# Assessments of the Direct and Indirect Effects of Anthropogenic Aerosols on Regional Precipitation over East Asia Using a Coupled Regional Climate-Chemistry-Aerosol Model

A Thesis
Presented to
The Academic Faculty

by

Yan Huang

In Partial Fulfillment
of the Requirements for the Degree
Doctor of Philosophy in the
School of Earth and Atmospheric Sciences

Georgia Institute of Technology
February 2005

# Assessments of the Direct and Indirect Effects of Anthropogenic Aerosols on Regional Precipitation over East Asia Using a Coupled Regional Climate-Chemistry-Aerosol Model

Approved by:


Dr. William L. Chameides, Chairman
School of Earth & Atmospheric Sciences
*Georgia Institute of Technology*

Dr. Michael H. Bergin
School of Earth & Atmospheric Sciences and Civil & Environmental Engineering
*Georgia Institute of Technology*

Dr. Robert E. Dickinson
School of Earth & Atmospheric Sciences
*Georgia Institute of Technology*

Dr. Rong Fu
School of Earth & Atmospheric Sciences
*Georgia Institute of Technology*

Dr. Filippo Giorgi
Physics of Weather and Climate Section
*Abdus Salam International Centre for Theoretical Physics, Italy*


Date Approved: February 16, 2005

# ACKNOWLEDGEMENTS

I would like to thank my thesis advisor, Prof. William L. Chameides, for his many years of patience, guidance, assistance and encouragement throughout my graduate study. His scientific insight and perspectives have made working with him being a rewarding and invaluable experience. I would also like to thank Dr. Filippo Giorgi, for the opportunity to work with him, and for his assistance and valuable insight in the regional climate research. I would also like to thank my other committee members, Prof. Michael Bergin, Prof. Robert Dickinson and Prof. Rong Fu, for their interest in my research and helpful discussions, comments and suggestions on this thesis.

Sincere thanks to Prof. Congbin Fu at the Institute of Atmospheric Physics, Chinese Academy of Sciences, for the opportunity he provided me to work at NCAR, where I began my regional climate modeling study. Many thanks to Dr. Xunqiang Bi, Dr. Yongqiang Liu, Dr. Chao Luo, Dr. Yun Qian, Dr. Allison Steiner, Dr. Qian Tan, Dr. Hui Wang and Dr. Hongbin Yu, for their helpful discussion and valuable suggestions in this study. The friendship and help of the research group, including Dr. Nicholas Meskhidze, Dr. Jing Zhang, as well as many other friends at the School of Earth and Atmospheric Sciences, has made my life at Georgia Tech more enjoyable.

Finally, I would like to thank my husband, Sihong, and my sons, Wenhan and Kevin, for their constant support, encouragement and love throughout these years.

# TABLE OF CONTENTS

# LIST OF TABLES

TABLE

# LIST OF FIGURES

FIGURE

# SUMMARY

In this thesis work, an aerosol module is developed and coupled to a regional climate model to investigate the direct and indirect effects of anthropogenic aerosols (sulfate and carbonaceous aerosols) on climate with a focus on precipitation over East Asia. This fully coupled regional climate-chemistry-aerosol model is capable of understanding the interactions between the aerosol perturbation and climate change.

The aerosol module consists of six prognostic equations for $SO_2$, $SO_4^{2-}$, hydrophobic and hydrophilic BC and hydrophobic and hydrophilic OC, including emission, advection, dry and wet deposition, and chemical production and conversion. The simulated aerosol spatial and seasonal distributions are generally consistent with the observations. The magnitude of the simulated 'TOTAL' aerosol concentration and optical depth is about 2/3 of the observed value, suggesting the estimated climatic effects in this work are reasonable and conservative.

With the implementation of various aerosol effect, i.e., direct, semi-direct, 1st and 2nd indirect effect, the coupled model is used to assess the aerosols' impacts on climate over East Asia. The direct, semi-direct and 1st indirect effects generate a negative surface solar forcing, leading to a surface cooling, and the semi-direct effect also heats the atmosphere by BC absorption. This, in turn, increases the atmospheric stability and tends to inhibit the precipitation. The precipitation reduction is largest in the fall and winter, up to -10% with the inclusion of both direct and 1st indirect effects. The 2nd indirect effect using BH94 scheme produces a comparable magnitude in longwave heating as the solar cooling, leading to the nighttime temperature warming of 0.5K, and a reduction in the diurnal temperature range. The precipitation reduction from the 2nd indirect effect strongly

depends on the autoconversion scheme, with about -30% in the fall and winter, and -15% in the spring and summer using BH94 scheme, while less than -5% using TC80 scheme. By allowing the feedbacks between aerosols and climate, the coupled model generally decreases the discrepancies between the model-simulated and observed precipitation and aerosols over the region.

The EOF analysis of the climatological precipitation from last century over East Asia shows a decreasing mode in the EOF leading modes in the fall and winter, and is generally geographically consistent with the distribution of the model simulated precipitation reduction from anthropogenic aerosols. However, the model predicted precipitation reduction trend is larger than that in the observations, even without the inclusion of 2$^{nd}$ indirect effect.

# CHAPTER 1

# INTRODUCTION

## 1.1 Atmospheric Aerosols

Atmospheric aerosols (also referred to as particulate matter or simply PM) are a complex chemical mixture of solid and/or liquid particles suspended in the air. Their presence is often directly observable by the human eye as haze in many industrial regions, as well as the rural areas subjected to heavy biomass burning, caused by the scattering and absorption of sunlight. The sizes of the atmospheric aerosols widely range from a few nanometers (nm) to tens of micrometers (μm) in diameter. The so-called superfine particles (less than about 0.1μm) mainly arise from gas-to-particle conversion whereby gases such as sulfur dioxide ($SO_2$), nitric oxide and nitrogen dioxide ($NO_x$) and volatile organic carbon (VOC) are oxidized and condensed. The so-called coarse particles (greater than 1 μm) are usually produced mechanically, e.g. wind blowing over dusty region, evaporation of sea spray, etc. Between the superfine and the coarse mode particles are the fine particles (about 0.1 ~ 1 μm). This mode is also referred to as the accumulation mode because the aerosols in this size range accumulate from the coagulation and condensational growth of superfine particles and tend to remain in the atmosphere for relatively long times (i.e., a few days) because of their relatively low sedimentation and coagulation rates. This mode is of particular interest in regard to the Earth's energy budget and climate change due to their efficient interaction with the solar radiation, (i.e., most of the solar energy is in the visible part of the spectrum ~ 0.5μm, and

the particles of about the same size as the wavelength scatter light efficiently), and their optimum size as cloud condensation nuclei (CCN) and as ice nuclei (IN) (Charlson et al., 1990; Twomey, 1974; Penner et al., 2001; Ramaswamy et al., 2001). Fine mode aerosols generally have atmospheric lifetimes of days to about a week (Penner et al., 2001), and, as a result, can be highly variable in the spatial and temporal distributions.

Atmospheric aerosol particles may be emitted directly as particles (primary sources) or formed from gaseous precursors (secondary sources) via the aforementioned gas-to-particle conversion of $SO_2$, $NO_x$, and VOC, etc. Some of the atmospheric sources are natural, e.g. volcanic emission and ocean sea spray; while others, such as industrial emissions, biomass burning and soil dust emissions from agriculture activities are anthropogenic. Globally, the atmospheric aerosol flux is estimated at about 3440 Tg per year, of which 10% comes from anthropogenic sources (Andreae, 1995; IPCC 1995). However, the anthropogenic aerosols, mainly consisting of sulfate and carbonaceous aerosols (black carbon and organic carbon), has substantially increased since pre-industrial times (IPCC, 1995), and even exceeds the natural sources globally, and dominates over the urban/industrial areas (Kiehl and Briegleb, 1993; Andreae, 1995, etc). Such a large perturbation of the global and regional aerosols from the anthropogenic sources is a major climatic and environmental concern.

## 1.2 Aerosol and Climate

In general, aerosols influence the climate via two ways: the direct effect by scattering and absorbing incoming solar radiation, and the indirect effect by acting as cloud condensation nuclei (CCN) and/or ice nuclei (IN), which modify the microphysics, radiative properties and lifetime of clouds. The direct effect from scattering by non-

absorbing aerosols such as particulate sulfate cools the Earth system (so-called the whitehouse effect, as opposed to the greenhouse effect by $CO_2$, $CH_4$, $N_2O$, etc) (Angstrom, 1929; Coakley et al. 1983; Charlson et al., 1990 and 1992; Schwartz, 1996). Absorption by aerosols such as black carbon and mineral dust, on the other hand, warm the earth by heating the atmosphere. This heating, in turn, can hinder the condensation and flatten the temperature gradient, which damps the convection and draws less water into the atmosphere, leading to a loss of cloud cover, a decrease in cloud albedo, and a further warming of the Earth system. This tendency to warm the Earth by "cloud-burning" from aerosol absorption is called the "semi-direct effect" (Hansen et al., 1997). The aerosol indirect effect is also split into two components: the 1$^{st}$ type indirect effect, in which an increase in aerosols leads to an increase in the cloud droplet concentration and a decrease in cloud droplet size, and, as a result, an increase in cloud albedo ( also termed as "cloud albedo effect") (Twomey, 1974); and the 2$^{nd}$ indirect effect, where the aforementioned reduction in cloud droplet size also tends to lower the precipitation efficiency, and increase the liquid water content, thereby the increasing cloud lifetime (also termed as "cloud lifetime effect") (Albrecht, 1989) and cloud thickness (Pincus and Baker, 1994). Therefore, both direct and indirect effects tend to reduce the amount of solar radiation reaching to the Earth's surface, while the semi-direct effect also increases solar heating in the atmospheric column. However, the magnitude of the indirect effect is far more uncertain than that of the direct effect (Schwartz and Andreae, 1996; Ramanathan et al., 2001a).

In addition to aerosols' impact on temperature, the direct and indirect effects can also affect the precipitation. This is more apparent in the case of the indirect and semi-direct

effects, which alter the cloud properties. However, other pathways may also be important. For example, both direct and indirect effects lead to less solar radiation reaching the Earth's surface, while the semi-direct effect increases solar heating through the atmosphere column. These in turn can alter the atmospheric stability, possibly leading to modifications in precipitation patterns induced by convection and monsoonal circulations (Ramanathan et al., 2001b; Boucher et al., 1998; Graf, 2004). The reduction in surface solar radiation by aerosol direct and indirect effects also likely modify the hydrological cycle through the surface energy budget alteration and subsequent reduction in evaporation to the extent that it can spin down the water cycle (Liepert et al., 2004).

Moreover, aerosols can affect the environment in a variety of different ways. Fine particles may adversely affect human health, especially in regard to cardio-vascular illnesses (Dockery and Pope, 1994) and reduce visibility by their scattering and absorption of radiation (Husar et al., 1981; Ball and Robinson, 1982; Husar et al., 2000). Concerns about the impact on visibility and human health have led to proposals to reduce the concentration of fine particles through regulations and emission control in the United States (US EPA, 1996), and China (China SEPA, 2003), etc. (Due to the heavy air pollution in China, the regulatory standard for ambient air quality of $PM_{10}$ (the aerosol particles with diameter less than 10 μm) from China SEPA is 2 ~ 3 times higher than that from U.S. EPA.) Aerosols can also affect photosynthesis and C-uptake rates of ecosystems subject to large aerosol loadings by perturbing leaf temperatures and the amount of photosynthetic active radiation (PAR) available to green plants (Chameides et al., 1999a and b; Bergin et al., 2001a; Steiner, 2004). In addition, sulfate and nitrate are the primary causes of acid rain, which affects large industrial regions over the world

(NAPAP, 1990; Ding et al., 1995; Wang and Wang, 1995). In this thesis work, the aerosols' direct and indirect effects on regional climate over East Asia will be explored and assessed.

## 1.3 Direct and Indirect Radiative Effect of Aerosols

The radiative effect of aerosols is usually quantified with a concept of radiative forcing, which denotes an externally imposed perturbation (e.g., changes in the aerosols' concentrations) on the radiative energy budget (both solar and long-wave) of the Earth's climate system (Ramaswamy et al., 2001). Conventionally, a positive radiative forcing indicates a net energy increase in the earth-atmosphere system, thus a warming effect; and a negative radiative forcing means a net energy loss, thus a cooling effect.

As originally portrayed by Angstrom (1929, 1961, and 1964), the central determinant of aerosol radiative forcing is the aerosol optical depth (AOD, called 'turbidity' in Angstrom's papers), an index of the attenuation of radiation as it passes through the atmosphere due to the presence of the atmospheric aerosols. The AOD is the vertical integral of the aerosol concentration weighted with the effective cross-sectional area of the particles intercepting (both scattering and absorption, the sum is extinction) the solar radiation at the wavelength of interest.

### 1.3.1 Observational Evidences

Observational evidences for the direct and indirect radiative effects of anthropogenic aerosols have been reported from in-situ and satellite data. The direct effect of aerosols comes from their scattering and absorption of solar radiation, and can be identified as an increase in AOD (or extinction), and/or a decease in solar radiation penetrating through

the atmosphere. For the most part, continental hazes tend to be concentrated over distinct regions of the world, such as the urban/industrialized areas of North America and Europe, the Indian subcontinent, eastern China, western Africa, etc (Husar et al., 2000). Studies of visibility indicate an increasing solar extinction from the 1940s to the 1970s due to anthropogenic aerosols in the eastern United States (Husar et al., 1981). Ball and Robinson (1982) estimated a 7.5% loss of the annual mean solar radiation for the eastern United States from sulfate and other anthropogenic aerosols relative to pre-industrial times.

Over China, analysis of meteorological data by China Meteorological Administration (CMA) indicates significant decreasing trends in sunshine duration for 1954-1998, especially in the eastern part of the country. This trend is likely related to the large increase in atmospheric anthropogenic aerosol loading and in turn increasing aerosol extinction over the region (Kaiser and Qian, 2002). Xu et al. (2003) also suggested that a reduction of about 16% in the amount of PAR reaching the surface over the Yangtze delta region as a result of the direct radiative effect of aerosols. The derived aerosol optical depth from the data of daily direct solar radiation, sunshine duration, etc at 46 solar radiation stations over China from 1961-1990 suggested a significant increase in aerosol optical depth with maximum over the Sichuan Basin of southwestern China (Luo et al., 2001). In-situ measurement of aerosol radiative, physical and chemical properties in Beijing (urban) and Lin'An (rural and located in Yangtze delta region) in China indicates an aerosol extinction coefficient of 488 $Mm^{-1}$ in Beijing and 353$Mm^{-1}$ in Lin'An, which is about 3 ~ 4 times higher than that measured in Atlanta (about 120$Mm^{-1}$)

during the Atlanta supersite 1999 experiment (Bergin et al., 2001b; Xu et al., 2002 and 2003; Carrico et al., 2003).

While the in-situ data provide the evidences of direct effect over certain regions, remote sensing from satellites delivers the most reliable information about global aerosol distributions. The measurable quantity from space is the aerosol optical depth, which is derived from the solar radiation reflected to space (Kaufman, et al., 1997). Advanced Very High Resolution Radiometer (AVHRR) satellite imagery shows an enhanced aerosol optical depth in the industrial regions of Northern Hemisphere, and prominent plumes downwind of the industrial polluted, biomass burning and dust regions (Durkee et al., 1991; Husar et al., 1997). The aerosol optical depth and reflectivity derived from the Earth Radiation Budget Experiment (ERBE) satellite and MODerate resolution Imaging Spectroradiometer (MODIS) also illustrate regional plumes over several continental aerosol regions (Penner et al., 2002; Yu et al., 2003 and 2004).

With regard to the indirect effects of aerosols, they arise from the interaction between aerosol and clouds, in which anthropogenic aerosols acting as cloud concentration nuclei (CNN), enhance cloud albedo by increasing the number concentration of cloud droplets ($N_c$) and reducing the cloud effective radius ($r_e$). Therefore, an increase in cloud reflectivity, CCN and/or $N_c$, and a decrease in $r_e$ could be an indication of the 1$^{st}$ indirect effect.

Numerous studies have found that CCN concentrations are greater in anthropogenic polluted continental air than in the marine air, and continental clouds tend to have a greater $N_c$ and smaller mean droplet diameters than do marine clouds. This contrast is also seen in the downwind of polluted regions vs. the upwind clean regions (Warner and

Twomey, 1967; Meszaros, 1992; Hudson and Li, 1995; Pruppacher and Klett, 1997). The measurement of CCN concentration in well-aged continental air generally exceeds 1000cm$^{-3}$, while that of background clean marine air rarely exceed 100 cm$^{-3}$ (Radek and Hobbs, 1976; Twomey et al., 1978; Hudson, 1991; Frisbie and Hudson, 1993). And the measured cloud reflectance from ACE-2 (the second Aerosol Characterization Experiment, Raes et al., 2000) demonstrates the higher reflectance of clouds in polluted air than that in marine air (Brenguier et al., 2000).

Ship tracks and aircraft observations have shown higher cloud reflectivity embedded in marine stratus cloud, and enhanced $N_c$ and decreased droplet sizes resulting from an increase of aerosols from the ships engine exhaust, comparing with nearby unperturbed regions of clouds (Coakley et al., 1987; Scorer, 1987; Radke et al., 1989a and b; King et al., 1993; Kuang and Yung, 2000).

Using data from ISCCP (International Satellite Cloud Climatology Project), the analysis of the cloud effective radius in warm clouds, column droplet concentration in low-level clouds, and the relationship between cloud albedo and cloud droplet size, demonstrated that there were systematically smaller effective cloud droplet radius and larger cloud number concentration for continental clouds compared to the maritime clouds and for clouds in mid-latitude Northern Hemisphere, where the industrial sources are concentrated (Han et al., 1994 and 1998a). A negative correlation exists between satellite-derived cloud albedo and cloud droplet size for most clouds over continental areas and all optically thick clouds, but an opposite correlation in optically thinner clouds over marine areas (Han et al., 1998b; Nikajima et al., 2001). AVHRR satellite data over

the Amazon Basin and Cerrado also demonstrated that smoke increases the cloud reflectance and reduces the droplet size (Kaufman and Fraser, 1997).

While the direct and 1st indirect effects have been extensively observed during last several decades, it is only recently that scientists began to investigate the semi-direct effect from absorbing aerosols, such as black carbon. As noted earlier, the semi-direct effect causes surface cooling and atmospheric warming, which alters the temperature gradient, and thus is associated with a reduction in cloud formation. Measurements during the Indian Ocean Experiment (INDOEX, Ramanathan et al., 2001c) suggest a reduction of tropical cloudiness, presumably due to the presence of soot, and thus an indication of semi-direct effect (Ackerman, 2000). Satellite data over the Amazon region during the biomass burning season also shows the effect of Amazon smoke on the inhibition of cloud formation (Koren et al., 2004).

### 1.3.2 Modeling Studies

Since the first quantitative study of anthropogenic aerosols on climate (Charlson et al., 1990), numerous quantitative estimates of the direct and indirect effects of tropospheric aerosols have been carried out, which require knowledge of the aerosols' spatial and temporal distribution and their radiative properties. Due to the inhomogeneous nature of aerosols, regional and global scale chemical transport models of aerosols and their precursors have been developed based on several processes including emission, transport, conversion and removal. These works include sulfur cycle models (e.g. Langner and Rodhe, 1991; Langner et al., 1992; Benkovitz et al., 1996; Chin and Jacob, 1996; Chin et al., 1996; Benkovitz and Schwartz, 1997; Kasibhatla et al., 1997; Chin et al., 2000a and b; Koch, 2001; etc); and later developed carbonaceous aerosol models (Penner et al., 1993;

Cooke and Wilson, 1996; Liousse et al., 1996; Cooke et al., 1999; Scholes and Andreae, 2000; Koch, 2001). Because these models differ in their resolution, representation of physical processes and the complexity of the chemical schemes, the Comparison of Large Scale Sulfate Aerosol Models (COSAM) found that estimates of the concentration and atmospheric column loading are highly model-dependent (Barriel et al., 2001; Roelofs et al., 2001). Overall, the globally averaged anthropogenic aerosol column burden estimated by different models agrees to within a factor of 2.5, and around 0.53 Tg S, 1.52 Tg C and 0.27 Tg C for sulfate, organic carbon and black carbon, respectively (Penner et al., 2001).

With the aerosol distribution, the aerosol radiative transfer scheme is used to estimate their radiative-climate effect. Generally, the radiative effects of aerosols are described by three optical parameters: 1) the specific extinction coefficient $\alpha_e$, which is the extinction (both scattering and absorption) per unit dry mass; 2) the single scattering albedo $\omega_0$, which is defined as a ratio of scattering to total extinction; and 3) the asymmetry parameter $g$, which is a measure of the amount of radiation scattered forward relative to that scattered backward. The value of $g$ ranges from -1 (totally backward scattering) to +1 (totally forward scattering). All of above three parameters are dependent on aerosol physical properties (i.e. refractive index, size distribution, mixing state, etc), wavelength and environmental relative humidity. The extinction coefficient increases with the relative humidity because hygroscopic aerosols uptake water to increase their mass and surface area, and therefore scatter more solar radiation. The value of $\omega_0$ ranges between unity and zero, and it is critical to the net effect of atmospheric aerosols in the radiation balance (Heintzenberg et al., 1997). For the pure scattering aerosols, $\omega_0$ is unity. For strong absorbing aerosols, $\omega_0$ is $<<$ 1 and reaches zero if the aerosol acts like a black

body. The observed $\omega_0$ is close to unity in remote marine areas (Bodhaine, 1995), and 0.90 for polluted continental areas (IPCC, 1995), and 0.82 ~ 0.85 for biomass burning areas (i.e. the African savanna region) (Eck et al., 2001).

Starting from the box model, one-, two-, three-dimensional models, offline (using the prescribed aerosol distribution from aerosol chemical transport models) and now commonly online coupled models, have been developed to evaluate the direct and 1st indirect radiative forcing of anthropogenic sulfate, organic carbon and black carbon since pre-industrial times. The studies of sulfate direct radiative forcing include: Charlson et al. (1991 and 1992), Kiehl and Briegleb (1993), Taylor and Penner (1994), Penner et al., (1994), Kiehl and Rodhe (1995), Chuang et al. (1997), Haywood et al. (1997), Hansen et al. (1998), Haywood and Ramaswamy (1998), Myhre et al. (1998), Koch et al. (1999), Kiehl et al. (2000) and Jacobson (2001), etc. On the other hand, assessments of direct radiative forcing due to anthropogenic black carbon and organic carbon aerosols have been carried out by Penner et al. (1992 and 1998), Hansen et al. (1993), Haywood and Shine (1995), Hansen et al. (1997), Haywood and Ramaswamy (1998), Myhre et al. (1998), Cooke et al. (1999), Jacobson (2001), Koch (2001), etc.

When considering the direct effect by black carbon, another complication arises from the way in which chemical species are mixed in aerosols. Black carbon can absorb up to twice as much light when present as internal mixture with ammonium sulfate (in the same particles) compared to external mixture (separate particles) (Ackerman and Toon, 1981; Horvath, 1993; Liousse, et al., 1993; Fuller et al., 1999), which may introduce a range of a factor of two in the magnitude of forcing by black carbon (Haywood and Shine, 1995; Jacobson, 2000).

While the direct effect of anthropogenic aerosols consider the aerosol-radiation interaction only, the indirect effect investigation needs to relate the aerosol and cloud microphysics (Schwartz and Slingo, 1995; Haywood and Boucher, 2000), which can be represented via: i) a measurement-based empirical relationship, in which a relationship between $N_c$ and aerosol mass or number concentration is derived from measurements (i.e. Jones et al., 1994; Hegg, 1994; Boucher and Lohmann, 1995; Jones and Slingo, 1996; Lohmann and Feichter, 1997; Rotstayn, 1999; Kiehl et al., 2000); or ii) a prognostic method including parameterization of cloud nucleation processes, in which $N_c$ is calculated from formulas that explicitly relate cloud droplet nucleation to the aerosol concentration, as well as other relevant parameters such as the vertical velocity and an activation parameter (i.e. Chuang and Penner, 1995; Chuang et al, 1997; Lohmann et al., 2000; Ghan et al., 2001a, b and c; Chuang et al., 2002). As discussed in Haywood and Boucher (2000), the prognostic approach (sometimes referred to as a "mechanistic" approach) accounts for other preexisting aerosol types and variations in the cloud vertical updraft and avoids the problem of prescribing a unique relationship between aerosol mass and cloud droplet concentration. In fact, substantial variation exists in the empirical relationships suggested by studies of analyzing the measured $N_c$ and aerosol concentration (Leaitch et al., 1992; Leaitch and Isaac, 1994; Hegg et al., 1993; Novakov et al., 1994; Feingold et al., 2003; Rosenfeld and Feingold, 2003). While the prognostic method represents a more comprehensive approach, it also adds to models one degree of complexity by introducing a process not yet fully understood. Haywood and Boucher (2000) also suggest that the empirical relationships commonly used in the previous modeling studies show the same qualitative behavior of the prognostic method.

Based on the numerous studies during the last decade, the Intergovernmental Panel on Climate Change (IPCC) reported the "best estimate" global annual mean direct forcing of -0.4 W $m^{-2}$ for sulfate, +0.2 W $m^{-2}$ for fossil fuel black carbon, -0.1 W $m^{-2}$ for fossil fuel organic carbon, and -0.2 W $m^{-2}$ for biomass burning carbonaceous aerosol since pre-industrial times. For the 1$^{st}$ type indirect forcing, a range of 0 ~ -2.0 W $m^{-2}$ was given due to the very low scientific understanding level (Ramanathan et al., 2001a). Anderson et al (2003) also argued that the magnitude and uncertainty of aerosol forcing may be larger than is usually considered in models. Though the uncertainty is substantial, the anthropogenic aerosol radiative forcing appears to be comparable in magnitude to current anthropogenic greenhouse gas forcing (+2.5 W $m^{-2}$ ) but opposite in sign, and thus may have offset and even overcome the warming of greenhouse gases (Charlson et al., 1992; Kiehl and Briegleb, 1993).

On the regional scale, due to the relatively short lifetime (~ a week or less), aerosols occur in substantial and temporal variations with peak concentrations near the source. It would be expected that the radiative and climatic effects of aerosols are more pronounced over the regions with high industrial emissions and/or heavy biomass burning rural areas. A series of recent studies investigated the role of anthropogenic aerosol in modifying the climate over East Asia using a coupled regional climate chemistry model initiated by the CHINA-MAP project (Chameides et al., 1994; Chameides, 1995), a research program aiming at understanding the environmental and climatic effect of China Metro-Agro-Plex. The model system was developed by Qian and Giorgi (1999) and Qian et al. (2001) by coupling a regional climate model of Giorgi et al (1993a and b) and Giorgi et al (1999), and a simplified version of a sulfur chemistry module based on the a full chemistry

transport model of Chameides et al. (1999a) and Luo et al (2000). Using the coupled model (including sulfate and BC), Giorgi et al. (2002 and 2003) carried out a series of regional simulations to investigate the direct and 1$^{st}$ indirect radiative forcing and climatic effects of anthropogenic sulfate and fossil fuel soot over East Asia. They found that direct forcing was dominant over the cold seasons, while the indirect forcing was dominant in the summer monsoonal season. Tan et al. (2002) also implemented a tracer convective transport scheme in the coupled model to study the sulfur species ($SO_x$) transport from East Asia. Using the model-calculated anthropogenic aerosols and satellite-derived cloud optical depths, Chameides et al. (2002) found a correlation between these two dataset, an indication of the indirect effect.

## 1.4 Climatic Response to the Aerosol Effects

### 1.4.1 Impact on Surface Temperature

As mentioned above, there have been numerous attempts to quantitatively estimate the direct and indirect radiative forcing by anthropogenic aerosols. A related issue is whether there is any empirical evidence indicating how the climate system responds to this aerosol forcing and whether any aerosol fingerprint exists in the observed climate record? Climate responses are the meteorological results of the forcings, including changes in temperature, wind, precipitation and their probability distribution (NRC, 1996). The overall negative forcing by both direct and indirect effects leads to a reduction in surface received solar radiation, which likely causes a cooling in surface temperature. Studies investigating the global observed temperature trend demonstrated that the simulated surface temperature trend combining both aerosol and greenhouse gases effects in the climate models agrees better with the observational temperature record than

simulations which only included aerosols, or greenhouse gases, or neither (Taylor and Penner, 1994; Santer et al., 1995 and 1996; Hansen et al., 1995, 1997 and 2001). Karl et al. (1995) found that the diurnal temperature range (DTR) decreased over industrial regions, which may be partially attributable to the anthropogenic aerosol forcing. A significant cooling trend is also found over some regions of China, most notably the Sichuan Basin, where especially high anthropogenic aerosol loadings exist (Li et al., 1995; Qian and Giorgi, 2000; Zhai and Pan, 2003).

### 1.4.2 Impact on Precipitation

As discussed earlier in Section 1.2, both the direct and indirect effects can also affect the precipitation by the modifications of cloud properties, atmospheric stability, surface evaporation, etc from aerosols. The investigation of the aerosol-precipitation linkage began with the speculation of how aerosol might modify weather and climate (Gunn and Phillips, 1957; Warner, 1968; Hobbs and Radke, 1969; Hobbs et al., 1974; Junge, 1975). The practice of weather modification through cloud seeding (using dry ice, silver iodide, etc) to stimulate precipitation, to dissipate cloud or fog and to suppress hail has been carried out at a local scale since the late 1960s (Dennis, 1980; Roger and Yau, 1989; Huang and Xu, 1994). In addition, studies of the BC aerosols from the nuclear war fires found that the smoke heating induces cloud formations and precipitation, and on the other hand, the smoke shielding stabilizes the lower troposphere and hinder precipitation (Crutzen et al., 1984; Cotton, 1985; Malone et al., 1985 and 1986; Golding et al., 1986; Giorgi and Visconti, 1989; etc). Recently, satellite observation of the Tropical Rainfall Measuring Mission (TRMM) indicated rain suppression due to air pollution from forest fires (Rosenfeld, 1999) and from industrial pollution (Rosenfeld, 2000). Using both

satellite and aircraft observation, Rosenfeld et al. (2001) also showed that cloud forming within desert dust contain small droplets and produce little precipitation by coalescence. Ackerman et al (2003) also suggested an enhancement of cloud cover and suppression of nocturnal drizzle in stratocumulus polluted by haze based on a large-eddy simulation.

While most of the previous investigations of the climatic effects of aerosols have focused on the direction and magnitude of the perturbation on surface and atmospheric temperatures from aerosols using global and/or regional climate models, by contrast, there have been relatively few attempts to assess the impact of aerosols on precipitation. Among these few are two recent studies which both assessed the impact of anthropogenic aerosols on precipitation over East Asia, but reached different conclusions. Menon et al. (2002b) studied the direct and semi-direct effect of aerosols over China and India using a global climate model driven by observed aerosol optical depth and an assumed single scattering albedo over the region. They concluded that anthropogenic aerosols have increased precipitation in southeast China but suppressed precipitation over northeast China. These precipitation changes in their model simulations were essentially attributable to the absorption (as opposed to the scattering) of radiation by the assumed aerosol distribution. Giorgi et al. (2002 and 2003), on the other hand, used a regional coupled climate/chemistry model that included the direct and 1$^{st}$ indirect effect of anthropogenic sulfate and soot. They concluded that aerosols tend to inhibit precipitation throughout China. For current sulfur emissions, they found that the impact on precipitation from the direct effects from aerosol scattering and absorption was negligible, but became quite pronounced with inclusion of the 1$^{st}$ indirect effect. A more recent study by Ackerman et al. (2004), focused more generally on the 2$^{nd}$ indirect effect by

simulating the marine stratocumulus clouds polluted by aerosol particles with a fluid dynamics model. They argued that the climatic impacts of 2nd indirect effect are likely to be small. Another study by Takemura et al. (2005) simulated the climate response to the aerosol direct and indirect effects with a coupled global aerosol transport-radiation-climate model, and they found that the precipitation and cloud water changes are strongly affected by a variation of the dynamical hydrological cycle, with a strong signal of 2nd indirect effect over the regions where a large amount of anthropogenic aerosols and cloud water co-exist.

In summary, the primary shortcomings of the above studies regarding the aerosol effects on precipitation are as following: not including all the direct, semi-direct, 1st and 2nd aerosol effects, and/or not considering all three main anthropogenic aerosols ($SO_4^{2-}$, BC and OC), and/or using an offline approach, and, in turn, lack of feedbacks between aerosol and climate.

## 1.5 Objectives and Outline of This Thesis

In this thesis work I carry out an investigation of atmospheric aerosol effects on climate with a focus on impacts on precipitation using a fully coupled climate-chemistry-aerosol regional model applied to a domain covering East Asia and centered on China. The coupled climate-chemistry aspect of the model allows for a more complete treatment of the feedbacks that may exist between aerosols and climate. A regional climate-chemistry-aerosol model is an especially suitable tool for understanding the interaction between aerosol and climate, because the model operates on a more appropriate spatial scale to resolve inhomogeneities in aerosol concentrations, precipitation and clouds.

East Asia was chosen for this regional focus for a variety of reasons. East Asia, one of the most populous and rapidly developing regions of the globe (United Nations, 1996), has large atmospheric loading of anthropogenic aerosols due to the rapid industrialization, urbanization and domestic heating. Several experimental and modeling studies (e.g. ACE-Asia, Huebert et al., 2003; ChinaMAP, Chameides et al., 1995) have focused on understanding the aerosol characteristics and their climatic effects over this region.

This study is motivated by two scientific questions. First, what are the impacts of the various effects of aerosols, individually and in concert, on precipitation over East Asia within the context of a regional coupled climate-chemistry-aerosol model? But perhaps more importantly, to what extent are the aerosols impacts on precipitation predicted by this model actually reflected in climate record for the region? One of the major sources of uncertainty in both global and regional climate models is the simulation of precipitation because so many of the relevant processes occur at the sub-grid scale (Giorgi and Mearns, 1991; Pan et al., 2001 and Frei et al., 2003). If climate models are able to correctly predict the affect of aerosols on precipitation, it provides some further support for the use of such models in assessing this and other impacts of aerosols on the environment, as well as in their use in assessing the effects of other environmental perturbations on precipitation.

The investigation has largely consisted of the development and application of a three-dimensional regional coupled climate-chemistry-aerosol model to assess how the various aerosol effects influence the climate over East Asia. The model was originated from NCAR regional climate model (RegCM2) (Giorgi et al., 1993a and b) with a sulfate module developed by Qian et al. (2001), modified tracer convective transport (Tan et al.,

2002) and the implementation of carbonaceous aerosols. All three main anthropogenic aerosol components ($SO_4^{2-}$, BC and OC) and direct, semi-direct, 1st and 2nd indirect effects are included in the model. In addition to model development and application, an analysis of the long term precipitation record over East Asia was performed in an attempt to find if an aerosol fingerprint exists which is consistent with the model-predicted effects of aerosols on precipitation over the region. The thesis is organized as follows.

Chapter 2 presents the implementation of the aerosol module including sulfur chemistry and carbonaceous aerosols. The simulated aerosol characteristics are evaluated with the observations of both spatial and seasonal patterns.

Chapter 3 describes how the various aerosol effects are represented in the coupled climate-chemistry-aerosol model based on the aerosol radiative properties and their interaction with clouds and precipitation. The magnitude and relative importance of each effect on radiative forcing and in turn the climate responses (esp. precipitation) are assessed. An empirical orthogonal function (EOF) analysis of long term precipitation trend for the last century over East Asia is then presented to evaluate the model-predicted effects of aerosols on precipitation.

Chapter 4 summarizes the main conclusions and implications of this study and discussion of future investigation.

# CHAPTER 2

# REGIONAL SIMULATION OF ANTHROPOGENIC SULFATE AND CARBONACEOUS AEROSOLS OVER EAST ASIA

## 2.1 Introduction

The spatial and temporal distributions of aerosols (such as sulfate and carbonaceous particles) tend to be highly inhomogeneous on the regional scale (~ 1000s of kilometers) due to their relatively short lifetimes. Moreover, the measurements of atmospheric aerosols concentration (both horizontally and vertically) in non-urban areas are scarce. For these reasons, three-dimensional chemical transport models that simulate the emissions, transports, conversion and removal processes of sulfur and carbonaceous species are important tools to characterize their spatial distributions on global/regional scales, and to assess their climatic effects, whose uncertainties are large (Schimel et al., 1996). One of the first attempts to simulate aerosols globally was carried out by Langner and Rodhe (1991), who estimated the global distribution of sulfate aerosols in the context of a global sulfur cycle study, using an "off-line transport model, in which the meteorological information (e.g. temperature, precipitation, cloud, etc) was specified and interpolated from the outputs of global circulation models. Since then, a number of studies have been carried out using this off-line approach to study sulfate aerosols globally, i.e., Chin et al. (1996), Chuang et al. (1997); Pham et al. (1995), Kasibhatla et al. (1997), etc. During the last decade, more sophisticated coupled chemistry-climate global/regional models have been developed, which: i) make use of significantly more temporally and physically detailed information about the processes that influence the

aerosol formation and their interaction with clouds (e.g. Chin et al., 2000a and 2000b; Qian et al., 2001; Tan et al., 2002, etc); ii) include organic aerosol compounds (Hegg et al., 1997; Novakova et al., 1994 and 1997, etc), which scatter at least as much light as sulfate, and soot aerosols (Haywood and Shine, 1995; Koch, 2001; etc), which absorb solar radiation; and; iii) allow for climate-aerosol feedbacks.

Here, a three dimensional regional coupled climate-chemistry-aerosol model is developed to simulate sulfate and carbonaceous aerosols over East Asia, which is then used to investigate the climatic effects of anthropogenic sulfate and carbonaceous aerosols over this region (see Chapter 3). As noted earlier, East Asia is chosen because of its large atmospheric loading of anthropogenic aerosols due to the rapid economic and industrial development of this region (Streets and Waldhoff, 2000; Chameides et al. 2002). A major step towards the understanding of aerosols effect over East Asia was the inception of the CHINA-MAP project (Chameides et al., 1994; Chameides, 1995), a research program aimed at elucidating the environmental and climatic effects of rapid economic and industrial development in China. As part of this project, a fully coupled chemistry-transport model was developed for the region and used to study the effects of anthropogenic pollutants on agricultural productivity and air quality (Chameides et al., 1999a and b; Luo et al., 2000). In this thesis, a sulfur and carbonaceous aerosol module was developed and added to the regional climate model. In this chapter, I describe the aerosol module and the characteristics of anthropogenic sulfate and carbonaceous aerosols distributions over East Asia obtained using this module within the regional model developed during China-Map project.

## 2.2 Model Description

### 2.2.1 Regional Climate Model

The regional climate model (RegCM2) that forms the framework for the coupled model used in this thesis, is the second-generation grid-point limited area model developed by Giorgi et al. (1993a and b) with the augmentations described by Giorgi and Shields (1999) and Giorgi et al. (1999). Its dynamical core is essentially equivalent to the hydrostatic version of the NCAR/PSU (National Center for Atmospheric Research / Pennsylvania State University) mesoscale model MM5 (Grell et al., 1994), with the terrain-following sigma ($\sigma$) pressure vertical coordinate, which is defined as:

$$\sigma = \frac{p - p_t}{p_s - p_t} \tag{2.1}$$

where $p$ is pressure, $p_s$ and $p_t$ is the surface and top pressure respectively of the model. Surface processes are represented via the Biosphere-Atmosphere Transfer Scheme (BATS, see Dickinson et al., 1993) and boundary layer physics is formulated following the non-local scheme of Holtslag et al. (1990). Resolvable scale (large scale) clouds and precipitation are represented via the simplified explicit scheme described by Giorgi and Marinucci (1996) and Giorgi and Shields (1999), which includes a prognostic equation of cloud water content; while non-resolvable (small scale) convective clouds and precipitation are represented by the simplified form of the Kuo-type scheme of Anthes (1977) and Anthes et al. (1987). Radiative transfer calculations are carried out using the radiation package of the NCAR Community Climate Model, version CCM3 (Kiehl et al., 1996), which make use of a delta-Eddington approximation (Briegleb, 1992) to treat the radiative effects of different greenhouse gases ($H_2O$, $CO_2$, $O_3$, $CH_4$, $N_2O$, CFCs), cloud water and cloud ice, and a uniform background of boundary layer atmospheric aerosols

(Kiehl and Briegleb, 1993). Detailed descriptions of RegCM2 and its validation can be found in Giorgi et al. (1993a, 1993b and 1999).

Figure 2.1 shows the model domain and topographical field used in this work. Also shown in Figure 2.1 are the inner domain which excludes 12 lateral boundary grids and four Chinese sub-regions used for more detailed analysis of the model results: north China (NC), central China (CC), south China (SC) and southwest China (SW), and the aerosol measurement sites used for model-observation comparison. The domain encompasses 80x103 grids with a resolution of 60km and centered at (34N, 120E), covering East Asia and adjacent ocean areas. The model includes 14 vertical levels, with a tropospheric resolution of about $\sigma = 0.1$, five levels below about 850mbar and a top level at 80mbar. The lateral boundary conditions to drive the model simulation are obtained from the analyses of observations from the European Center for Medium-Range Weather Forecasts (ECMWF). The full simulation period is from June 01, 1994 to August 31, 1995, and the first two months are dropped to allow for model spin up. An evaluation of the RegCM2 simulation and performance for this domain and time period is provided in Chapter 3; a more detailed discussion can be found in Giorgi et al. (1999).

### 2.2.2 Treatment of Sulfate and Carbonaceous Aerosol

Measurements in rural and urban locales over East Asia, suggest that, with the exception of episodes of intense dust storms, the composition and radiative effects of particulate matter in the region are dominated by two components that are, in turn, largely of anthropogenic origin: namely, sulfate ($SO_4^{2-}$) and carbonaceous aerosols (Bergin et al., 2001b; Xu et al., 2002 and Bergin et al., 2004). To simulate the distributions of these two

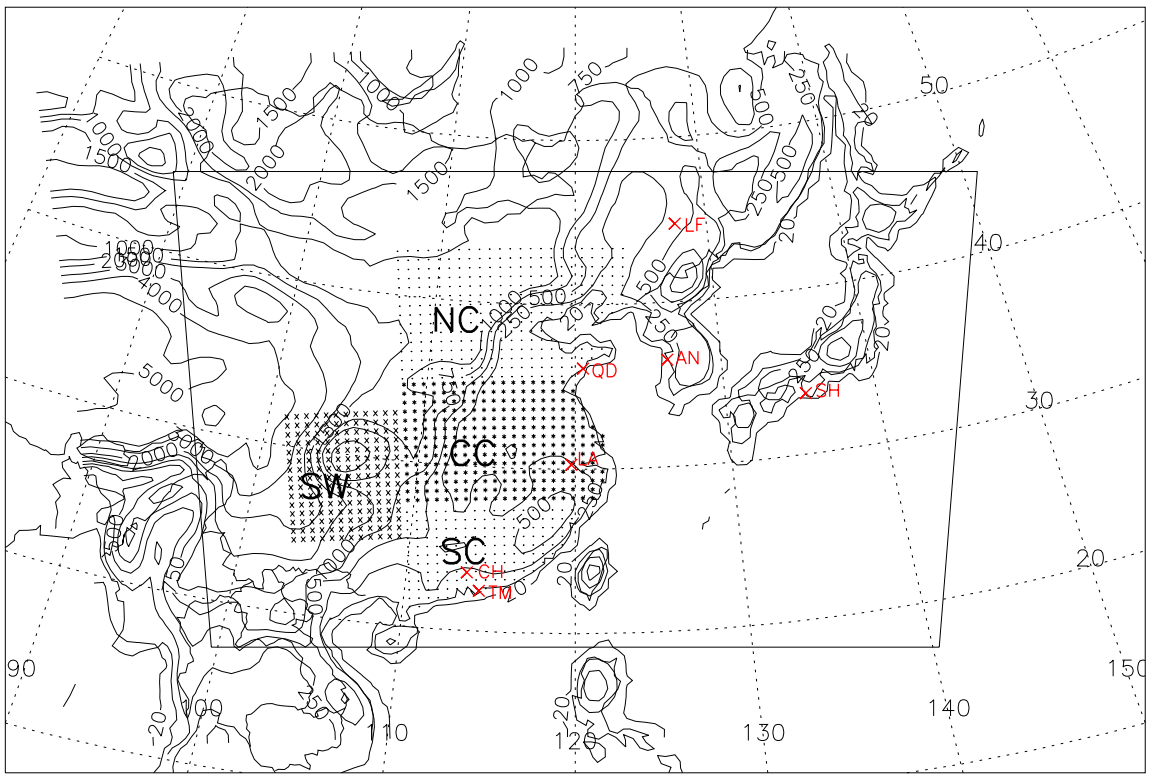


**Figure 2. 1** Regional model domain and topography. Units are in meters, and the contour levels are 20m, 250m, 500m, 750m, 1000m, 1500m, 2000m, 3000m, 4000m and 5000m. Also shown are the inner domain excluding 12 laterial boundary grids, and four shading sub-regions used in the analysis: NC – North China; CC – Central China; SC – South China and SW – Southwest China. The aerosol measurement sites used for the model-observation comparison are shown in red: LA- Lin'An, QD – QingDao, LF – LongFengShan, CH – Conghua, TM – Tap Mun, AN – Anmyon, SH – Shirahama.

aerosol components, a coupled chemistry-climate aerosol module was developed to solve the mixing ratio ($\chi$ in unit: kg kg$^{-1}$ air) of six chemical species: gaseous $SO_2$, particulate $SO_4^{2-}$, hydrophobic and hydrophilic black carbon ($BC_{phobic}$ and $BC_{philic}$), and hydrophobic and hydrophilic organic carbon ($OC_{phobic}$ and $OC_{philic}$) described as the following prognostic equation:

$$\frac{\partial \chi_i}{\partial t} = -\vec{V}\nabla \chi_i + F_{H,i} + F_{V,i} + S_i + T_{gas,i} + T_{hetero,i} + T_{ls,i} + T_{conv,i} + T_{below-cloud,i} + T_{dry,i} \quad (2.2)$$

where $i$ indicates the i$^{th}$ species. The first term on the r.h.s of Equation (2.2) represents the horizontal and vertical advection, $F_{H,i}$ and $F_{V,i}$ are horizontal and vertical turbulent diffusion, $S_i$ is the emission term, $T_{gas,i}$ is the tendency due to gas phase chemical conversion, $T_{hetero,i}$ is the tendency due to heterogeneous reactions, $T_{ls,i}$ and $T_{conv,i}$ are tendencies via large scale and convective cloud processes, respectively, $T_{below\text{-}cloud,i}$ is the rate of removal via below cloud scavenging, $T_{dry,i}$ is dry deposition term. All the advection and diffusion terms are the same as used in the MM5 for cloud water mixing ratio (Grell et al., 1994; Qian et al., 2001).

*2.2.2.1 Sulfur species*

The sulfur algorithm is based on that of Kasibhatla et al. (1997) with the revisions and enhancements of Qian et al. (2001) and Tan et al. (2002), where the detailed formulas can be found. A brief description of the terms on the right hand side of Equation (2.2), except for the advection and diffusion terms, is given below.

The gas phase oxidation pathway is initiated by the reaction of $SO_2$ with OH to produce $SO_4^{2-}$

$$T_{gas,so2} = - T_{gas,so4} = -k_{OH,SO2}[OH]\ \chi_{SO2} \quad (2.3)$$

where $k_{OH,SO2}$ is the temperature-dependent reaction rate constant from DeMore et al. (1994) and [OH], the OH concentration, is obtained from the regional chemical transport model simulation of Luo et al. (2000), which used the same domain as the RegCM2 application described here and was driven, in turn, by the meteorological fields calculated by the RegCM2.

Following Kasibhatla et al. (1997) and Chameides et al. (2002), an additional pathway to convert $SO_2$ to $SO_4^{2-}$ is included to account for the effect of heterogeneous reactions of $SO_2$ with the pre-existing aerosols. The reaction was assumed to only occur within the boundary layer and to have a pseudo 1$^{st}$ order reaction coefficient of $6x10^{-6}$ $s^{-1}$,

$$T_{hetero,so2} = - T_{hetero,so4} = -6x10^{-6}\ \chi_{SO2}, \quad \textit{within the boundary layer} \quad (2.4)$$

At pH's typical value of cloud water over East Asia (below 5), $SO_2$ has a relatively low solubility, and in the absence of aqueous-phase chemical conversion, most $SO_2$ in a cloud would remain in the interstitial air (Chameides, 1984). Hence, the rate of removal of $SO_2$ in clouds is limited by the rate of aqueous-phase conversion of $SO_2$ to $SO_4^{2-}$. This occurs via the dissolution of $SO_2$ in clouds to form $HSO_3^-$ and $SO_3^{2-}$ ions and then oxidation by dissolved $H_2O_2$ and $O_3$. Previous work indicated that reaction with $O_3$ only accounts for 10% of the $SO_2$ oxidation (Rasch et al., 2000), and hence the oxidation by $O_3$ is neglected in this work. The conversion process is assumed to be limited by the availability of $SO_2$ and $H_2O_2$, and is a function of the cloud liquid water content, cloud fractional cover and cloud lifetime (Giorgi and Chameides, 1986; Rogers and Yau, 1989 and Kasibhatla et al., 1997). As noted above, the RegCM2 simulates two types of clouds: large-scale or resolvable clouds and convective clouds.

In large scale clouds, the tendency of $SO_2$ in Equation (2.2) is given by

$$T_{ls,so2} = \frac{1}{dt} frc_{ls}[\exp(-\frac{w_L dt}{A}) - 1]\min(\chi_{SO2}, \chi_{H2O2}) \quad (2.5)$$

where $frc_{ls}$ is the fractional cover for the large scale clouds (equal to 1 except where convective clouds are also present, then 0.7), $w_L$ (g $m^{-3}$) is the liquid water content, which is a prognostic variable calculated by the dynamical portion of the RegCM2, $A$ (=360 g $m^{-3}$ $s^{-1}$) is a parameter derived from the cloud-chemistry simulation of Chameides (1984), which is related the $SO_2$ equilibrium dissolution in clouds, $dt$ is the time step (=200s), and the term 'min($\chi_{SO2}$, $\chi_{H2O2}$)' is used to ensure that the $SO_2$ conversion is limited by the availability of $H_2O_2$ whenever $H_2O_2 < SO_2$.

The $SO_4^{2-}$ produced by the oxidation of $SO_2$ in clouds, and the ambient $SO_4^{2-}$ entrained into the clouds, are partially removed by the precipitation process. Previous observations suggest that $SO_4^{2-}$ particles are entirely dissolved into the cloud water, hence the in-cloud wet removal coefficient is essentially equal to unity (Hegg and Hobbs, 1987; Seinfeld and Pandis, 1998). Therefore, in large scale clouds, the tendency of $SO_4^{2-}$ is given as

$$T_{ls,so4} = [\exp(-r_{rem} dt) - 1][\frac{1}{dt} frc_{ls} \chi_{SO4} - T_{ls,SO2}] \quad (2.6)$$

where $r_{rem}$, is the autoconversion frequency for the production of rain water from cloud water (Giorgi and Chameides, 1986; Giorgi et al. 1999), given by the autoconversion rate ($P_{autocv}$ , see Chapter 3, Section 3.2.3) divided by the cloud water mixing ratio ($w_L$).

In addition to chemical conversion and wet removal, convective clouds can affect the horizontal and vertical distribution of tracers through convective entrainment and transport. The treatment of convective transport and wet removal for $SO_x$ tracers in the

model closely follows that of water vapor and thus makes use of the pre-existing algorithms within the RegCM2. We first calculate the total amount of $SO_x$ that is entrained into a convective cloud at the k vertical level by assuming that the amount of tracer that enters the cloud is proportional to the amount of water vapor that enters the cloud and the relative concentrations of the tracer and water vapor at that level,

$$En(k)_i = qv_{tendency}(\frac{\chi_i}{qv}) \tag{2.7}$$

$$S_i = \sum_{cloudbase}^{cloudtop} En(k) \tag{2.8}$$

where $qv$ is the mixing ratio of water vapor, and $qv_{tendency}$ is the tendency of water vapor at k level caused by the horizontal convergence, $En(k)_i$ is the rate at which tracer $i$ (i.e. $SO_2$ and $SO_4^{2-}$, and carbonaceous aerosols) is entrained into the cloud at the k vertical level and $S_i$ is the column integrated amount of tracer $i$ entrained into the cloud from cloud base to cloud top. So the amount of $SO_2$ and $SO_4^{2-}$ convergence for the k level by cloud entrainment is $En(k)_{SO2}$ and $En(k)_{SO4}$, and the total convergence in the convective column is $S_{SO2}$ and $S_{SO4}$, respectively.

Next, a fraction of the column integrated entrained $SO_2$ in the cloud is oxidized to $SO_4^{2-}$. Following the formulation used for large scale clouds, $P_{oxid}$, the fraction of the entrained $SO_2$ that is oxidized is given by

$$P_{oxid} = 1 - exp(-\tau_{conv} w_L / A) \tag{2.9}$$

where $\tau_{conv}$ = 30min, the typical lifetime of a mature stage of convective cloud (Rogers and Yau, 1989) and $w_L$ = 2g $m^{-3}$ is assumed for the liquid water content of a convective cloud (Giorgi and Chameides, 1986). Thus, $S_{SO2}P_{oxid}$ and $S_{SO2}(1-P_{oxid})$ represent the amount of $SO_2$ entrained in the column that is oxidized to $SO_4^{2-}$, and not oxidized,

respectively. Since $SO_2$ remains largely in the gas phase, the non-oxidized portion of $S_{SO2}$ is then returned back to the k vertical layer within the convective column as $SO_2$, according to a relative humidity dependent, parabolic vertical weighting factor *w(k)*, which is also used for water vapor detrainment for convective clouds in the RegCM2 (Anthes, 1977).

The total amount of $SO_4^{2-}$ in the convective column is the sum of the newly converted $SO_4^{2-}$ from $SO_2$ (i.e., $S_{SO2}P_{oxid}$) and the pre-existing $SO_4^{2-}$ entrained into the cloud (i.e., $S_{SO4}$). Since virtually all of this $SO_4^{2-}$ resides in the cloudwater, a fraction of it will be removed in precipitation and a fraction will be returned to the atmosphere. This fraction is determined using the same approach used in the RegCM2 to partition between the water in the convective cloud that is removed from the cloud in precipitation and the fraction that is returned to the atmosphere. In the RegCM2, $P_{convg}$ is the fraction of water that is not removed in precipitation; it is dependent on the column averaged relative humidity ( $\overline{RH}$ ), and calculated as

$$P_{convg} = \begin{cases} 2(1-\overline{RH}), & when\ \ \overline{RH} \geq 0.5 \\ 1, & when\ \ \overline{RH} < 0.5 \end{cases} \tag{2.10}$$

Thus, the amount of $SO_4^{2-}$ in the column returned to the atmosphere is given by ($S_{SO2}P_{oxid}$ + $S_{SO4}$) $P_{convg}$; and the amount returned to the k level is obtained by multiplying this quantity by the same vertical factor *w(k)* as in the case of $SO_2$.

Therefore, the tendency for $SO_x$ at k vertical level due to the convective cloud processes can be expressed as

$$T_{conv,so2} = -En(k)_{SO2} + S_{SO2}\,(1-P_{oxid})\,w(k) \tag{2.11}$$

$$T_{conv,so4} = -\,En(k)_{SO4} + S_{SO4}\,P_{convg}\,w(k) + S_{SO2}\,P_{oxid}\,P_{convg}\,w(k) \tag{2.12}$$

where the 2nd term of the right hand side of Equation (2.11) represents the amount of non-oxidized $SO_2$ that is redistributed to the convective column, and the 2nd and 3rd terms of right hand side of Equation (2.12), represent the amount of the entrained $SO_4^{2-}$ that is redistributed, and the amount of $SO_2$ that is oxidized within the clouds and redistributed into the atmosphere convective column as $SO_4^{2-}$, respectively.

Below cloud scavenging of $SO_2$ follows the parameterization of Levine and Schwartz (1982), which is dependent on the precipitation rate and the mixing ratio of $SO_2$. The tendency for $SO_2$ is given as

$$T_{below\text{-}cloud,\ SO2} = -k_{scav}\ Precip^{0.68}\ \chi_{SO2} \tag{2.13}$$

where *Precip* is the below cloud precipitation rate (in mm $hr^{-1}$), and $k_{scav}$ is a pseudo 1st order scavenging coefficient of $6.5 \times 10^{-5}$ $s^{-1}$.

Sulfate aerosols are generally found in the accumulation mode (i.e., submicron to micron in diameter). Previous study suggests that at the typical large scale precipitation rate of 2 mm $hr^{-1}$, the lifetime of accumulation mode aerosols in the precipitation column is about 50 hours (Balkanski et al., 1993), which is much longer than the model time step (about 3 min). Thus, the below cloud scavenging of $SO_4^{2-}$ particles is not effective, and assumed to be zero.

Dry deposition for $SO_2$ and $SO_4^{2-}$ are parameterized using prescribed deposition velocities obtained from Clean Air Status and Trends Network (CASTNET), i.e. for $SO_2$, the dry deposition velocity over land varies by month, with the highest value of 0.42 cm $s^{-1}$ in July and lowest of 0.25 cm $s^{-1}$ in wintertime. Adopted from Langner and Rodhe (1991), the $SO_2$ dry deposition velocity is constant at 0.8cm $s^{-1}$ over water, while the $SO_4^{2-}$ dry deposition velocity is set to 0.2 cm $s^{-1}$ over both land and water.

*2.2.2.2 Carbonaceous aerosols*

Carbonaceous aerosols mainly arise from combustion processes, i.e. fossil fuel and biomass burning. Following the algorithm of Chameides et al. (2002), they are separated into two modes: a hydrophobic mode and a hydrophilic mode, and two chemical forms: organic carbon (OC) and black carbon (BC). OC and BC are assumed to be primary pollutants, directly emitted into the atmosphere, and when emitted they are assumed to be in hydrophobic form. These primary particles are then allowed to age into hydrophilic form at a rate characterized by a pseudo first-order rate coefficient of $k_{age}$ at $7.1 \times 10^{-6}$ $s^{-1}$ (equivalent to a lifetime of 1.6 days) (Cooke et al 1996).

Hydrophilic BC and OC are removed via wet deposition by large scale and convective clouds in the way same as sulfate, while hydrophobic BC and OC are not subject to wet removal. In convective clouds, both hydrophilic and hydrophobic BC and OC are vertically redistributed using the same vertical weighting factor described in the previous section.

The dry deposition velocity for hydrophilic BC and OC is assumed to be 0.2cm $s^{-1}$ and 0.025 cm $s^{-1}$ over water and land, respectively, while for hydrophobic BC and OC, it is assumed to 0.025 cm $s^{-1}$ everywhere (Ganzeveld et al, 1998).

Since no chemical conversion is involved for the carbonaceous aerosols, the prognostic equation (2.2) is simplified as

$$\frac{\partial \chi_i}{\partial t} = -\vec{V} \nabla \chi_i + F_{H,i} + F_{V,i} + S_i + T_{age,i} + T_{ls,i} + T_{conv,i} + T_{dry,i} \qquad (2.14)$$

where $i$ indicates BC and OC hydrophobic and hydrophilic components, $T_{age,i}$ is the aging process converting the hydrophobic mode of BC and CO to hydrophilic mode. The

tendencies in the right hand side of Equation (2.14) due to the aging and cloud process are given as

$$T_{age,phobic} = - T_{age,philic} = - k_{age}\, \chi_{phobic} \quad (2.15)$$

$$T_{ls,philic} = (1/dt)\, frc_{ls}\, [exp(-r_{rem} dt) - 1]\, \chi_{philic} \quad (2.16)$$

$$T_{conv,phobic} = -En(k)_{phobic} + S_{phobic}\, w(k) \quad (2.17)$$

$$T_{conv,philic} = - En(k)_{philic} + S_{philic}\, P_{convg}\, w(k) \quad (2.18)$$

where the subscript "phobic" indicates hydrophobic BC or OC, and "philic" hydrophilic BC or OC, all the parameters are assumed to be same as sulfate, if not specified.

*2.2.2.3 Emissions*

Table 2.1 lists the annual emissions assumed in our simulations for $SO_x$ (i.e., $SO_2$ + $SO_4^{2-}$), BC, and OC from area, large-point sources and biomass burning over the model-domain and Figure 2.2 and 2.3 illustrate the spatial distribution in these emissions. In the simulations, emissions from area sources and biomass burning are assumed to be entirely released into the bottom model layer (~ 40m), while emissions from large-point sources are assumed to be equally distributed in the second (~ 110m) and third (~ 300m) model layers above the surface.

The emissions over China for $SO_x$, including their spatial and seasonal pattern are obtained from 1995 emission inventory of Streets and Waldorf (2000). (Since our simulation period spans 1994 and 1995, this 1995 emission inventory was chosen instead of the 2000 TRACE-P emission inventory of Streets et al. (2003). In general, the model-simulated $SO_4^{2-}$ concentrations obtained using the 1995 inventory were more consistent with observed $SO_2$ and $SO_4^{2-}$ concentrations over China than that obtained using the 2000 inventory. A comparison of model-simulated and observed aerosol concentrations is

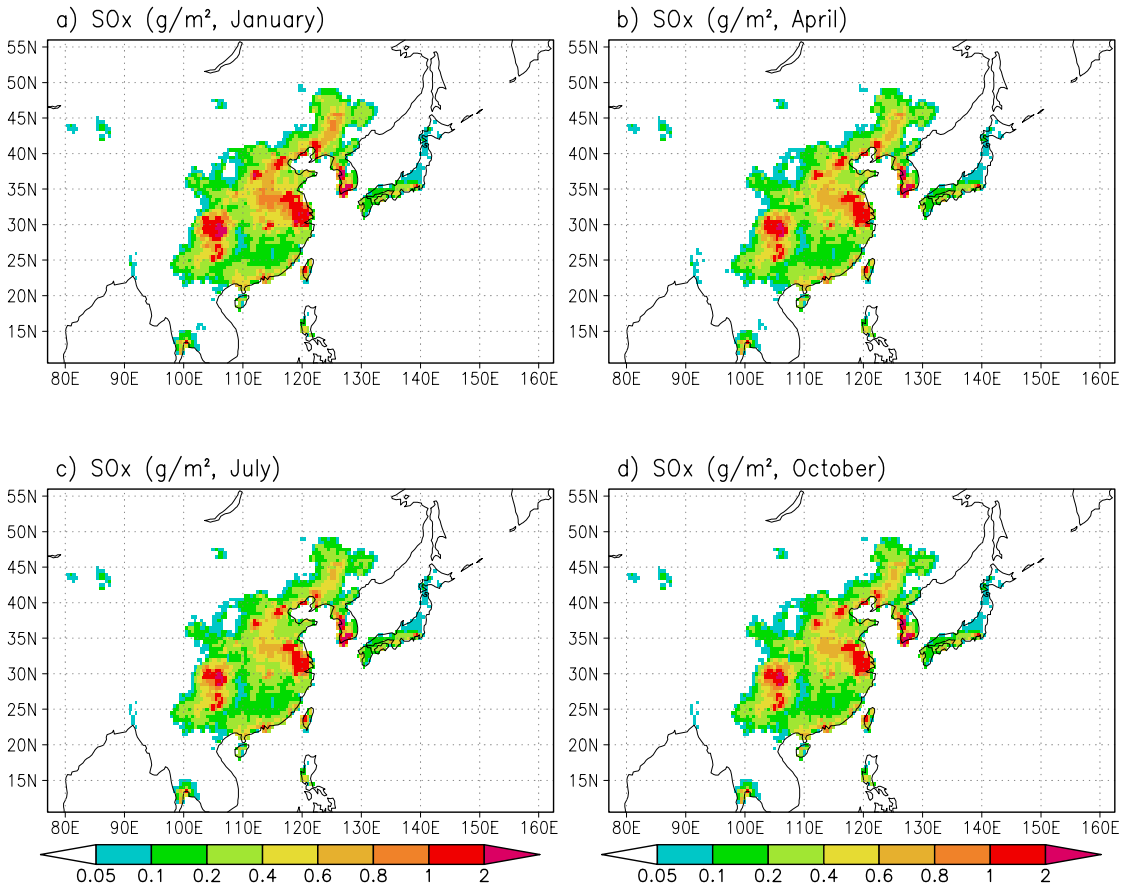


**Figure 2. 2** Monthly $SO_x$ emission (unit: g $SO_2/m^2$).

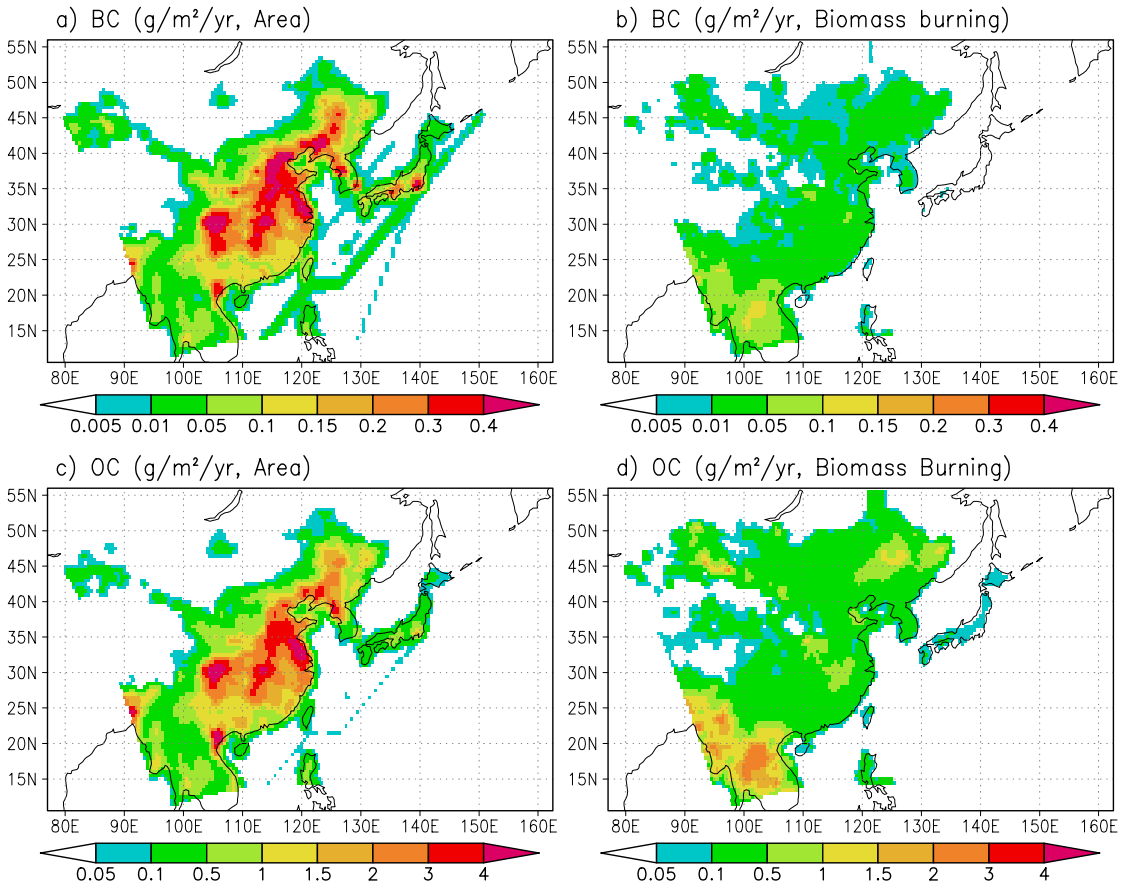


**Figure 2. 3** Annual BC and OC emission from Trace-P emission inventory (unit: g $C/m^2$). Note that OC is tripled (see context for detail).

presented in Section 2.3.1.) $SO_x$ emissions over the rest of East Asia are interpolated from the Global Emissions Inventory Activity (GEIA) inventory (Penner et al., 1994) as described by Luo et al. (2000). Figure 2.2 shows the monthly emission rates of $SO_x$ in January, April, July and October 1995. The most intense emissions arise from the Sichuan Basin and the eastern coastal area of China due to the relatively intense industrial activities in these regions. Over Northern China, the emission in winter is larger than that in summer, because of the domestic heating (mainly coal burning) that occurs in the area in the winter season. The monthly total emission over the entire domain is 1.354Tg S, 1.224Tg S, 1.150Tg S and 1.156 Tg S in January, April, July and October, respectively. Of the total $SO_x$ emissions, 98% was assumed to be $SO_2$ and 2% in the form of $SO_4^{2-}$.

**Table 2. 1** $SO_x$, BC and OC annual emission over the model domain (unit: Gg $SO_2$ or C)

| Species | Area source | Large point source | Biomass Burning | Total | References |
|---|---|---|---|---|---|
| $SO_x$ | 24683 | 5503 | 211.35[a] | 30397 | Streets & Waldorf (2000) |
| BC | 1201.50 | 7.45 | 264.80 | 1473.75 | Streets et al. (2003) |
| OC | 10417.50 | 16.77 | 5699.88 | 16134.15 | Streets et al. (2003)[b] |
| $SO_x$[c] | 18944 | 5771 | 211.35[a] | 24926 | Streets et al. (2003) |

Note: [a] Biomass burning for $SO_x$ is from Streets et al. (2003).

[b] OC emissions assumed to be three times that of Streets et al. (2003) (see Section 2.2.2.3 for detail)**.**

[c] $SO_x$ emission from Streets et al. (2003) (Trace-P emission inventory).

The emissions of OC and BC are based on the 2000 TRACE-P emission inventory of Streets et al. (2003). However, following Chameides et al. (2002) and Tan et al. (2004), the magnitude of the OC emissions over the model domain was assumed to be three times

that estimated by Streets et al. (2003) in order to produce simulated concentrations of OC that approach those that are typically observed in the region. Since the prime interest of this thesis is in assessing the effects of aerosols on climate over East Asia, and not explaining the presence of the aerosols themselves, it is appropriate to adjust the emissions to obtain a more realistic simulation of OC aerosol distribution. Moreover, by doing this instead of simply specifying the aerosol distribution, the ability to assess the strength of potential feedbacks between climate changes and aerosol concentrations is still retained.

Figure 2.3 illustrates the annual area source and biomass burning emissions for carbonaceous aerosols. In order to derive seasonally dependent emissions, Streets et al. (2003) allocated the annual emissions into monthly emissions, however, it results in a very large variation in the monthly emission rates (the ratio of the monthly maximum emission in January to the minimum emission in June is ~ 2), and produces unrealistic variations in our model-calculated BC and OC concentrations over China. Therefore, a weaker seasonal variation in OC and BC emissions is assumed with a ratio of 1.2 between maximum and minimum monthly emissions based on 1995 BC emission inventory from Streets et al. (2001).

*2.2.2.4 Boundary conditions for $SO_x$ and carbonaceous aerosols*

Considering the aerosol lateral boundary conditions, the so-called inflow/outflow boundary conditions are used by assuming a nominal background level at 10pptm for all aerosol species and their gas precursor. With these boundary conditions, all relevant species are not advected into the domain from the outside, but are freely advected out when they reach the domain boundaries and the flow is outward. These assumptions

neglect the contribution of anthropogenic and natural emissions from other regions, such as Europe, India and Southeast Asia. Due to the relatively short lifetime of sulfate and carbonaceous aerosols, and to the relative high emissions over East Asia, this external contribution should be small compared to the internal source (Roelofs et al., 2000). At the upper boundary, the concentrations of all chemical species are set to zero.

## 2.3 Model Simulation

In this section, I present the aerosol distributions obtained from two year-long simulations (June 01, 1994 ~ August 31, 1995) of the regional model with the aerosol modules described above, however without any feedbacks between the climate and aerosol allowed. (In the next chapter, where the climatic effects of aerosols are discussed, the effect of climate-aerosol feedbacks on the model-simulated aerosol distributions is presented). I first discuss the seasonal cycle and spatial distribution of the simulated sulfate and carbonaceous aerosols. Next, the model-simulated distributions are compared to the limited observations of aerosol surface concentrations and aerosol optical depths. Then, the relative contribution of the various chemical and physical processes to the atmospheric aerosol loadings is discussed. The comparisons between this work and the previous global and regional model simulations are also presented. Finally, the results from the experiment using the Trace-P 2000 emission inventory are discussed. As mentioned earlier in Section 2.2, the sulfate aerosol conversion rate depends on various quantities, such as oxidant OH and $H_2O_2$, and the wet removal process depends on the cloud processes, a detailed sensitivity analysis regarding these parameters can be found in Qian et al. (2001) and Tan et al. (2002). Suffice it to say, the sensitivities of the model to

uncertainties in these parameters are sufficiently small that our basic conclusions are not significantly affected by these uncertainties.

### 2.3.1 Simulated Seasonal Variations of $SO_x$ and Carbonaceous Aerosols

*2.3.1.1 Spatial distribution*

Figure 2.4, 2.5 and 2.6 illustrate the monthly averaged distribution in the model-calculated surface concentrations of $SO_2$, $SO_4^{2-}$ and BC, respectively, for January, April, July and October. (The distribution of OC is similar to BC, but approximately 10 times larger.) It can be seen from Figure 2.4, that $SO_2$ surface concentrations closely follow the emission distribution, exhibiting a large gradient between industrialized regions and more remote areas, with a maximum over South Korea, and two maxima over China (Sichuan Basin and central-eastern China). In terms of seasonal variation, $SO_2$ is highest in the winter and lowest in summer. This is largely attributed to the efficient chemical conversion (via gaseous and aqueous processes) and increased dry deposition in summer. (As discussed in Chapter 3, the simulated climate over East Asia is dominated by the Asia monsoon with a maximum in clouds and precipitation in the summer.) The distribution in $SO_4^{2-}$ surface concentrations are similar to that of $SO_2$, with maximum over Sichuan Basin and a secondary maximum over eastern China, and a seasonal cycle with a maximum in winter and a minimum in summer. As in the case of $SO_2$, the seasonal cycle of $SO_4^{2-}$ is dominated by the influence of the monsoonal circulation which leads to rapid removal by wet deposition and convective transport during the summer. However, because $SO_4^{2-}$ is largely a secondary pollutant, its distribution is somewhat more dispersed than that of $SO_2$. Following variations in prevailing winds over China (see Chapter 3), $SO_4^{2-}$ in summer maximizes over Sichuan Basin (~ $105^oE$), and extends

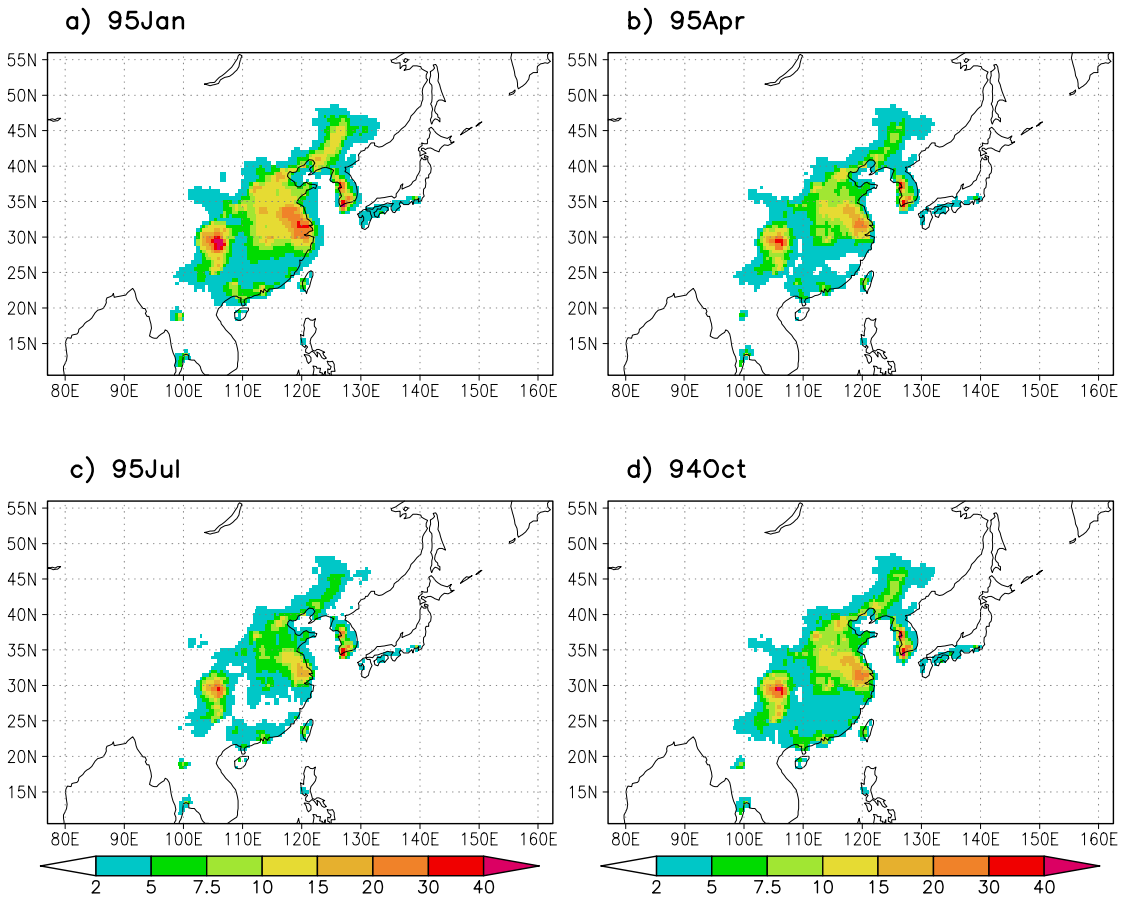


**Figure 2. 4** Monthly mean $SO_2$ surface concentrations for January, April, July and October. Unit: ppbv.

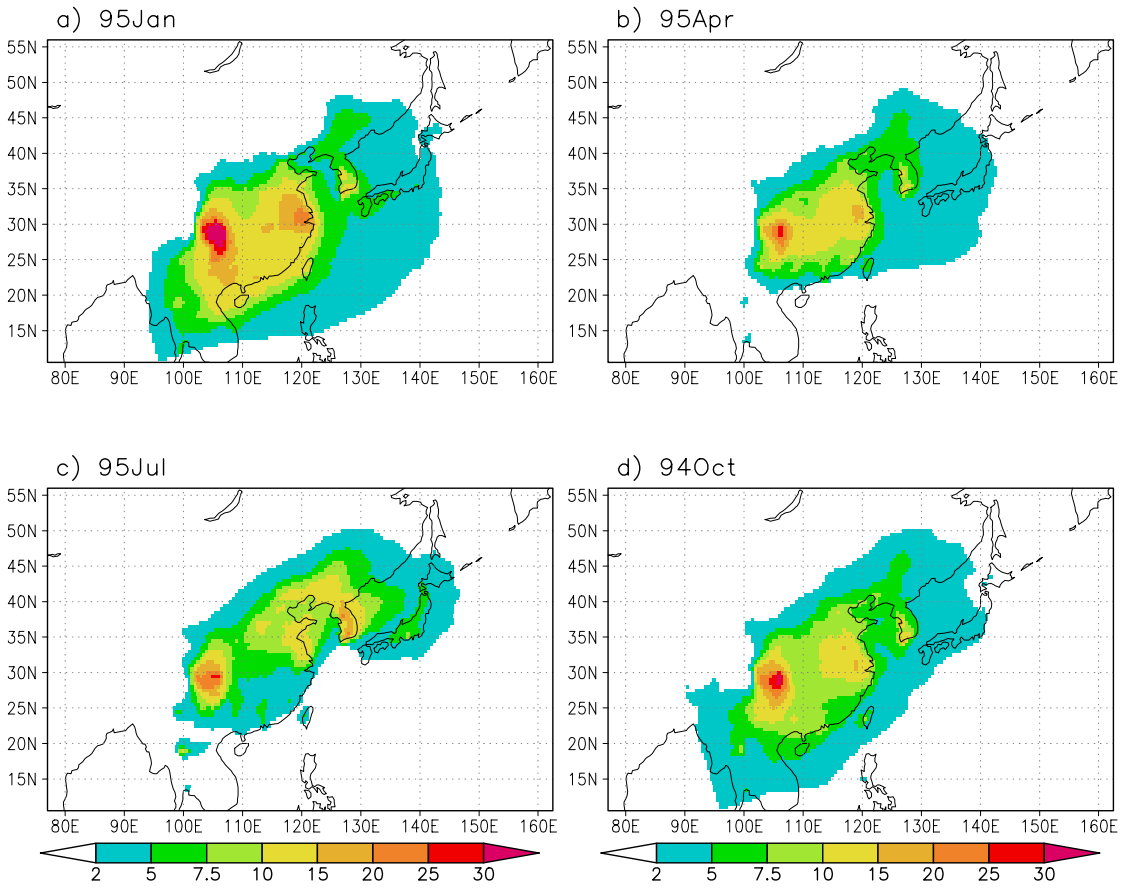


**Figure 2. 5** Similar to Figure 2.4, but for sulfate, unit: μg $SO_4^{2-}/m^3$.

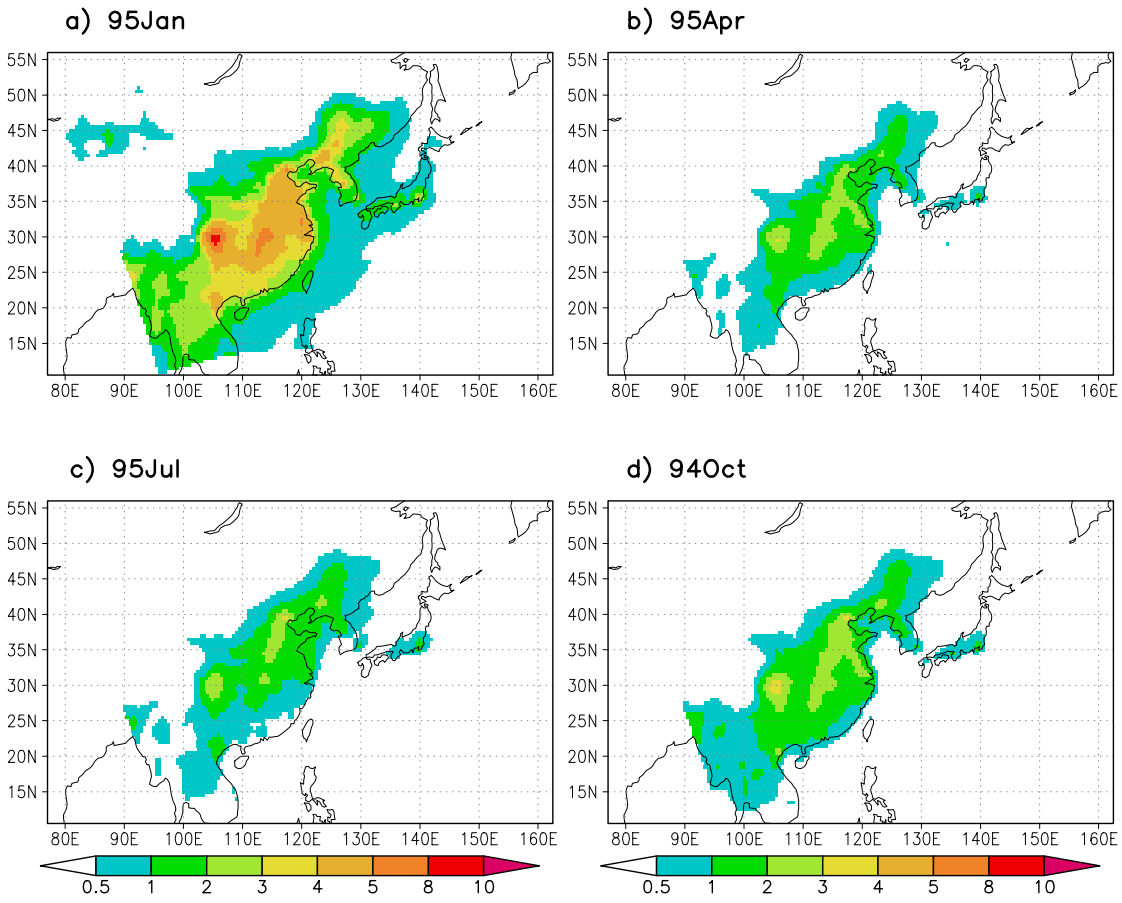


**Figure 2. 6** Similar to Figure 2.4, but for BC, including both hydrophobic and hydrophilic BC component, unit: μg C/m$^3$.

towards the northeast of China, reaching to 45°N latitude, while in other seasons, the maximum $SO_4^{2-}$ concentration area spreads from 105°E to the east coast of China, bounded around 35°N.

As for carbonaceous aerosols (Figure 2.6, including both hydrophobic and hydrophilic components), the spatial gradients tend to be smoother than that of sulfur species, with high values extending eastward from ~ 105°E to the entire eastern coast of China. Since hydrophobic component is closely related to the emission, while hydrophilic one is subject to wet removal, the spatial distribution and seasonal variation of carbonaceous aerosols are shaped by both emission and wet removal, with highest concentration in wintertime, and lowest in other seasons. Unlike $SO_4^{2-}$ with a marked maximum in the Sichuan Basin, carbonaceous aerosols show two maxima of similar magnitude: one over Sichuan Basin and one over north eastern China. This difference reflects the high carbonaceous aerosol emissions over northern China.

Figure 2.7 presents the model simulated aerosol optical depth (AOD) derived from the aerosol concentrations including all aerosol species ($SO_4^{2-}$, BC and OC) (see Chapter 1 and Chapter 3 for the description of the aerosol radiative properties and how to calculate AOD). It can be seen that AOD is highest in January with a broad region of over 0.4 extending from Sichuan Basin to the east coast of China, and lowest in July with a region of over 0.2 extending from Sichuan Basin towards north eastern of China. The seasonal variation in the magnitude of AOD is largely due to the change in wet removal of aerosols, which in turn is caused by the aforementioned monsoonly-driven variations in precipitation over the region and to a lesser extent the higher emission rates in winter as a result of domestic heating. The seasonal variation in the AOD spatial distribution

reflects the variations in the wind patterns over china, with prevailing westerly winds in the winter and prevailing southerly and south-westerly winds in the summer (see Chapter 3).

In addition to AOD, aerosol single scattering albedo $\omega_0$ is another critial parameter to assess the climatic effects of aerosols, since it is related to the partition between scattering and absorption of solar radiation. Figure 2.8 illustrates the monthly averaged $\omega_0$ derived from the model-simulated aerosol composition at the surface. In comparison to the seasonal variation in aerosol concentrations and AOD, the model-calculated $\omega_0$ does not have a strong seasonal dependence, with values hovering between 0.88 ~ 0.92 over the entire period. The simulated $\omega_0$ values generally fall within the range typically observed at rural sites over the region (Xu et al., 2002; Bergin et al., 2004, etc).

*2.3.1.2 Vertical profiles*

Figure 2.9 and 2.10 show the model simulated seasonal vertical profiles of six gas/aerosol species ($SO_2$, $SO_4^{2-}$, hydrophobic and hydrophilic BC, and OC) averaged over the interior domain (land grids only) and four Chinese subregions (see Figure 2.1) in winter and summer, respectively. Generally, the concentrations of the primary gas precursor ($SO_2$) and aerosols (hydrophobic BC and OC) are larger at surface, and decrease more rapidly with altitude than the secondary aerosols ($SO_4^{2-}$ and hydrophilic BC and OC). In terms of seasonal variations, the concentrations of hydrophobic BC and OC are about 35% lower in summer than in winter at surface, due to more efficient convective transport in summer. $SO_2$ in summer is about 40% ~ 50% lower near surface and within/above the boundary layer than in winter, which is attributed to the efficient

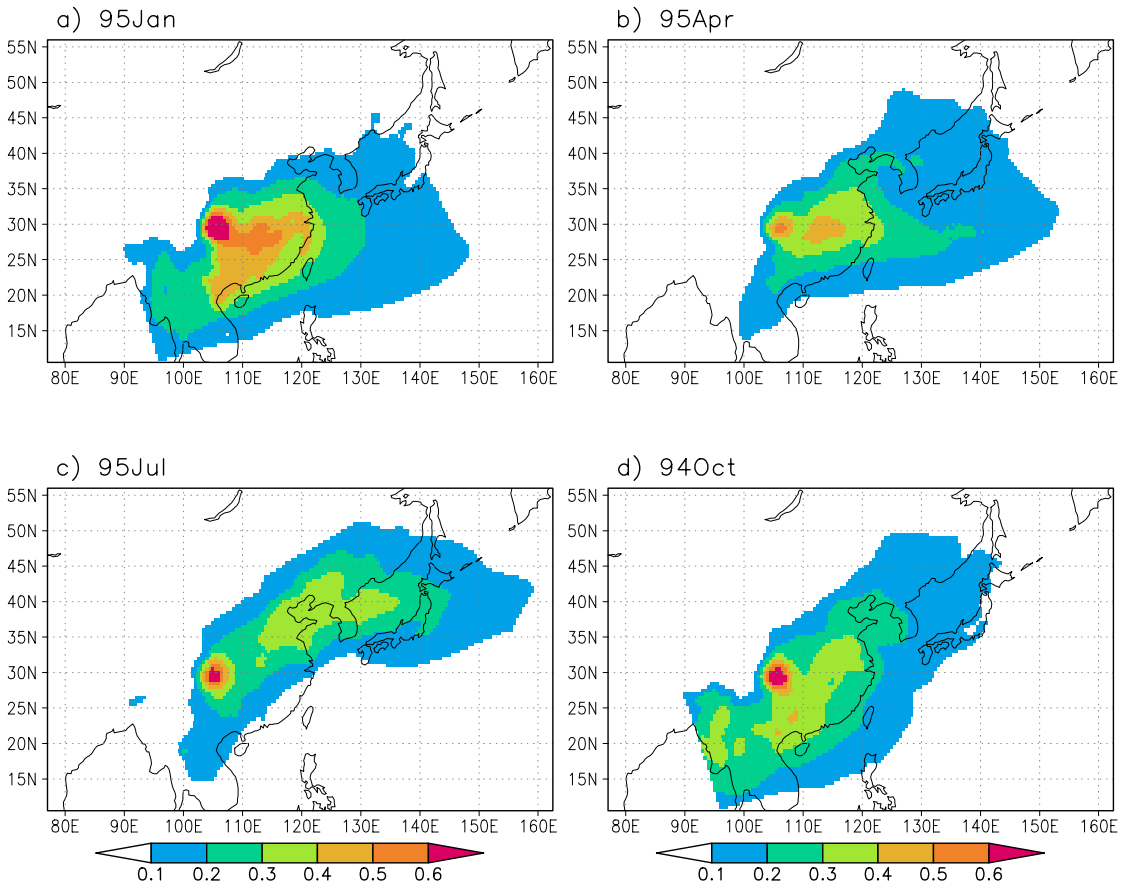


**Figure 2. 7** Similar to Figure 2.4, but for aerosol optical depth (AOD) derived from model-simulated aerosol column burden.

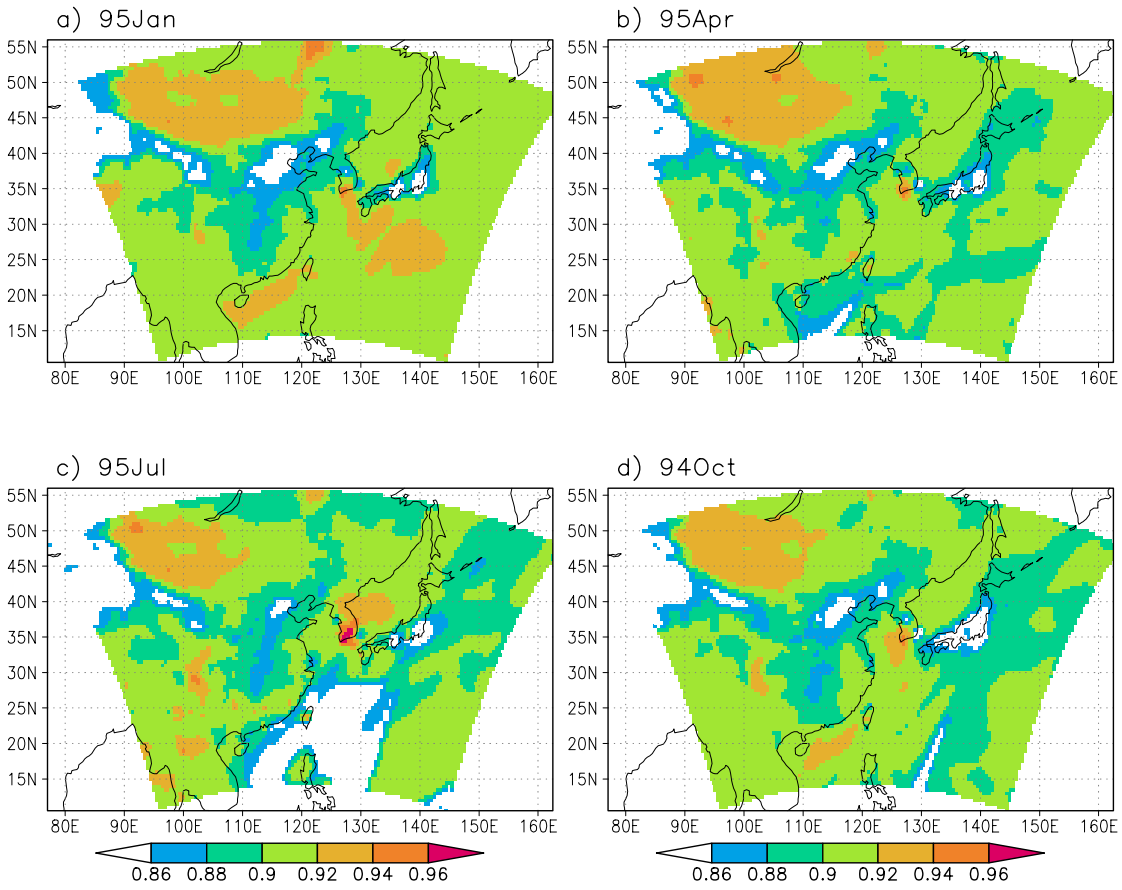


**Figure 2. 8** Similar to Figure 2.4, but for aerosol single scattering albedo ($\omega_0$) derived from model-simulated aerosol composition at the surface.

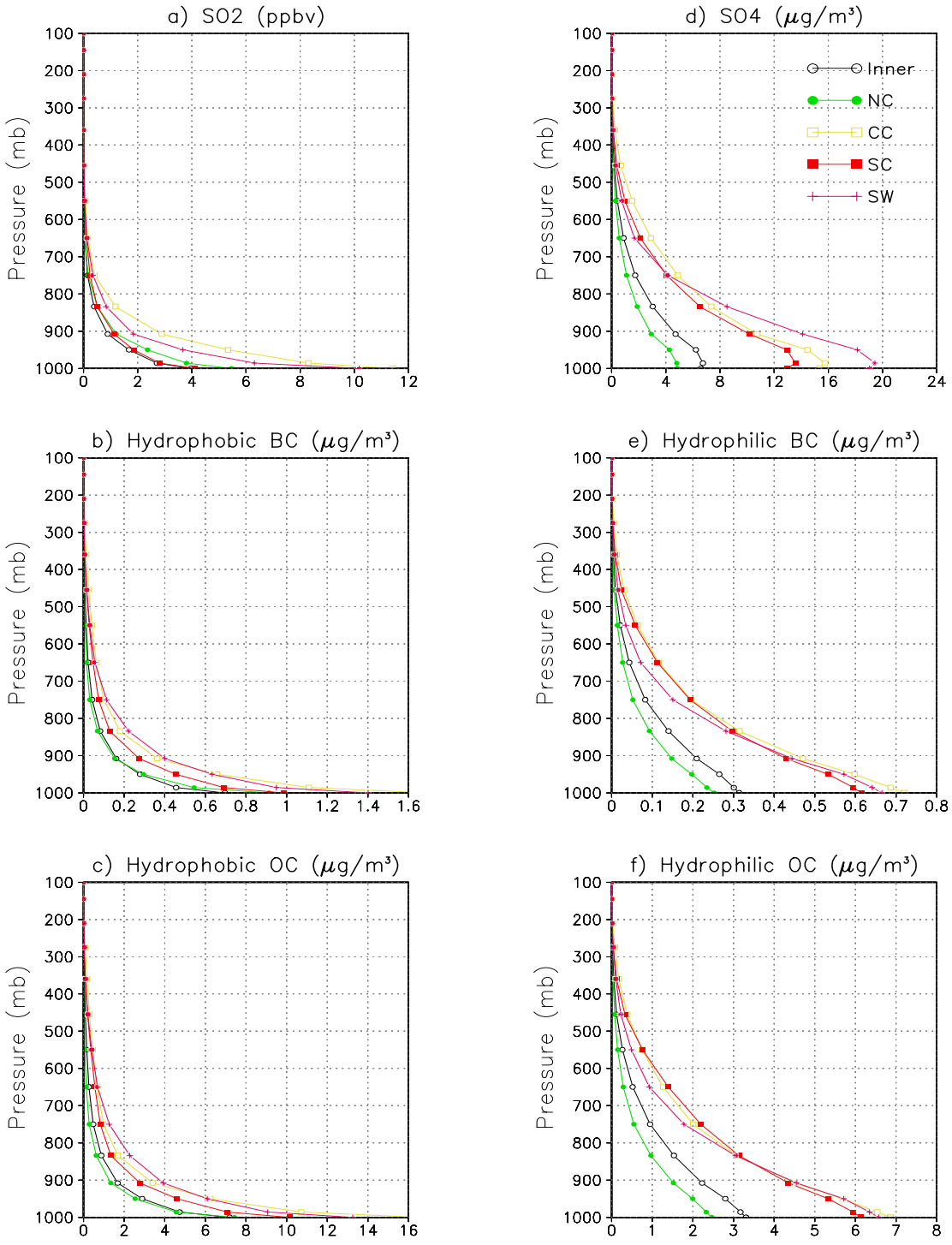


**Figure 2. 9** Vertical profiles of concentration: a) $SO_2$, b) hydrophobic BC, c) hydrophobic OC, d) $SO_4^{2-}$, e) hydrophilic BC and f) hydrophilic OC averaged over the interior model domain and four Chinese subregions (see Figure 2.1) in winter. Unit: $SO_2$ in ppbv, others in μg /$m^3$.

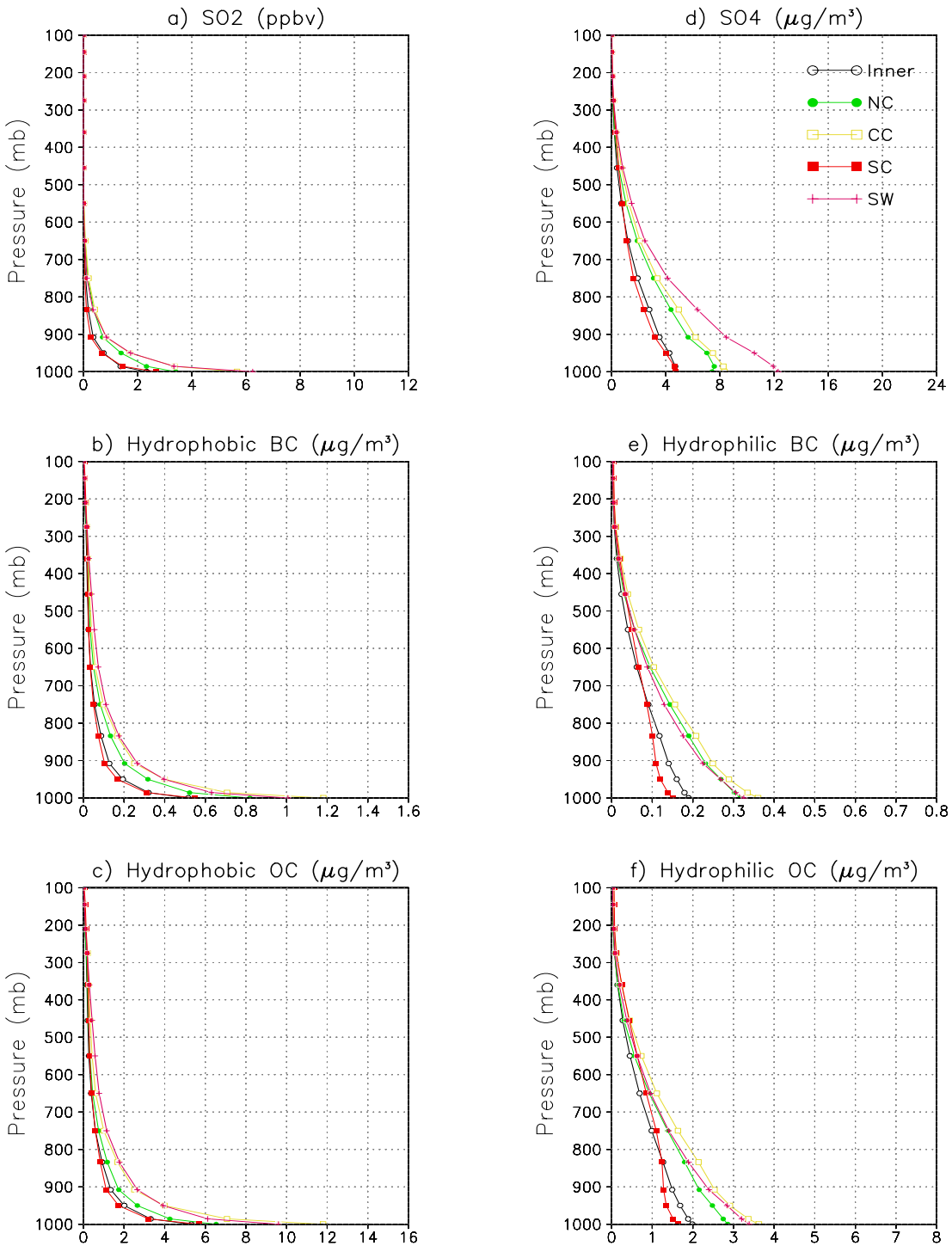


**Figure 2. 10** Similar to Figure 2.9, but for summer.

chemical conversion and dry deposition, in addition to the convective transport in summer. On sub-regional scales, we again see that Sichuan Basin and Central China have the highest concentrations both in winter and summer. Further inspection of Figure 2.9 and 2.10 show that the sub-regional average concentration of $SO_4^{2-}$, hydrophilic BC and OC near surface are about 1/3 ~ 2/3 lower in summer than in winter for all subregions, with an exception of North China, where the concentrations are about 50 ~ 60% larger in summer than that in winter. This could be due to the southerly and southwesterly winds in summer that bring more pollutants to this area from the polluted Sichuan Basin and Central China.

### 2.3.2 Comparison with Observations

#### *2.3.2.1 Surface concentration*

Very limited non-urban observations of sulfur compounds and carbonaceous aerosols over East Asia are available. Figure 2.11 compares the model-calculated and observed annual cycles of $SO_2$ surface concentrations at three non-urban Chinese sites (see Figure 2.1 for their locations): Lin'An (30.28N, 119.75E, rural/agricultural site, at Yangtze Delta region), Qingdao (36.13N, 120.53E, coastal/marine site, on the coast of the Shandong peninsula), and LongFengSan (44.75N, 127.60E, rural/forest site, at north-eastern China). The observed data at Lin'An were obtained hourly during August 1999 and July 2000 (Wang et al., 2002), and at Qingdao and Longfengsan spanning from August 1994 and July 1995 (Yan et al., 1997). The simulated values are calculated using distance-weighting from the concentrations obtained at 4 grids points around these sites. A comparison of these point measurements with the grid-box averaged model results is difficult due to the high horizontal variability of surface $SO_2$ and its dependence on local

meteorological conditions. With these caveats, it would appear that the model-simulations reasonably reproduce the observed seasonal variation with a winter peak and a summer low. Except for some relatively large departures in winter, the simulated concentrations fall within a factor of 2 of the observed values. At Lin'An, the simulations peak in January, while the observations peak in December with a local minimum in February. The underestimation at QingDao, particular in winter, suggests that this site might be unduly influenced by the local pollution (Of the three sites, this one is closest to an urban center). The overestimation at LongFengSan might be caused by overly rapid horizontal transport in the model from the more polluted cities lying to the south of LongFengSan.

**Table 2. 2** Model simulated surface aerosol concentration vs. observation (mean and standard deviation) at Lin'An in China (unit: $\mu g/m^3$), observations were obtained in November 1999 (Xu et al., 2002).

| | $SO_4^{2-}$ | BC | OC | TOTAL[a] |
|---|---|---|---|---|
| OBS | 21.2 | 3.4 | 31.4 | 90.0 |
| (STD) | (11.5) | (1.7) | (18) | (47) |
| MOD[b] | 18.69 | 1.99 | 20.94 | 57.01 |
| EMS00[c] | 12.59 | 1.99 | 6.98 | 29.08 |

Note:[a] For the model, TOTAL is calculated as the sum of $SO_4^{2-}$, BC, OC, ammonium and other organic elements. Ammonium is assumed to be present as $(NH_4)_2SO_4$ and other organic elements are assumed to be 40% of OC (Chameides et al., 2002). For the observation, TOTAL is the measured concentration of $PM_{2.5}$, $\sigma_{ep}$ and $\omega$ represents dry (RH<40%) conditions.

[b] MOD, the standard simulation using 1995 $SO_x$ emission inventory, 2000 Trace-P BC and OC emission inventory (see also Table 2.1, and Section 2.2.2.3 for detail).

[c] EMS00, the experiment using 2000 Trace-P emission inventory for $SO_x$, BC and OC (see also Table 2.1, and Section 2.3.4 for detail).

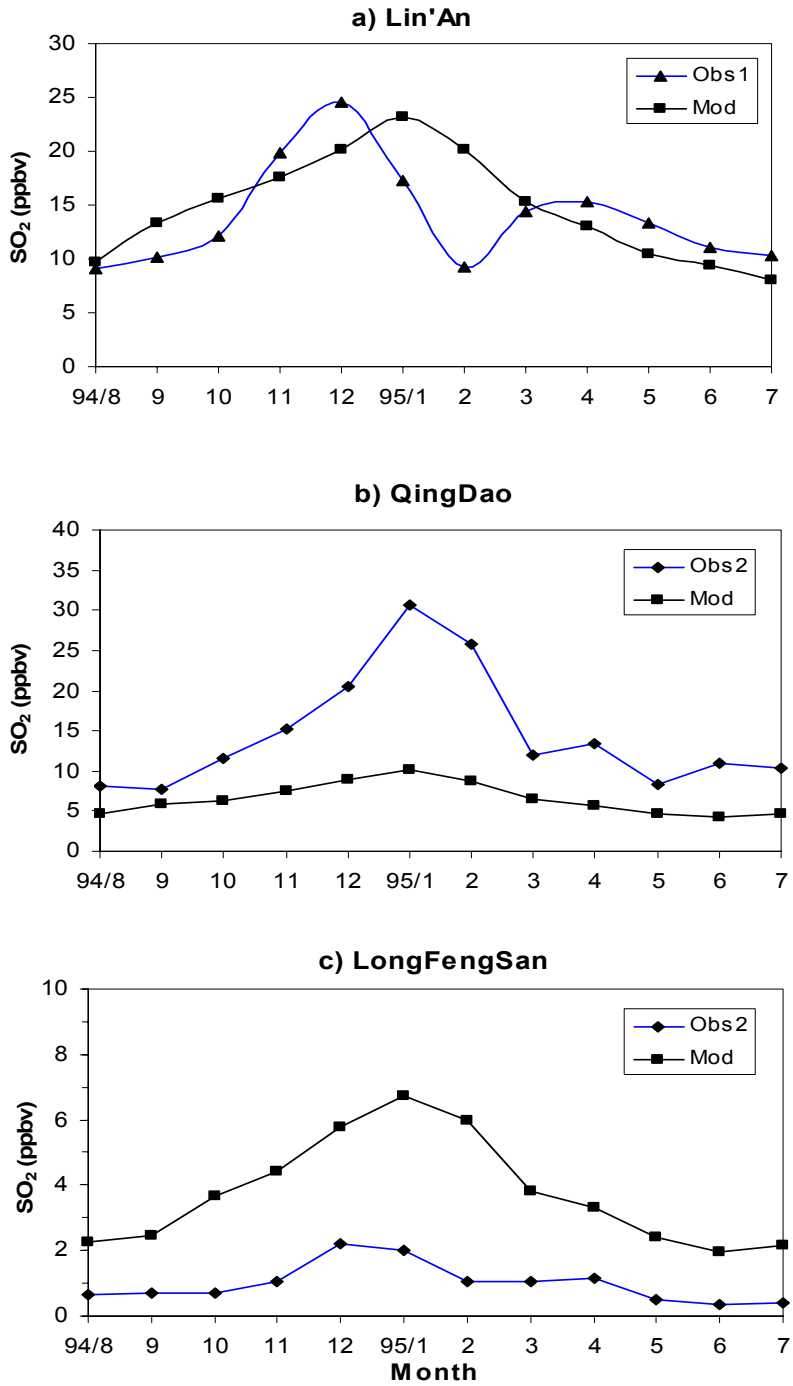


**Figure 2. 11** Seasonal variation of the simulated and observed monthly mean surface $SO_2$ concentration at three sites: a) Lin'An, b) Qingdao, and c) LongFengSan. Observation data were measured hourly during August 1999 and July 2000 at Lin'An indicated as 'obs1' (Wang et al. 2002), and during August 1994 to July 1995 at the other two sites indicated as 'obs2' (Yan et al, 1997). Model simulation was averaged based on 6 hourly model output.

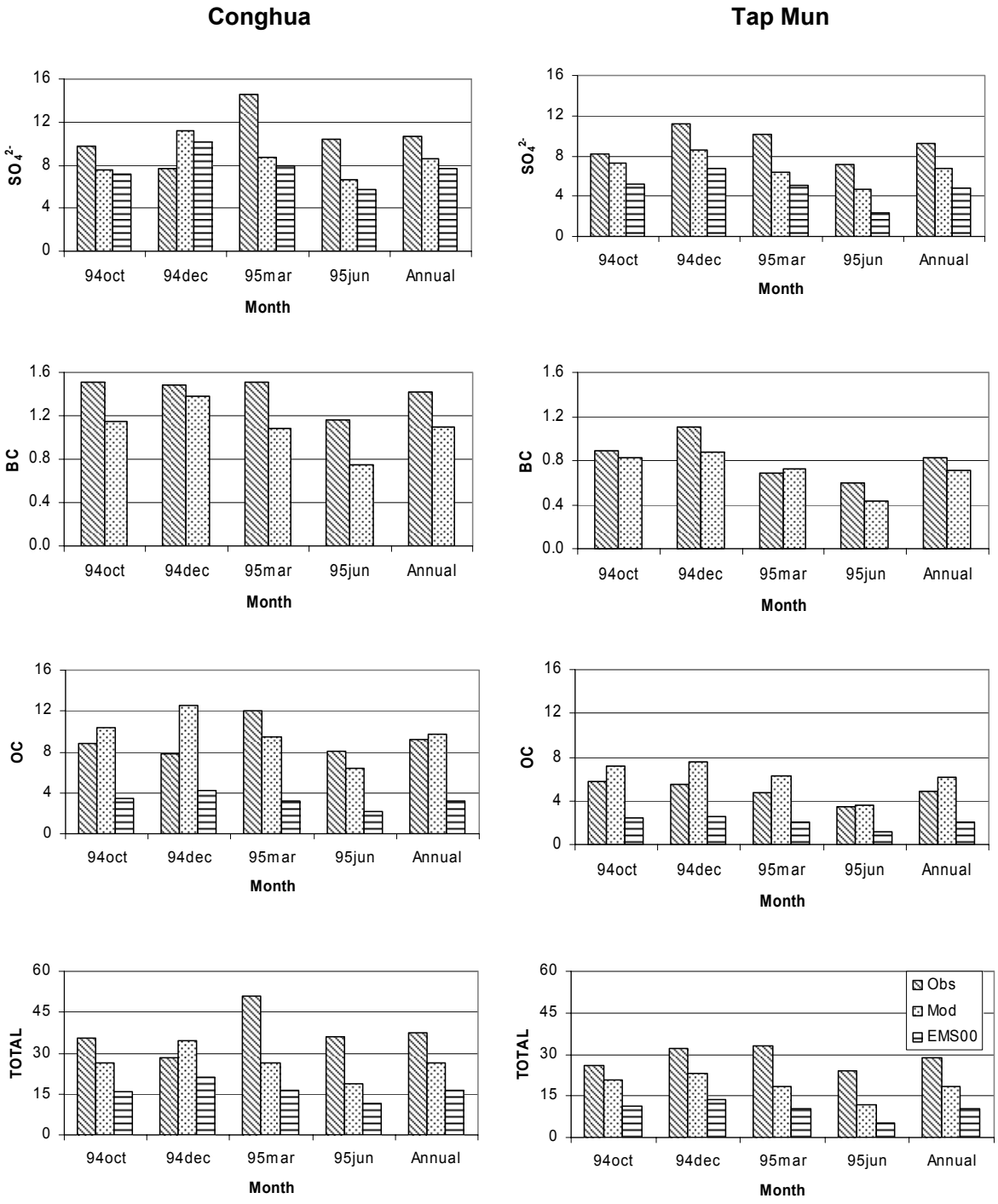


**Figure 2. 12** Comparison of the simulated and observed monthly mean aerosol surface concentrations at Conghua (left column) and Tap Mun (right column), unit: $\mu g/m^3$. Observations were measured over 24hr integrated time periods on every sixth day during the months of Oct02, Dec02, Mar03 and Jun03 (Bergin et al., 2004). See also Table 2.2 for the definition of 'TOTAL', MOD and EMS00.

In Table 2.2 and Figure 2.12, I compare the model simulated surface aerosol concentrations with observations at three non-urban sites over China (Lin'An, see above; Conghua, 23.55N, 113.57E, background station, at Pearl Delta region; Tap Mum, 22.47N, 114.35E, background station, at Hong Kong, also see Figure 2.1). It can be seen that the simulated aerosol concentrations are generally consistent with the observations for the three components simulated; e.g. concentrations are highest at Lin'An; and $SO_4^{2-}$ and OC are roughly equivalent in concentration. The largest discrepancies are for BC and OC at Lin'An where the simulated concentrations are a factor of ~ 1.5 less than the observations, despite our tripling of the OC emission in the Streets et al. (2003) inventory. At Conghua and Tap Mun, the model simulated aerosol concentrations agree well with the observations for all three components with less than 20% difference throughout the year. And the simulated seasonal variation is also consistent with the observed with a minimum in June and higher in other months. However, the simulation underestimates $SO_4^{2-}$ concentration by about 40% at both sites in March and June, which could be due to the excessive sulfate wet removal simulated in spring and early summer. In December, the observed $SO_4^{2-}$ and OC concentrations are lower than simulation by about 40% at Conghua (located about 40 miles north of Guangzhou, the most polluted city in Pearl Delta region), due to the relatively high precipitation and dominant surface northerly flows observed on the sampling days (Bergin et al., 2004).

Table 2.2 and Figure 2.12 also include a comparison between the 'TOTAL' aerosol concentration implied by our model simulations and the averaged concentration of $PM_{2.5}$ observed at the three sites. It has been found that $PM_{2.5}$ is generally responsible for ~ 90% or more of the aerosol scattering and absorption at rural sites in China (Bergin et al.,

2001; Xu et al., 2002). Thus a comparison between the 'TOTAL' aerosol concentration implied by our model simulations and observed $PM_{2.5}$ provides an indication of whether the simulated concentrations can be expected to reasonably reproduce the aerosols' radiative effects over the region. As shown, the total simulated aerosol concentrations are lower than the observed $PM_{2.5}$ concentrations by about 30% at the three sites. The shortfall in the model calculations, are due in part to our neglect of nitrate and other aerosol components, as well as a neglect of aerosol-climate feedbacks. As discussed in Chapter 3, when aerosol-climate feedbacks are included, the discrepancies between model-simulated and observed aerosol concentrations decrease somewhat. Nevertheless, the tendency of the model to underestimate the aerosol loadings over this region, suggests that the climatic effects of the aerosols produced by the model (see next chapter) are likely to be conservative estimates of their actual effects.

*2.3.2.2 Aerosol optical depth*

Another useful parameter for assessing the model's ability to simulate aerosol radiative effects is aerosol optical depth (AOD). Figure 2.13 presents a scatter-plot between model-simulated and observed spatially and annually averaged AOD's over four subregions of China (see Figure 2.1) where our model predicts the largest aerosol loadings. The observed AODs are taken from Zhou et al. (1999) and were derived from surface solar irradiance measurements made at meteorological stations from 1979-1990. Here again, reasonable agreement is obtained. The spatial pattern is well-reproduced with $R^2$ approaching 0.9. The slope of only 0.66 suggests, like the comparison between model-calculated 'TOTAL' and observed $PM_{2.5}$ that the model underestimates the total burden by 30% - 40% and thus that aerosol-climatic effects simulated in this work will be

conservative. The small negative intercept (-0.11) in the regression illustrated in Figure 2.13 likely arises from the inclusion of only anthropogenic aerosols emitted from within the model domain in our simulations, while the observed AOD relates to the anthropogenic aerosols as well as natural aerosols and anthropogenic aerosol emitted from outside the model domain. Finally, while not included in the regression illustrated in Figure 2.13, it should be noted that our model-simulated AOD's over the western half China are significantly smaller than Zhou et al.'s (1999) observed AOD's. Chameides et al. (1999a) have argued that the AOD's for this portion of China may have been unduly influenced by local sources of pollution and thus not representative of the region.

The AERONET aerosol climatology data (http://aeronet.gsfc.nasa.gov, Aerosol Robotic Network) can be also used to assess the simulated aerosol results. Figure 2.14 shows the comparison at 2 AERONET sites that are located in our model domain, have available data for an entire annual cycle, and are non-urban: Anmyon (36.52N, 126.32E, at west coast of the Korean peninsula) and Shirahama (33.69N, 135.36E, at east coast of Japan). It can be seen that at Anmyon, the model simulated AODs are reasonably close to the observation for the entire year (within about 20%). At Shirahama, the agreement is also quite good except for the month of June when the model underestimates the AOD by a factor of ~ 6. This discrepancy may simply reflect an anomalous pollution episode that significantly impacted the data at the site in June.

### 2.3.3 The Relative Contribution of Budget Components

The sulfur and carbonaceous pollutants emitted into the atmosphere can be transported and removed by various processes, i.e. dry and wet deposition, and export from the model domain. In this section, I will discuss the relative contributions of these

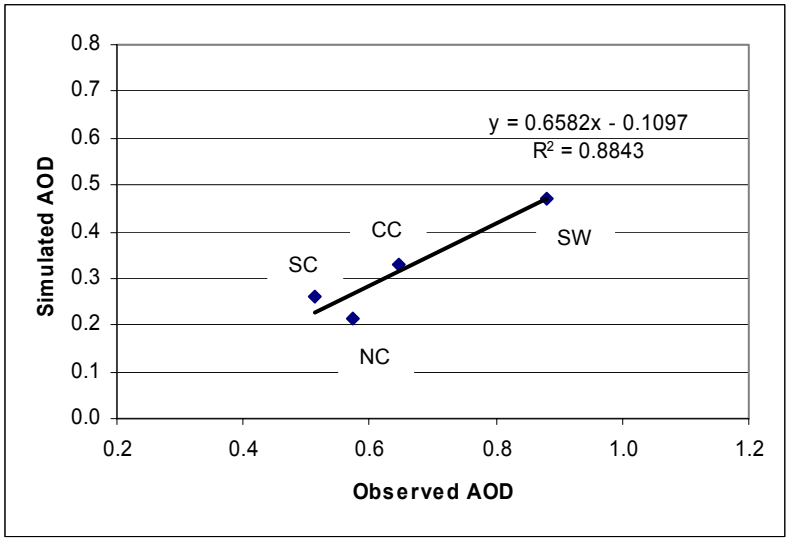


**Figure 2. 13** Annual mean aerosol optical depth at 550nm averaged over stations within 4 subregions in China (see Figure 2.1). Model simulated AOD is derived from the simulated column burden from 94Sep to 95Aug, and observed AOD from surface solar irradiance measurement during 1979-1990 (Zhou et al., 1999).

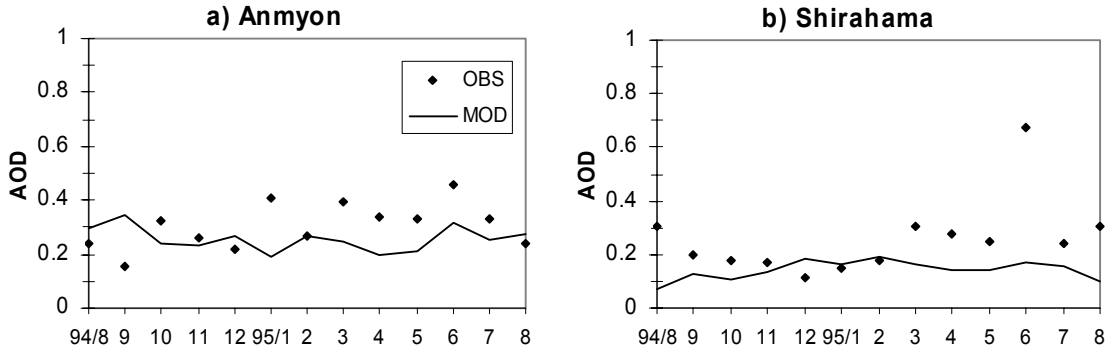


**Figure 2. 14** Simulated and observed seasonal variation of aerosol optical depth (AOD). Observations are shown in Diamond, from Aeronet aerosol climatology, and model simulation in line, at the grid points closest to the Aeronet sites (see Figure 2.1).

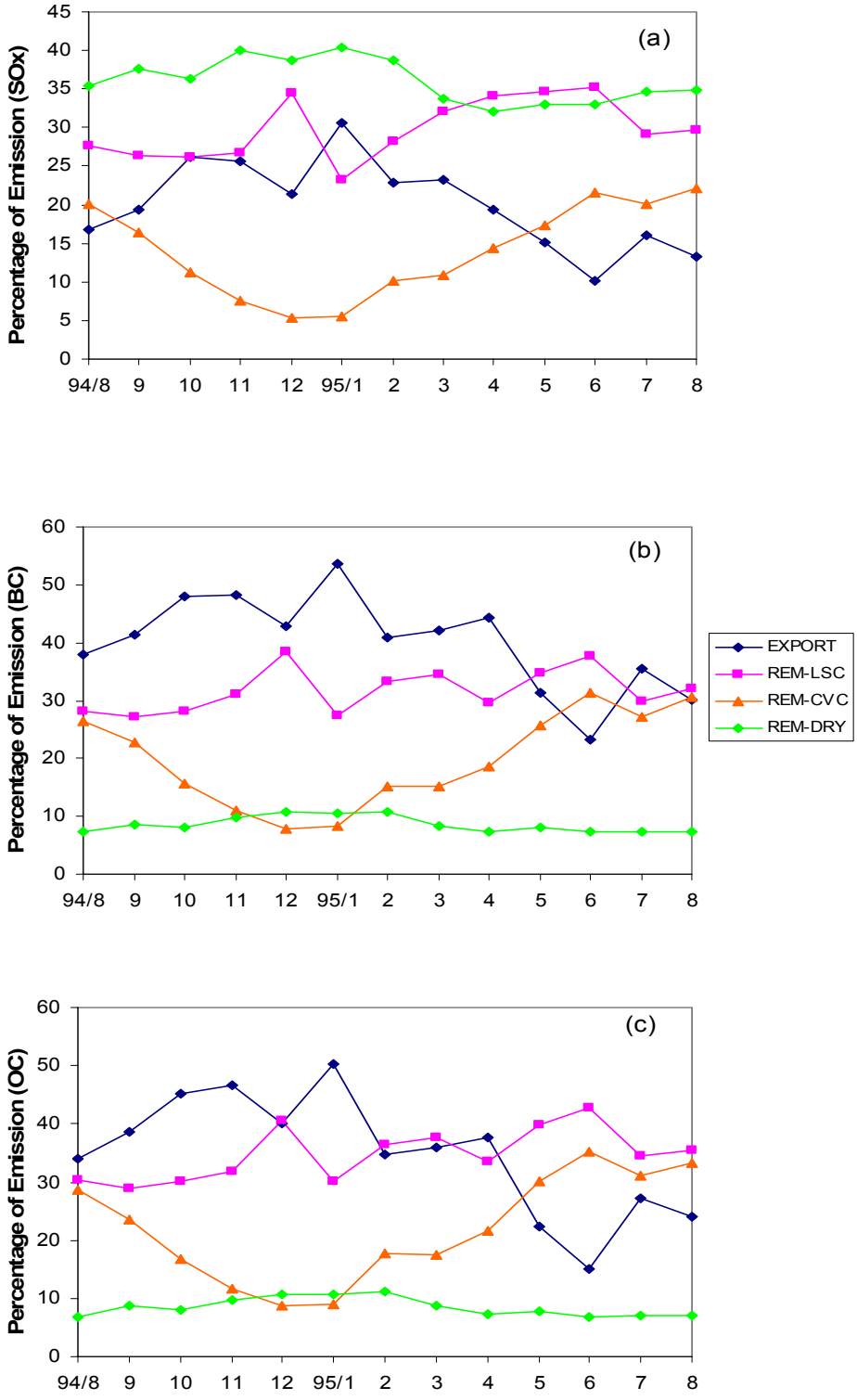


**Figure 2. 15** Percentage of total monthly emission due to export, dry deposition, wet removal by large scale and convective clouds averaged over the model interior domain.

different processes and their roles in regulating the simulated atmospheric aerosol loadings. Figure 2.15 illustrates the annual cycle of percentages of total monthly emissions due to export, dry deposition, wet deposition by large scale clouds and convective clouds averaged over the model inner domain (see Figure 2.1) for sulfur, BC and OC compounds. Table 2.3 and 2.4 present the annual mean column burden, lifetime and budget terms for all six species simulated in the model.

**Table 2. 3** Annual mean different components of $SO_2$ and $SO_4^{2-}$ budgets averaged over the interior model domain. Units are mg S/$m^2$ for column burden, mg S/($m^2$ day) for the budget terms, and day for lifetime. In parentheses are reported the percentage of the total sources or sinks accounted for each species.

| | $SO_2$ | $SO_4^{2-}$ |
|---|---|---|
| Emission | +2.54 (+100%) | +0.05 (+3%) |
| Dry deposition | -0.75 (-30%) | -0.23 (-13%) |
| Wet deposition | -0.16 (-7%) | -1.01 (-60%) |
| Export | -0.08 (-3%) | -0.48 (-27%) |
| Gas conversion | -0.36 (-14%) | +0.36 (+23%) |
| Hetero- conversion | -0.24 (-9%) | +0.24 (+15%) |
| Aqueous conversion | -0.93 (-37%) | +0.93 (+59%) |
| Column burden | 1.55 | 2.98 |
| Lifetime | 0.60 | 1.92 |

*2.3.3.1 Budget terms of $SO_x$, BC and OC*

For sulfur compounds (Figure 2.15a and Table 2.3), most removal occurs via dry deposition (of $SO_2$ primarily) and wet deposition (of $SO_4^{2-}$) in large scale clouds. Wet deposition in convective clouds is a relatively small sink, but it makes a non-negligible

contribution of ~ 20% during the summer months reflecting the influence of the monsoonal circulation. Export of sulfur compounds out of the model domain varies from about 10% to 30%, and is largest in the winter, when convective wet deposition is smallest, and smallest in the summer, when convective wet deposition is largest.

Inspection of Table 2.3 reveals that, on an annual basis, about 60% of the $SO_2$ emitted into the atmosphere is converted to $SO_4^{2-}$, a value close to the global average estimated by IPCC (1995). Of this 60%, 37% occurs via in-cloud aqueous-phase processes, 14% by gas-phase reactions, and 9% by the heterogeneous pathway included in the model. In total, the conversion of $SO_2$ represents almost 97% of the total source of $SO_4^{2-}$ to the model domain, with only about 3% coming from the direct emissions.

The simulated annual mean column burden for $SO_2$ and $SO_4^{2-}$ are 1.55 mg S $m^{-2}$ and 2.98 mg S $m^{-2}$, and the corresponding residence times for these species in the model domain are 0.6 and 1.9 days, respectively.

In the case of carbonaceous aerosols, wet removal by large-scale clouds dominates over that of convective clouds with a similar seasonal variation and magnitude as that of sulfur compounds. However, dry deposition tends to be a relatively small sink (~ 10%), reflecting the relatively small deposition velocities assumed for these species over land. As a result, export of BC and OC are larger components of the overall budget, ranging from 15 and 20% to 50 and 55% for OC and BC, respectively. Thus these results suggest that carbonaceous aerosol pollution from East Asia may be more likely to have long-range air quality and climatic impacts than that of the sulfur oxides.

Inspection of Table 2.4 reveals that between 80 and 90% of the hydrophobic BC and OC emitted into the model is converted to hydrophilic form before removal or export.

This agrees with the so-called '$S_{cf}$" global simulations of Koch (2001) in which hydrophobic BC and OC were not subject to wet removal as in my model. Of the exported BC and OC, Table 2.4 reveals that the ratio of hydrophilic-to-hydrophobic is about 3:1 and 4:1, respectively.

The model simulated annual mean column burden for hydrophobic and hydrophilic BC is 0.3 ~ 0.4 mg C $m^{-2}$, with 30% higher for the latter one. (The column burden for OC components is about 10 times higher than BC.) The corresponding residence times for these species are around 1.4 days and 2.3 days for the hydrophobic and hydrophilic components, respectively.

**Table 2. 4** Similar to Table 2.3, but for hydrophobic and hydrophilic BC and OC. Units are mg C/$m^2$ for column burden, mg C/($m^2$ day) for the budget terms, and day for lifetime.

| | $BC_{phobic}$ | $BC_{philic}$ | $OC_{phobic}$ | $OC_{philic}$ |
|---|---|---|---|---|
| Emission | +0.216 (+100%) | 0 | +2.12 (+100%) | 0 |
| Dry deposition | -0.008 (-4%) | -0.011 (-6%) | -0.08 (-4%) | -0.11 (-6%) |
| Wet deposition | 0 | -0.11 (-60%) | 0 | -1.21 (-63%) |
| Export | -0.026 (-12%) | -0.064 (-34%) | -0.18 (-8%) | -0.59 (-31%) |
| Aging conversion | -0.18 (-84%) | +0.18 (+100%) | -1.89 (-88%) | +1.89 (+100%) |
| Column burden | 0.301 | 0.418 | 3.07 | 4.44 |
| Lifetime | 1.40 | 2.26 | 1.45 | 2.36 |

*2.3.3.2 Comparisons with the previous work*

Also important for model evaluation is a comparison with previous model results. Especially useful in this regard is the project COSAM (Comparison of large scale Sulfate Aerosol Models) intended to increase the understanding of the global distribution of

sulfate aerosols (Barrie et al., 2001). Ten General Circulation Models (GCMs) that included a sulfur cycle module participated in this project; the resulting sulfur budgets for the SouthEast Asia (SEA) region defined by 15-45N and 105-140E, were presented by Roelofs et al. (2001). We also compare our results to the regional model study of Qian et al (2001), who used a similar sulfur module and focused on the same East Asia region. Qualitatively, the features of the sulfur cycle are modeled quite consistently, i.e., i) the relative importance of dry deposition as a major sink for $SO_2$, ii) the importance of wet over dry deposition for removal of $SO_4^{2-}$, iii) the importance of aqueous over gas conversion from $SO_2$ to $SO_4^{2-}$, iv) larger seasonal cycle for $SO_2$ than $SO_4^{2-}$. The major discrepancy lies in the seasonal cycle of $SO_4^{2-}$, where some of the aforementioned models found an opposite seasonality associated with the change of $SO_2$ oxidation efficiencies. This could be due to the lack of emission variation in their works, and the different treatment of chemical conversion and removal in the convective clouds. While my simulated $SO_2$ and $SO_4^{2-}$ column burden and lifetime agrees with the regional study of Qian et al. (2001), my $SO_2$ is relatively lower with a shorter lifetime than the COSAM average for the region. This latter discrepancy is possibly caused by the absence of natural sulfur sources, and the advection of sulfur from the other regions outside the model domain, and the additional heterogeneous conversion pathway assumed in this work.

Due to the lack of regional budget analysis for carbonaceous aerosols, the results of global model study by Koch (2001) (case $S_{cf}$) are used here for a qualitative comparison. As stated earlier, Koch (2001) found that about 76% of the hydrophobic BC is converted to hydrophilic BC, and that wet deposition removes about 72% of the hydrophilic BC.

These are very close to the model results in this work (80% conversion, 60% wet removal). The resultant lifetime for hydrophobic BC are similar (~ 1-2 days) in both work, while for hydrophilic BC, its lifetime simulated from this work is much shorter than that of Koch (2001) (2.3 days vs. 5.4 ~ 8.4days). A possible explanation is that aerosols tend to wet or dry removal more over the relatively polluted regions (like East Asia), and in turn short lived.

### 2.3.4 Experiment Using Trace-P Emission Inventory

In this section, I compare the simulated aerosol loadings using Trace-P 2000 emission inventory (Streets et al., 2003) for all $SO_x$, BC and OC (indicated as 'EMS00' experiment) with the above standard simulation. Table 2.1 shows that in the EMS00 run the total $SO_x$ emission over the entire domain decreases by about 18%; there is 25% decrease in area sources but a 5% increase in elevated large point source. OC emissions are decreased by a factor of 3, and thus set to the original values from the 2000 emission inventory. It can be seen from Table 2.2 and Figure 2.12 that the simulated surface OC concentration varies linearly with emissions, and thus the OC concentrations for EMS00 are 1/3 of the standard run. The simulated reduction of surface $SO_4^{2-}$ varies spatially, being -33% at Lin'An, -10% at Conghua, and from -20 ~ -50% for the months of December, March, October to June at Tap Mun. The variability in the $SO_4^{2-}$ reduction reflects that spatial variations in the difference between the two $SO_x$ emission inventories used here. The simulated 'TOTAL' aerosol concentrations at these sites decrease by 40 ~ 50%.

In terms of the spatial distribution, Figure 2.16 presents the ratios of 'TOTAL' aerosol concentration at surface and aerosol optical depth relative to the standard simulation discussed in previous sections. As mentioned earlier, EMS00 experiment

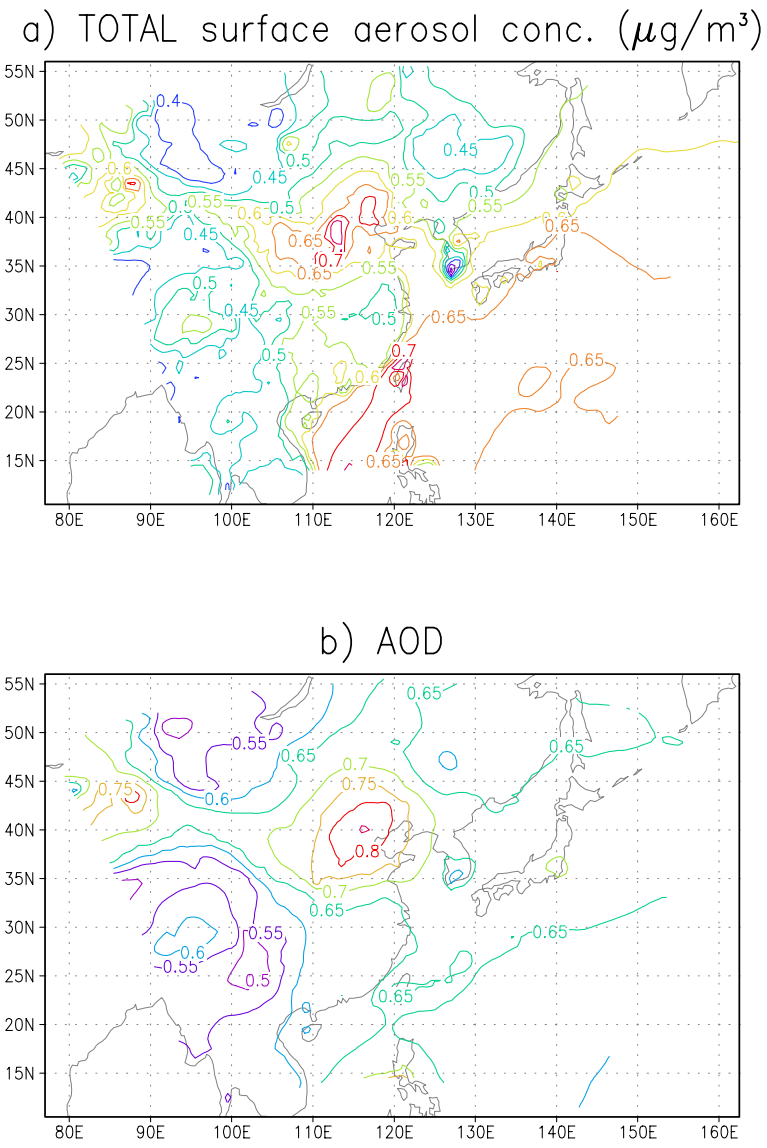


**Figure 2. 16** Ratio of simulated 'TOTAL' aerosol concentration at surface and aerosol optical depth using Trace-P 2000 emission inventory relative to the standard simulation.

produces 1/3 of the OC than the standard run uniformly over the domain, therefore, the pattern of the ratios in Figure 2.16 is indicative of the reduction of $SO_4^{2-}$, and in turn caused by the spatial variation assumed in the $SO_x$ emission rate for the two runs. It can be seen that using the Trace-P 2000 emission rate, the simulated 'TOTAL' surface aerosol concentration decreases by 40 ~ 50% over the continental China, with the least reduction of ~ 30% over the northeastern China. On the other hand, the reduction of AOD appears to be 10% less than that of 'TOTAL', which might be in part due to the increased elevated $SO_x$ point sources.

## 2.4 Conclusions and Discussion

In this chapter, the development and evaluation of the sulfur and carbonaceous aerosol modules coupled to the three-dimensional regional climate model over East Asia were discussed. The main conclusions can be summarized as follows:

1) The $SO_2$ spatial and seasonal distributions are closely tied to the emission rate, with sharp gradients between the highly polluted regions and more rural areas. Chemical conversion (especially aqueous conversion) and dry deposition are the two major sinks, removing 60% and 30% of the total $SO_2$ emission, respectively. $SO_2$ concentrations are highest in winter and lowest in summer due to the efficient gaseous and aqueous conversion and high dry deposition velocity in summer, and the high emission in winter as well.

2) The $SO_4^{2-}$ shows a smoother horizontal gradient and less seasonality than $SO_2$. Nevertheless there is a marked maximum over Sichuan Basin, and a broad region of high concentration extending to the eastern/northeastern coast of China. Wet deposition

removes 60% of the total $SO_4^{2-}$ sources, and export term transports 27% of $SO_4^{2-}$ out of the domain.

3) Spatially, carbonaceous aerosols (BC and OC) are smoother than that of sulfur species, with two maximum over Sichuan Basin and northeastern China. The concentration of BC and OC are higher in winter and lower in summer due to the efficient wet removal for hydrophilic component in summer and higher emission in winter. Aging process transforms more than 80% of the hydrophobic BC and OC to hydrophilic component, which is removed by wet deposition (~ 60%) and export (~ 30%).

4) The concentration of the primary gas precursor ($SO_2$) and aerosols (hydrophobic BC and OC) decreases rapidly with the altitude, while the secondary aerosols ($SO_4^{2-}$, hydrophilic BC and OC) exhibit a smaller vertical gradient, and can penetrate into the mid-high altitude, favorable to transport further away.

5) Comparison with the limited available observations shows that our simulated $SO_4^{2-}$, BC and OC aerosol concentrations are generally consistent with the observations in rural areas over East Asia. The simulated 'TOTAL' aerosol concentration and aerosol optical depth are about 2/3 of the observed values, suggesting that the estimated climatic effects by the model are expected to be conservative of their actual effects.

6) Using the Trace-P 2000 emission inventory, the 'TOTAL' aerosol concentration and aerosol optical depth decreases by 40-50% and 30-40% over the continental China, respectively, with a large reduction over the mid-low reaches of the Yangtze river, and the least reduction over the northeastern China.

Overall, the aerosol module developed and coupled with the regional climate model in this work is capable of representing the anthropogenic sulfur and carbonaceous aerosol

cycle over East Asia, and will be a useful tool to assess their climatic effect reasonably and conservatively. Further validations are necessary when more aerosol observations over this region (both vertical and horizontal) become available. It is also necessary to re-evaluate emission inventory, in particular, the organic carbon aerosol.

# CHAPTER 3

# REGIONAL SIMULATION OF ANTHROPOGENIC AEROSOL EFFECTS ON CLIMATE OVER EAST ASIA

## 3.1 Introduction

The direct and indirect aerosol effects on climate have been extensively investigated, and a number of studies have shown that anthropogenic aerosols can have significant climatic impacts, especially at the regional scale (Charlson et al., 1990 and 1992; Kiehl and Briegleb, 1993; Kiehl et al., 2000; Penner et al., 2001; Ramanathan et al., 2001a, etc). As discussed in Chapter 1, the direct effect from aerosol scattering can cool the earth system, while aerosol absorption can heat atmosphere, flatten the temperature gradient, lower the atmospheric humidity, leading to the cloud-burning, which is the so called 'semi-direct' effect (Hansen et al., 1997). The aerosol indirect effect, in which particulate aerosols act as cloud condensation nuclei, modify the microphysics, radiative properties and lifetime of clouds, includes two components: the 1$^{st}$ indirect effect, in which the cloud albedo increases with the increase in aerosols (Twomey, 1974); and the 2$^{nd}$ indirect effect, where the aerosol increase tends to decrease the precipitation efficiency, and increase the liquid water content, thereby increase cloud lifetime (Albrecht, 1989) and cloud thickness (Pincus and Baker, 1994).

Both direct and indirect effects are believed to reduce the solar radiation reaching the surface, and thus cool the Earth system. In addition, the direct, semi-direct and indirect effects can also affect the precipitation, via the alteration in cloud properties (i.e., semi-direct and indirect effects), atmospheric stability (i.e. direct and semi-direct effects,

which cool the surface and heat the atmosphere), and surface energy balance (i.e. all four effects), possibly leading to modifications in precipitation pattern induced by convective and monsoonal circulations and spin down of the hydrological cycle (Boucher et al., 1998; Ramanathan et al., 2001b; Graf, 2004; Liepert et al., 2004).

There have been numerous studies by previous investigators on the climatic effects of anthropogenic aerosols since l990s. For the most part, these studies have focused on the establishing the existence of the direct and indirect effects and estimating their impact on radiative forcing, surface temperature and cloud radiative properties. However, relatively few studies assessed the impact of aerosols on precipitation using different modeling system, such as global climate model, regional climate model or fluid dynamic model (i.e., Menon et al., 2000b; Giorgi et al., 2002 and 2003; Ackerman et al., 2004; Takemura et al., 2005, see Chapter 1, section 1.4.2 for detailed discussions).

In this chapter, a more comprehensive assessment of the effect of anthropogenic aerosols on precipitation over East Asia is carried out using the coupled climate-chemistry-aerosol regional model. Significant advances in this study relative to previous studies, include: the inclusion of all three major components of anthropogenic aerosols (i.e., sulfate, black carbon and organic carbon); the simulation of the distributions of these fields in a fully interactive manner with the meteorological fields thereby allowing for feedbacks between chemical and climatic processes; the simulation of the direct, semi-direct, and $1^{st}$ and $2^{nd}$ indirect effects, individually and in concert, allowing us to assess the relative impacts of the various effects on precipitation; and comparison of the model-predicted precipitation trends over East Asia with an analysis of the long-term precipitation record for the region.

## 3.2 Implementation of Direct and Indirect Aerosol Effects

As discussed in Chapter 1, the radiative effects of aerosols are described by three optical parameters: 1) the specific extinction coefficient $\alpha_e$; 2) the single scattering albedo $\omega_0$, and 3) the asymmetry parameter $g$. The aerosol radiative/cloud effects are calculated using these aerosol radiative properties, along with the on-line model-calculated concentrations for $SO_4^{2-}$, BC, and OC and the pre-existing RegCM2 radiation scheme. The sulfate radiative properties follow that of Kiehl and Briegleb (1993): the size distribution of sulfate is assumed to be log-normal with a dry geometric mean radius of 0.05μm and a standard deviation of 2.0 and a hydroscopic growth function ($f_s$), taken from Charlson et al. (1984); the single scattering albedo in the visible spectral region is equal to unity; and for visible wavelengths, the specific extinction coefficient for dry sulfate is $5.3 m^2\ g^{-1}$ and the asymmetry parameter is 0.70. And hydrophilic and hydrophobic OC are assumed to have the same radiative properties as $SO_4^{2-}$, except that hydrophobic OC does not uptake water following Chameides et al. (2002).

Following the discussion of Chameides et al. (2002), the aerosol optical depth (AOD) at wavelength ($\lambda$) arising from the model simulated anthropogenic aerosol distributions can be calculated as

$$\tau_a(\lambda) = \int_0^{TOA} \sigma_e(\lambda) dz = \int_0^{TOA} (\sigma_a(\lambda) + \sigma_s(\lambda)) dz \qquad (3.1)$$

where z is the altitude, TOA indicates the top of the atmosphere (also the model top level of 80mbar), and $\sigma_e$ is the aerosol extinction coefficient, which is, in turn, equal to the sum of the $\sigma_a$ and $\sigma_s$, the aerosol absorption and scattering coefficients, respectively. The extinction, scattering and absorption coefficients all have units of $m^{-1}$.

The scattering coefficient at each altitude is calculated as the sum of $\sigma_s^{SO4}$, $\sigma_s^{OC}$ and $\sigma_s^{BC}$, which are the scattering coefficients for $SO_4^{2-}$, OC and BC, respectively. Each of the individual scattering coefficients is given by $\sigma_s^i=[I]\alpha_s^i f_s$, where $[I]$ is the mass concentration of the $i^{th}$ species, i.e., $SO_4^{2-}$, hydrophobic and hydrophilic BC and OC, and $\alpha_s^i$ is the $i^{th}$ species' specific scattering coefficient. Aerosol absorption is assumed to arise only from BC aerosols, and their radiative properties will be discussed in detail in the next section.

### 3.2.1 Absorption and Semi-direct Effect by Black Carbon

Absorption and the semi-direct effect arise from absorption by BC. In this section I describe the radiative parameterizations used in this study to characterize BC absorption.

Both hydrophobic and hydrophilic BC aerosols are modeled assuming a log-normal size distribution with a geometric mean radius of 0.0118μm and a standard deviation of 2.0 (WCP, 1986). Following the discussion of Jacobson (2000), three mixing treatments for BC, each with different optical properties, are available in 3-D models: an external-mixture in which BC exists as chemically distinct particles, an internal mixture in which BC co-exists with other particulate components, and a core-coated mixture in which BC exists as a core surrounded by a coating of the other components. In this work, hydrophobic BC is assumed to be externally mixed, while hydrophilic BC is treated as a core-coated mixture.

The wavelength-dependent radiative properties for the externally-mixed hydrophobic BC are taken from WCP (1983). The specific extinction coefficient is about $13 m^2 g^{-1}$ at 0.55μm (scattering coefficient of $3 m^2 g^{-1}$ and absorption coefficient of $10 m^2 g^{-1}$). The single scattering albedo ($\omega_0$) ranges from about 0.3 at 0.3μm to almost zero at

wavelengths greater than 2.0μm. The asymmetry factor (0.22 at 0.55μm) is lower for BC than sulfate throughout the solar spectrum since the smaller BC particles should preferentially scatter more solar radiation in the backward hemisphere (Seinfeld and Pandis, 1997).

The radiative properties assumed for the core-coated hydrophilic BC is based on Jacobson (2000). Absorption by these particles is assumed to be equal to that of externally-mixed BC multiplied by an absorption amplification factor ($A$) from Figure 2b of Jacobson (2000) and an absorption humidification factor ($f_a$) from Redemann (2001). $A$ is approximately 1.5 at visible wavelengths and 1.2 in the near infrared. The parameter $f_a$ is used to account for enhanced absorption by BC in the core of particle that has expanded due to water-uptake by a sulfate aerosol shell; $f_a$ increases from 1 to 1.15 when relative humidity increases from 30% to 80%.

Based on the above discussion, the wavelength-dependent radiative properties for core-coated hydrophilic BC can be shown as

$$\left.\begin{aligned} \omega_{0(philic)} &= \frac{\sigma_s}{\sigma_s + \sigma_a} = \frac{f_s \alpha_s^{phobic} [BC]_{philic}}{(f_s \alpha_s^{phobic} + A f_a \alpha_a^{phobic})[BC]_{philic}} \\ \alpha_{e(philic)} &= f_s \alpha_s^{phobic} + A f_a \alpha_a^{phobic} \end{aligned}\right\} \quad (3.2)$$

where $f_s$ is the scattering coefficient factor for hydrophilic BC due to hygroscopic growth (which is assumed to be the same as sulfate), $\alpha_s^{phobic}$ and $\alpha_a^{phobic}$ are specific scattering and absorption coefficient for hydrophobic BC, $\omega_{0\,(philic)}$ and $\alpha_{e(philic)}$ are single scattering albedo and extinction coefficient of hydrophilic BC. The asymmetry factor ($g$) is assumed to be same for both BC categories. Therefore, the absorption coefficient ($\sigma_a$) used to calculate AOD can be formulated as $\sigma_a = ([BC]_{phobic} + A f_a [BC]_{philic})\ \alpha_a^{phobic}$.

### 3.2.2 First Indirect Effect

As mentioned in Section 3.1, the first indirect effect modifies the distribution and concentration of CCN, and hence the number concentration, size distribution and radiative properties of cloud droplets. In the CCM3 radiation package, cloud radiation is calculated in terms of two quantities: the cloud liquid water content $w_L$ and the cloud effective radius $r_e$ . The cloud liquid water content is calculated by the model's explicit and cumulus cloud parameterizations. In the absence of anthropogenic aerosols, $r_e$ is assigned the value of 10 μm, typical of clouds affected by a background CCN population (Briegleb, 1992).

The parameterization for aerosol 1st indirect effect is typically based on the assumption that aerosols affect $r_e$, at a fixed $w_L$ (Twomey, 1974). The connection between $r_e$ and the prognostic variables related to the aerosol mixing ratio ($\chi$) and its chemical properties is in turn typically developed in two steps. First, a relationship is used to relate the aerosol mass concentration (i.e., $\chi$ times air density) to the number concentration of cloud droplets ($N_c$). As discussed in Chapter 1, two methods have been used in previous studies for this first step: 1) an empirical method, or 2) a prognostic method. The second step involves the establishment of a relationship between $N_c$ and $r_e$ (i.e., Martin et al., 1994) .

Following Qian and Giorgi (1999), the 1st indirect effect is represented here using the empirical relationship between $N_c$ and $\chi$ derived by Hegg (1994), then relating $N_c$ to $r_e$ using the formulation of Martin et al. (1994). It is assumed that the 1st indirect effect is caused by the presence of $SO_4^{2-}$ and hydrophilic BC and OC, and that all three components affect $N_c$ in the same way:

$$N_c = 10^6 \, (90.7 \, (10^9 \rho_a \, \chi_{tot})^{0.45} + 23) \tag{3.3}$$

$$r_e = \left(\frac{3 w_L}{4 \pi \rho_w \kappa N c}\right)^{1/3} \tag{3.4}$$

where $\rho_a$ and $\rho_w$ is the density of dry air and water, respectively, $\chi_{tot}$ is the total mass mixing ratio of sulfate and hydrophilic BC and OC, $w_L$ is the cloud water content, all in SI units, and, $\kappa$, the cube of the ratio of the mean volume radius ($r_v$) and the effective radius ($r_e$) of the cloud-droplet spectrum, is assumed to be 0.67 over continent and 0.80 over ocean (Martin et al., 1994).

### 3.2.3 Second Indirect Effect

The 2nd indirect effect, related to the increase in cloud amount and lifetime from the increase in CCN from aerosols, is implemented in the model by altering the cloud-microphysics parameterizations so that the rate of precipitation is affected by the concentration of anthropogenic aerosols. Before describing these alterations, it is useful to review how precipitation from large-scale or resolvable clouds and from convective clouds is produced in the standard version of the RegCM2. (A more detailed description can be found in Giorgi et al. (1999).)

In the standard version of the RegCM2 (referred to here as the Standard Model), precipitation from resolvable clouds is represented using a simplified version of Hsie et al. (1984) scheme, which includes a prognostic equation for cloud water content and a Kessler-type autoconversion term for converting cloud water into rain water (Kessler (1969), hereafter referred as KS69):

$$P_{autocv} = k_{cl} \, (w_L - w_{th}) \tag{3.5}$$

where $P_{autocv}$ is the rate of rain water formation (kg $kg^{-1}s^{-1}$) and cloud water removal for resolvable clouds , $k_{cl}$ ($s^{-1}$) is the autoconversion rate assumed in the RegCM2 to be $10^{-4}$ $s^{-1}$, and $w_{th}$ is the cloud-water conversion threshold, which in the RegCM2 is assumed to be a function of temperature (see Giorgi et al. (1999) for detail). Thus, since $P_{autocv}$ only depends upon $w_L$, which is assumed to be unaffected by aerosols, precipitation rates in the standard version of the RegCM2 is independent of the concentrations of aerosols. In order to include the 2nd indirect effect, $P_{autocv}$ must be modified so that it is dependent upon the cloud microphysical parameters ($N_c$ and $r_e$), that are in turn affected by aerosols.

For convective clouds, the Kuo-type scheme of Anthes (1987) is used in the RegCM2. Precipitation is triggered when the column-integrated water vapor convergence exceeds a given threshold in convectively unstable conditions. Depending on the column averaged relative humidity, part of the water vapor convergence is removed as precipitation and the other is redistributed back to the atmosphere. In convective clouds, $r_e$ typically varies very little throughout the depth of clouds due to the strong entrainment (Martin et al., 1994) and this suggests that the 2nd indirect effect should not be particularly strong in this type of cloud. Therefore, the aerosol effects on convective precipitation are neglected in this study.

In order to include the 2nd indirect effect, I modified the precipitation rate in the standard RegCM2 by replacing the KS69 parameterizations with two alternate parameterizations: one with a strong dependence on $\chi_{tot}$ and the other with a relatively weak $\chi_{tot}$ dependence. The first is based on Lohmann and Feichter (1997) who used an autoconversion scheme derived by Beheng (1994, hereafter referred to as BH94); in this

approach the autoconversion rate depends on $N_c$ as well as $w_L$ in the following manner (in SI units)

$$P_{autocv} = \frac{\gamma_1 6 \cdot 10^{28} n^{-1.7} (10^{-6} N_c)^{-3.3} (10^{-3} \rho_a \frac{w_L}{b})^{4.7}}{\rho_a} \propto {w_L}^{1.4} {r_e}^{9.9} \propto {w_L}^{4.7} {\chi_{tot}}^{-1.5} \qquad (3.6)$$

where n (=10) is the width parameter of the initial cloud droplet spectrum, described by a $\Gamma$ function, $\gamma_1$ (=150) is a tunable parameter, and b is the cloud cover fraction. Substituting $N_c$ with $r_e$ from Equation (3.4), it can be seen that $P_{autocv}$ in this parameterization is proportional to ${w_L}^{1.4} {r_e}^{9.9}$; alternatively, substituting for $\chi_{tot}$ in Equation (3.3), $P_{autocv}$ varies as ${w_L}^{4.7} {\chi_{tot}}^{-1.5}$.

A second parameterization is based on the work of Jones et al. (2001) and Menon et al. (2002a) who adopted an autoconversion parameterization from Tripoli and Cotton (1980, hereafter referred to as TC80) as following

$$P_{autocv} = \frac{0.104 g E_c {\rho_a}^{4/3} {w_L}^{7/3} H}{\mu (\rho_w N_c)^{1/3}} \propto {w_L}^2 r_e \propto {w_L}^{2.3} {\chi_{tot}}^{-0.15} \qquad (3.7)$$

where $E_c$ is the collision/collection efficiency of cloud droplets set to 0.55, $g$ is the acceleration due to gravity, $\mu$ is the dynamic viscosity of air ($1.83 \times 10^{-5}$ kg m$^{-1}$ s$^{-1}$), and $H$ is the Heaviside function

$$H = \begin{cases} 1, & when \ w_L > w_{th} \\ 0, & when \ w_L \le w_{th} \end{cases} \qquad (3.8)$$

where $w_{th}$, as in Equation (3.5), is the cloud-water threshold for autoconversion to occur so that autoconversion only occurs when $w_L$ exceeds $w_{th}$. This parameterization couples $P_{autocv}$ and aerosols through its dependence on $N_c$, which in turn is a function of aerosol concentration via Equation (3.3). Substituting from Equation (3.4) or Equation (3.3), it

can be found that $P_{autocv}$ is proportional to $w_L^2 r_e$ or $w_L^{2.3}\ \chi_{tot}^{-0.15}$. Thus it would be expected that TC80 is much less sensitive to changes in $\chi_{tot}$ than that of BH94.

The TC80 parameterization used in this model is further enhanced by allowing the threshold for autoconversion in Equation (3.8) to depend on the aerosol concentration (Jones et al., 2000). For example, Rogers and Yan (1989) suggested that autoconversion will only proceed when the number concentration of cloud droplets greater than 20μm in radius ($N_{c20}$) exceeds ~ $10^3$ $m^{-3}$. Since $r_e$ decreases as aerosol concentrations increase, it might be expected that the number of large cloud droplets would also decrease when aerosols increase and this would in turn presumably tend to delay the initiation of autoconversion. To incorporate this effect into TC80, I use a Heaviside function in Equation (3.7) that depends upon $N_{c20}$ instead of $w_L$ , i.e.,

$$H = \begin{cases} 1\,, & when\ \ \mathrm{N_{c20}} > 10^3 \\ 0\,, & when\ \ \mathrm{N_{c20}} \le 10^3 \end{cases} \tag{3.9}$$

where $N_{c20}$ is in units of $m^{-3}$. $N_{c20}$ is calculated in this model assuming a modified gamma cloud droplet size distribution constrained by $w_L$ and $N_c$ (Pruppacher and Klett, 1997), with $N_c$ in turn determined by $\chi_{tot}$ via Equation (3.3).

Comparison of the above three autoconversion rates (Equations (3.5)-(3.7)) as a function of $w_L$ and $r_e$ is presented in Figure 3.1, where $w_{th}$ for KS69 is assumed to be 0.2g $kg^{-1}$ for simplicity. Inspection of Figure 3.1 reveals that: i) without aerosol 2nd indirect effect ($r_e$ is assumed the background value of 10μm), the autoconversion rate is largest for TC80 scheme, then BH94 scheme, and least for KS69 scheme. At low $w_L$, TC80 and BH94 are quite similar in their dependence upon $w_L$, but distinctly different from that of KS69 because of the different threshold formulations used for these parameterizations.

With the increase of $w_L$, the magnitude of $P_{autocv}$ for BH94 approaches that of KS69 because of BH94's relatively weaker dependence on $w_L$. By comparison, $P_{autocv}$ for KS69 tends to be significantly smaller than that of TC80 for typical values of $w_L$ in large-scale clouds (i.e., $w_L$ usually less than 0.3 g $kg^{-1}$); ii) with the inclusion of 2nd indirect effect ($r_e$ is assumed to decrease to 7.5μm due to the increase in $\chi_{tot}$), $P_{autocv}$ for BH94 decreases an order of magnitude from 1mm/day to 0.1 mm/day at $w_L$ = 0.3 g $kg^{-1}$, while only slight decrease in $P_{autocv}$ is seen using TC80 scheme. Thus, it would be expected to find a stronger 2nd indirect effect with BH94 than with TC80. Finally, it should be mentioned that BH94 and TC80 autoconversion scheme were developed for the warm convective cloud systems with relatively larger cloud water content of 0.5 ~ 2 g $kg^{-1}$ and larger vertical velocity of 10 cm $s^{-1}$ ~ 1m $s^{-1}$, while for the large scale clouds, they are much smaller at less than 0.3 g $kg^{-1}$ and 1mm $s^{-1}$ ~ 1cm $s^{-1}$ (Pruppacher and Klett, 1997). It is necessary to tune these two autoconversion schemes to appropriately represent precipitation in large scale clouds with smaller vertical velocities. In addition, as discussed in Nenes et al. (2003), vertical updraft velocity is a parameter as important as aerosol concentration in terms of cloud droplet formation and number concentration. These issues will be investigated in the future work.

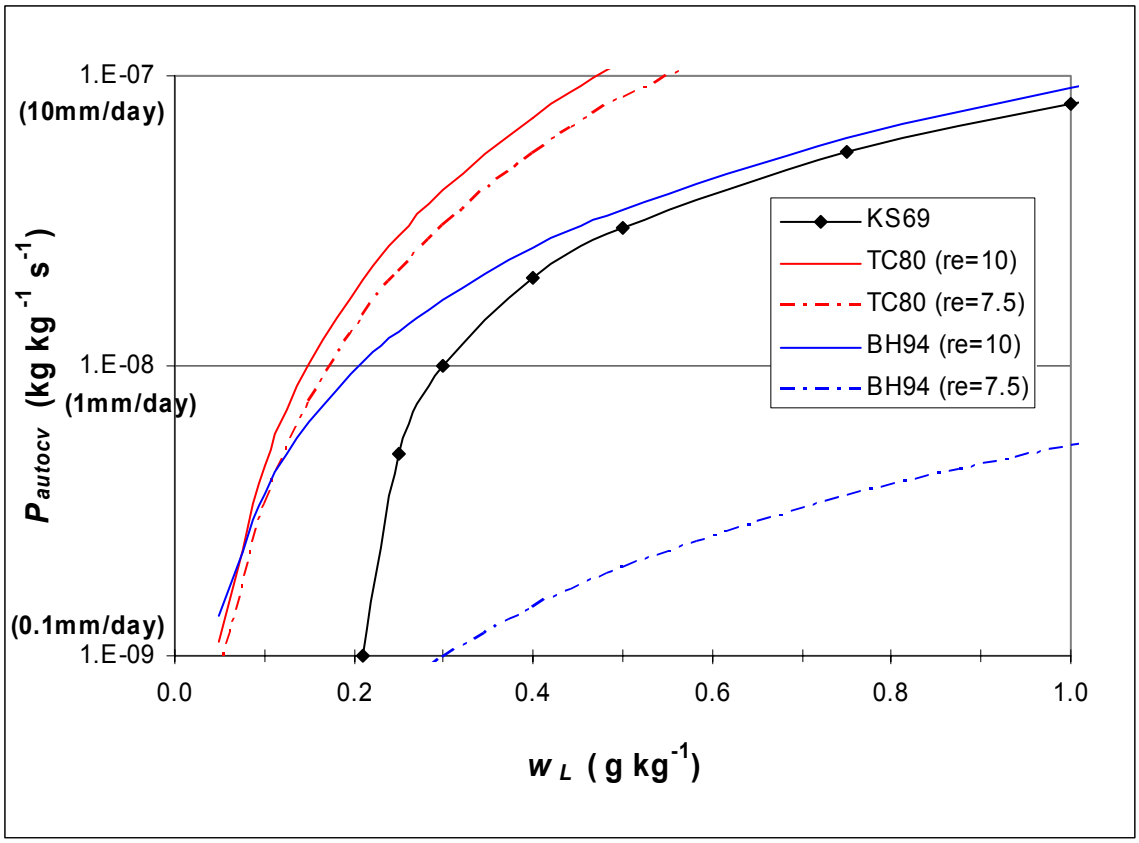


**Figure 3. 1** Variations in $P_{autocv}$, the autoconversion rate, as a function of $w_L$, the liquid water content at cloud effective radius $r_e$ = 10μm and 7.5μm, for three versions of the parameterization: KS69, based on Kessler [1969] with $w_{th}$ = 0.2 g kg$^{-1}$, BH94, based on Beheng [1994], and TC80 based on Tripoli and Cotton [1980]. (Note: KS69 is unaffected by variations in $r_e$, and in turn $\chi_{tot}$, the total concentration of particulate sulfate and hydrophilic OC and BC, and so only one plot is shown for this parameterization.

## 3.3 Model Simulation

In order to evaluate the RegCM2-simulated direct and indirect aerosol impacts on climate over East Asia, a series of model runs (Table 3.1) were conducted spanning a period from June 01 1994 to August 31 1995, with the first 2 months serving as spin-up for the subsequent 13-month simulation period. The main control run (CONT) uses the Standard Model with the KS69 parameterization and all aerosol radiative and cloud effects inactive. Two additional control runs, in which all aerosol radiative and cloud effects are neglected, were carried out: TCCONT and BHCONT using the TC80 and BH94 parameterizations, respectively, instead of KS69 scheme. In the DIRBC and DIR0 experiments, aerosol direct effects are included, with all species and without BC (i.e., BC emissions set to zero), respectively, using the Standard Model. In the experiment INDIR1, the direct and 1$^{st}$ indirect effects are included using the Standard Model. TCIND2 and BHIND2 include the 2$^{nd}$ indirect of aerosols only using the TC80 and BH94 parameterizations, respectively. Finally, TCALL and BHALL include all aerosol effects and all aerosol species using the TC80 and BH94 parameterization, respectively.

The observational climate dataset used here to evaluate model performance and to assess the anthropogenic aerosol effects is developed by the Climate Research Unit (CRU) of the East Anglia University, as described by Mitchell et al. (2003). This consists of monthly surface air temperature and precipitation over land gridded at a resolution of 0.5 degree from 1901 to 2000. It is also used to evaluate the long term trends of precipitation (see Section 3.3.5).

**Table 3. 1** List of Experiments

| Experiments | Description |
|---|---|
| CONT | Standard Model (using KS69 autoconversion parameterization) without radiative and cloud effects of aerosols |
| TCCONT | Control run with TC80 autoconversion parameterization without radiative and cloud effects of aerosols |
| BHCONT | Control run with BH94 autoconversion parameterization without radiative and cloud effects of aerosols |
| DIR0 | Standard Model with direct aerosol effect from scattering only (i.e., no BC, no aerosol-cloud interactions) |
| DIRBC | Standard Model with direct aerosol effect from both scattering and absorbing species (i.e., BC included, no aerosol-cloud interactions) |
| INDIR1 | Standard Model with direct, semi-direct and 1$^{st}$ indirect aerosol effects included |
| TCIND2 | 2$^{nd}$ indirect effect only with TC80 parameterization |
| BHIND2 | 2$^{nd}$ indirect effect only with BH94 parameterization |
| TCALL | All aerosol effects included with TC80 parameterization |
| BHALL | All aerosol effects included with BH94 parameterization |

### 3.3.1 Control Simulations: No Aerosol-Climate Coupling

The simulated climatic conditions over East Asia were discussed in detail by Giorgi et al. (1999), which showed a summer monsoon season with a predominant low level southerly and southwesterly circulation and a maximum in precipitation and cloudiness, and a winter dry season with prevailing westerly winds in the mid and high latitudes and an easterly in the sub-tropical regions. A brief summary is given here. Figures 3.2a and b present the monthly mean surface air temperature and precipitation averaged over the interior model domain (see Figure 2.1, land grid only) for the three control runs (i.e., CONT, TCCONT, and BHCONT) and the CRU observations over the 13-month simulation period.

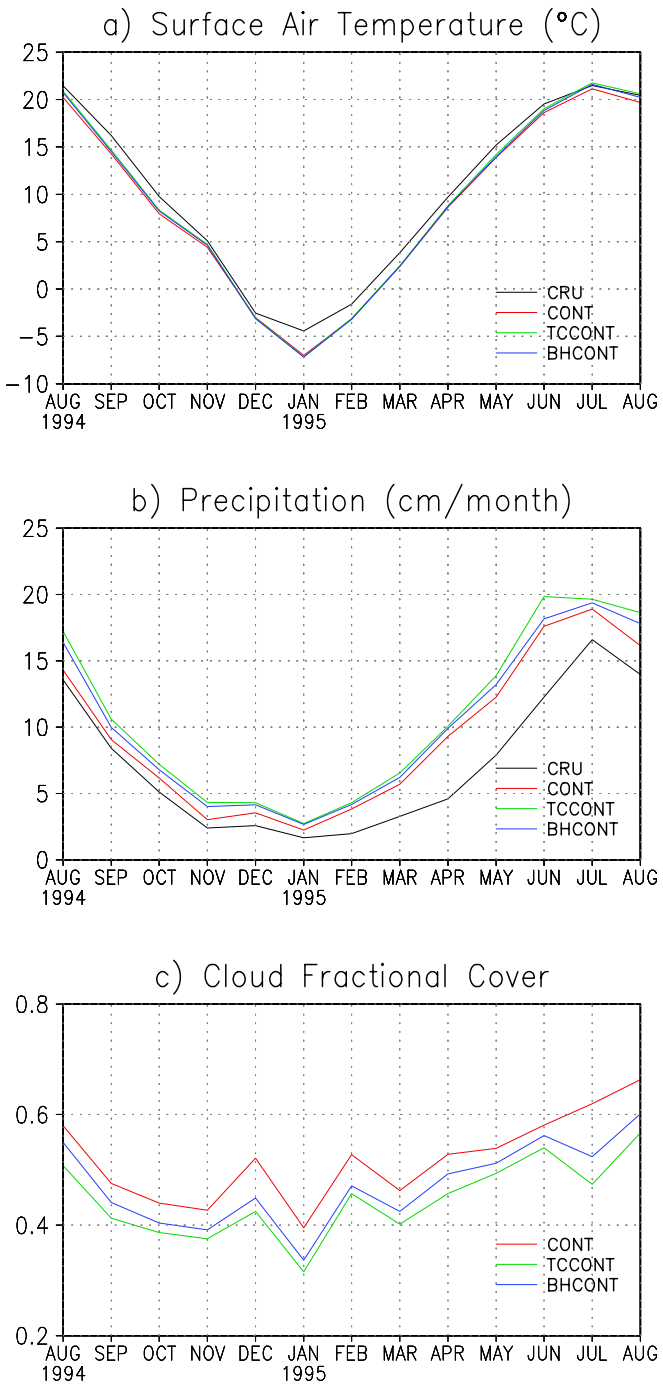


**Figure 3. 2** The annual cycle in observed and simulated monthly means averaged over the interior model domain (see context): (a) surface air temperature ($^0$C); (b) precipitation (cm month$^{-1}$); and (c) simulated cloud fractional cover. Results are shown for the three control runs.

In general, the model reproduces the seasonality of the East Asia climate, with dry cold winter and wet warm summer. The simulated average air temperature generally agrees well with the observations; however there is a cold bias in the simulations of ~ $1^0$C in summer and ~ $2^0$C in winter. Seasonally, the cold bias is largest in January, reaching $3^0$C over the entire continental region. Giorgi et al. (1999) discussed the possible causes of the winter cold bias, and suggested three contributing factors: the absence of urban heat island effects in the model, which are especially pronounced in the winter; the difference between the area averaged elevations of the model grids and the elevations of the meteorological stations (e.g, in mountains regions, observing stations are generally located in valleys and lower–elevation sites); and the model's tendency to overestimate cloudiness in the upper troposphere.

The observed precipitation over East Asia is generally low in winter and high in summer due to the East Asian monsoonal circulation. The model captures this overall seasonal variation, as well as the onset of the monsoonal rains in the spring, but tends to overpredict the spring and summer precipitation by 20 ~ 40%. Giorgi et al. (1999) proposed a number of possible explanations: observed-station rainfall may be lower than actual precipitation due to the effects of wind, wetting losses, evaporation, etc (Legates and Willmott, 1990); the occurrence of localized high precipitation events during the summer in the model (often referred to as numerical point storms) can also cause an over-prediction in precipitation.

Figure 3.2b also shows that the control runs using the TC80 and BH94 autoconversion parameterizations tend to produce more precipitation over the model domain than that obtained from the standard control run using KS69. The largest

precipitation increase is seen in the fall and winter (8.4% and 16.9% for TC80 scheme; 6.1% and 11.4% for BH94 scheme) and less increase in spring and summer (around 5%). It appears that most of the excess precipitation in the runs with TC80 and BH94 arise from clouds with $w_L$ below $w_{th}$, and thus is traceable to the different treatments for autoconversion at low $w_L$ (i.e., KS69 with a threshold of $w_L > w_{th}$, TC80 with a threshold of $N_{c20} > 10^3$ $m^{-3}$ such that autoconversion can occur at low $w_L$ provided anthropogenic aerosol concentrations are low, and BH94 without a threshold.

Since the CONT run already tends to over-predict precipitation, the use of the TC80 and BH94 parameterizations increases the discrepancy between observed and simulated precipitation. (I will show in Sections 3.3.2.3 and 3.3.3.2 that inclusion of the aerosol-climate coupling tends to decrease precipitation, and thereby bring the simulated precipitation obtained in all three control runs more in line with the observations.) On the other hand, using the TC80 and BH94 parameterizations leads to less cloudiness (see Figure 3.2c), and thus slightly surface higher temperatures, and in turn, a small reduction of the model's cold bias (see Figure 3.2a).

### 3.3.2 Aerosol Direct, Semi-direct and 1st Indirect Effect

This section discusses the results from the experiments that simulate the direct, semi-direct and 1st indirect effect using the standard KS69 scheme, i.e., DIR0, DIRBC, and INDIR1 in Table 3.1. Table 3.2 reports the changes in the seasonally mean surface solar radiation, surface air temperature and precipitation between these experiments and the CONT run averaged over the model inner domain (land grids only). Figure 3.3 and 3.4 illustrate the spatial distribution of the seasonal mean precipitation change between DIR0, INDIR1 and CONT runs.

**Table 3. 2** Difference in surface radiative forcing ($RF_{sfc}$ in W $m^{-2}$), surface air temperature $\Delta T$ (in Kelvin), and precipitation $\Delta P$ (in cm $month^{-1}$) relative to CONT run, averaged over the model inner domain (defined in the text, land grid only) for the experiments using standard KS69 scheme. The relative precipitation change is shown in parenthesis.

| | SON | DJF | MAM | JJA | Annual |
|---|---|---|---|---|---|
| *$RF_{sfc}$* | | | | | |
| DIR0 | -1.62 | -1.35 | -2.03 | -2.35 | -1.84 |
| DIRBC | -3.53 | -2.76 | -3.64 | -3.78 | -3.43 |
| INDIR1 | -5.59 | -4.17 | -6.87 | -9.62 | -6.56 |
| *$\Delta T$* | | | | | |
| DIR0 | -0.23 | -0.20 | -0.10 | -0.05 | -0.14 |
| DIRBC | *-0.18* | -0.28 | -0.14 | -0.05 | -0.16 |
| INDIR1 | -0.41 | -0.46 | -0.29 | -0.26 | -0.35 |
| *$\Delta P$* | | | | | |
| DIR0 | -0.23 (-3.8) | -0.22 (-6.9) | -0.03 (-0.3) | -0.30 (-1.7) | -0.19 (-3.2) |
| DIRBC | -0.31 (-5.1) | -0.24 (-7.6) | -0.16 (-1.8) | -0.44 (-2.5) | -0.29 (-4.3) |
| INDIR1 | -0.61 (-10.1) | -0.43 (-13.4) | -0.50 (-5.5) | -1.12 (-6.4) | -0.66 (-8.8) |

*3.3.2.1 Solar radiation and surface temperature changes (DIR0 and INDIR1 experiments)*

The radiative forcing at the surface is negative due to the sulfate and OC scattering effect (DIR0 run). This is expected because sulfate and OC particles scatter the incoming solar radiation, and cause some to be reflected back to space. The 1st indirect effect reinforces these negative radiative forcing, due to the increased cloud brightness caused by the role of aerosol particles as cloud condensation nuclei. The spatial variation of the radiative forcing (not shown) generally mimics the spatial variation in aerosol loadings, i.e. the largest negative forcing appears over Sichuan basin and the broad regions along

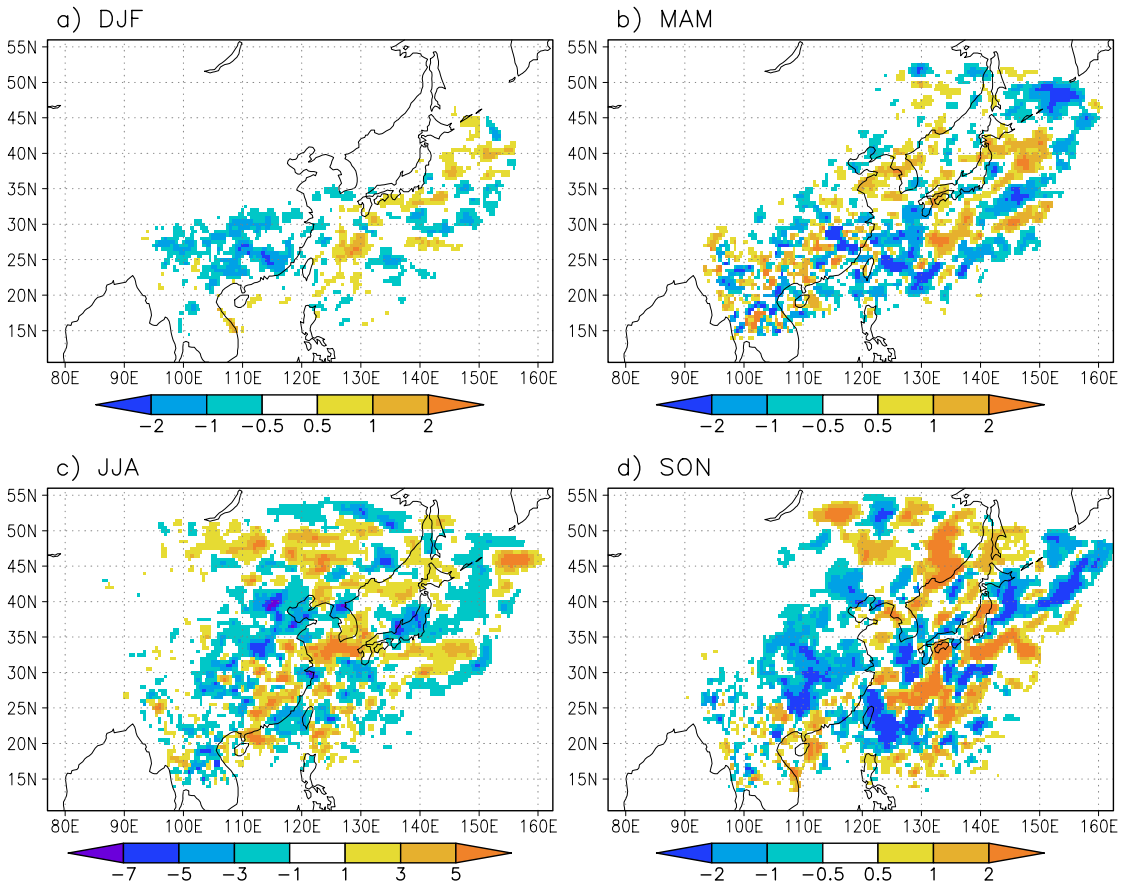


**Figure 3. 3** Seasonal mean precipitation change (DIR0 vs. CONT), unit: cm/month.

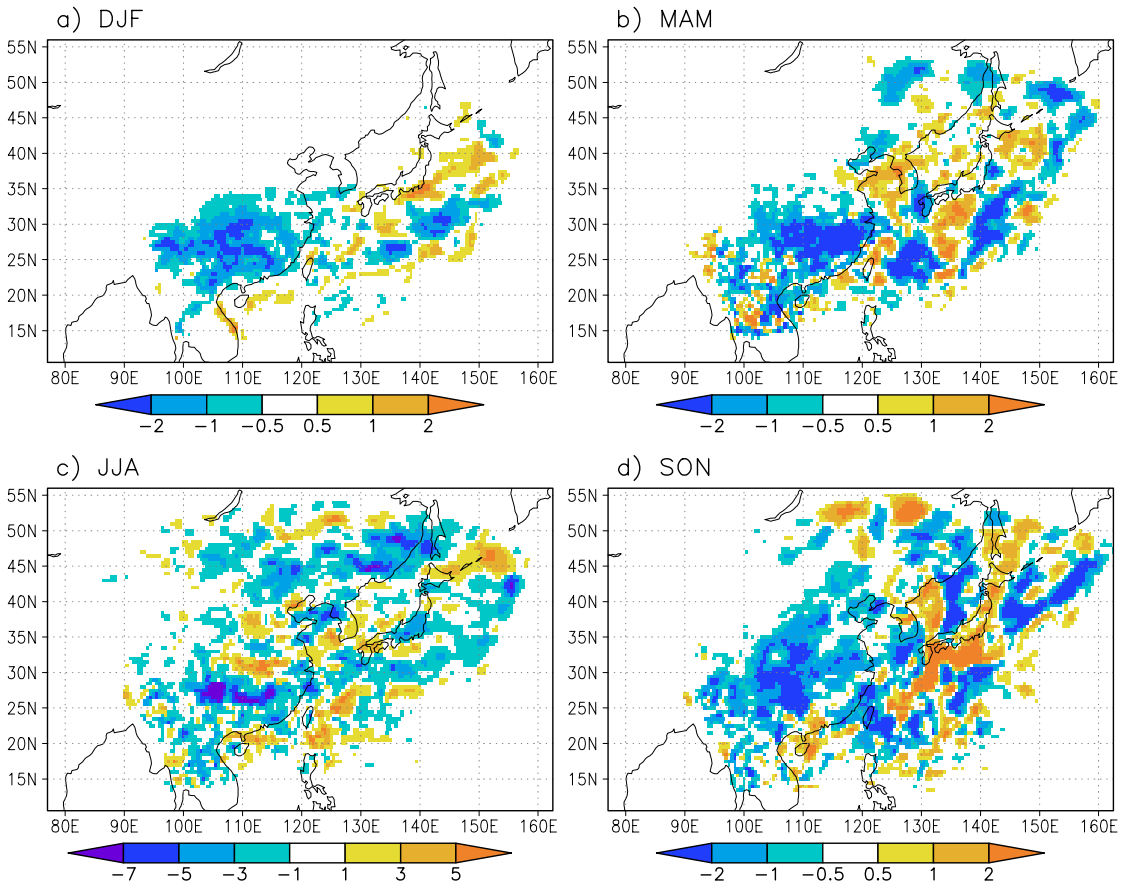


**Figure 3. 4** Similar to Figure 3.3, but for INDIR1 vs. CONT.

Yangtze River east of 110E, where the model-calculated AOD and aerosol concentrations are largest.

In terms of seasonal variations, Table 3.2 shows that the negative radiative forcing due to the direct effect (DIR0) is larger in spring (MAM) and summer (JJA), and smaller in fall (SON) and winter (DJF). However, the largest model calculated aerosol loadings are generally obtained during the fall and winter. This counterintuitive result is partially due to the less available incoming solar radiation in SON and DJF compared to MAM and JJA. It also appears to be caused by a complex interaction proposed by Yu et al. (2002) between low-level cloud cover and the aerosol-induced perturbation to surface solar radiation. Table 3.3 gives the seasonally averaged low-level cloud cover change (below 750hpa) and overall cloud cover for three experiments (DIR0, DIRBC and INDIR1) relative to the CONT run. Note that the low-level cloud cover tends to decrease in SON and DJF, but increase in MAM and JJA in the DIR0 experiment. The mechanism underlying this feedback, as discussed in Yu et al. (2002), is related to the development of boundary layer. The decrease of solar radiation by aerosols, cools the surface, and slows the development of boundary layer. During the relatively dry seasons (DJF and SON), less water is drawn into the atmosphere as a result of the surface cooling, and this leads to a decrease in low-level cloud cover. The result is a negative feedback which tends to decrease the negative forcing from aerosol scattering. During the wet seasons (MAM and JJA), on the other hand, the slowing in the development of boundary layer by aerosol scattering, tends to keep more moisture in the lower atmosphere, leading to more low-level clouds. The result in this case is a positive feedback that enhances the negative

forcing from aerosol scattering, As a result, the largest negative forcings in the model simulations for DIR0 experiment generally occur during the wet seasons (MAM and JJA).

**Table 3. 3** The changes in seasonal mean low level cloud cover (below 750hpa) (LLCLD) and overall cloud cover (CLD) relative to the CONT run, averaged over the model inner domain (land grid only) for the experiments using standard KS69 scheme (DIR0, DIRBC and INDIR1), unit: %.

| | *LLCLD* | | | | *CLD* | | | |
|---|---|---|---|---|---|---|---|---|
| | SON | DJF | MAM | JJA | SON | DJF | MAM | JJA |
| DIR0 | -0.46 | -0.41 | +0.09 | +0.30 | -0.68 | -0.45 | +0.01 | +0.13 |
| DIRBC | -0.56 | -0.78 | -0.24 | -0.48 | *-0.53* | -0.68 | -0.25 | -0.31 |
| INDIR1 | -0.87 | -1.14 | -0.19 | -0.06 | -1.39 | -1.17 | -0.42 | -0.16 |

The largest forcing from the 1st indirect effect occurs in summertime, because this is when clouds prevail. Similar to the direct effect (DIR0 run), the 1st indirect effect itself (INDIR1 vs. DIRBC) results in less low level and overall cloudiness in relatively dry months (fall and winter), and more cloudiness in summer (JJA), following the same mechanism discussed above.

The magnitude of mean surface radiative forcing over this region ranges -1.3 ~ -2.3 W $m^{-2}$ for sulfate and OC scattering (DIR0 run) and -4.2 ~ -9.6 W $m^{-2}$ for combined direct/semi-direct/1st indirect effect (INDIR1 run) with the maximum forcing up to -30 W $m^{-2}$ over the high aerosol loading areas. These results are compatible with those obtained by Giorgi et al. (2002 and 2003). The negative aerosol radiative forcings result in a model-simulated cooling at the surface of a few tenths degree Kelvin over the entire region (Table 3.2). Overall, the temperature decrease is larger in SON and DJF than that

in MAM and JJA. For example, the net seasonally- and regionally-averaged temperature decrease ranges from -0.3 K in JJA to -0.5K in DJF with the inclusion of direct, semi-direct and 1st indirect effects. Though the magnitude of the solar radiative forcing is larger in MAM and JJA, the surface temperature change is generally more sensitive to solar radiation change in dry seasons than wet seasons due to less latent heat compensation, thus the temperature decrease is larger in the fall and winter.

Spatially, similar to surface radiative forcing, the temperature (not shown for brevity) decrease from DIR0 run is well correlated with the aerosol loading, and thus the largest decrease are seen over Sichuan Basin and east of 110E along the Yangtze river regions. Over these regions the temperature decrease reaches up to -0.6 K in SON and DJF, but only -0.2 K in MAM and is negligible in JJA. Inclusion of 1st indirect effect doubles the cooling in DJF and SON, and also causes significant cooling in MAM and JJA (up to -0.6 K) over the Sichuan basin. As noted by Qian and Giorgi (2000), Giorgi et al. (2002) and Qian et al. (2003), the spatial distribution in this model-predicted temperature reduction, with a peaking over the Sichuan basin, is seen in the observational data, and suggests that China may have experienced an aerosol induced cooling superimposed over a larger scale, perhaps greenhouse effect induced warming.

*3.3.2.2 Soot effect (DIRBC vs. DIR0 runs)*

This section examines the radiative and climatic effects of core-coated internally mixed aerosols containing BC. As mentioned, black carbon strongly absorbs solar radiation, and thus heats the atmospheric column, and producing a positive radiative forcing for the earth and atmosphere system, which is believed to suppress cloud formation. Table 3.4 lists the seasonal mean solar radiation forcing (DIRBC vs DIR0) at

surface ($RF_{sfc}$) and top of the atmosphere ($RF_{TOA}$), within the atmospheric column ($RF_{atm}$), and the change of solar cloud forcing at surface (SWCF), as well as the cloud fractional cover (CLD) from the CONT run. In this Table, the atmospheric forcing is defined as the difference between surface and TOA forcing, and the cloud forcing as the difference between net solar radiation for cloudy and clear-sky atmosphere at surface (and thus is always negative). A positive change in cloud radiative forcing indicates less cloudiness, and vice visa. It can be seen that the cloudiness is largest in summer (JJA) and lowest in winter (DJF). Unlike the direct effect and 1$^{st}$ indirect effect, where both the surface and TOA radiative forcings are negative, soot aerosols generate a significant positive forcing at TOA (+1.1 ~ +2.4 W m$^{-2}$). This positive forcings has approximately the same magnitude as the negative forcing from the direct effect by sulfate/OC (DIR0 run), and thus the overall TOA forcing is around zero for DIRBC run (both scattering and absorption included). This cancellation was also found in the work of Ramanathan et al. (2001c) in the INDOEX experiment. In comparison with the previous studies by Giorgi et al. (2002), the BC forcing obtained here is about twice as large, mostly due to the different treatment of sulfate/OC and BC mixing states (an external mixture in their work produces about 1/3 less absorption than the core-coated treatment here, see the absorption amplification factor *A* in Section 3.2.1), and the relative lower prescribed BC mass concentration in their work (assumed to be 7.5% of sulfate amount with the same spatial and temporal distribution). On the other hand, the results here are generally consistent with the positive BC radiative forcing over Asia estimated from global modeling studies of a few tenths to 1 W m$^{-2}$ (Haywood et al., 1997; Myhre et al., 1998; Lohmann and Feichter, 2001, etc).

**Table 3. 4** Changes due to semi-direct effect (i.e. DIRBC vs DIR0) in seasonal mean $RF_{sfc}$, $RF_{TOA}$, $RF_{atm}$, and SWCF averaged over inner domain (land grid only), unit: W $m^{-2}$. Also listed is the mean cloud fractional cover from CONT run.

| | SON | DJF | MAM | JJA |
|---|---|---|---|---|
| $RF_{sfc}$ | -1.91 | -1.41 | -1.62 | -1.43 |
| $RF_{TOA}$ | 1.21 | 1.13 | 1.37 | 2.42 |
| $RF_{atm}$ | 3.12 | 2.54 | 2.99 | 3.85 |
| SWCF | 0.90 | 1.07 | 1.04 | 1.79 |
| CLD | 0.43 | 0.41 | 0.47 | 0.58 |

In contrast to the positive forcing at the top of the atmosphere, the radiative forcing at the surface by BC-absorption is negative (Table 3.4), and therefore tends to reinforce the negative surface forcing from scattering aerosols. Because the radiative forcing from the direct and semi-direct effects are similar in magnitude, $RF_{sfc}$ for DIRBC relative to the CONT is generally about twice as negative as that obtained for the DIR0. Thus, the annually averaged $RF_{sfc}$ increases from about -1.8 W $m^{-2}$ for DIR0 to -3.4 W $m^{-2}$ for DIRBC.

With regard to the atmospheric column, BC absorption significantly heats the atmosphere, especially in the lower levels where BC aerosols mainly reside. The model simulated atmospheric forcing from BC absorption is about +2.5 ~ +3.8 W $m^{-2}$, equivalent to a heating rate of about 0.1 K/day (not shown). The negative forcing at the surface from BC would actually be larger if it were not for a negative feedback involving clouds. Because of the positive atmospheric forcing from BC, the cloud cover fraction in DIRBC decreases by 0.1 ~ 0.8% and 0.2 ~ 0.4% for lower level and overall clouds, respectively, with the maximum cloud cover decrease occurring in summer (see Table 3.3). This, in turn, produces a positive change in solar cloud radiative forcing at the

surface of +0.9 ~ +1.8 W $m^{-2}$ (i.e., since less solar radiation is reflected by clouds, more solar radiation reaches the surface. In the absence of this cloud feedback (i.e., if SWCF equal to zero), the negative surface solar forcing by BC absorption would be enhanced by ~ -1 W $m^{-2}$.

In response to the greater reduction in solar radiation at the surface from DIRBC, the surface temperature generally decreases in all seasons except SON, with largest decrease of about 0.1 degree in DJF (Table 3.2). Note that in the fall (SON), the surface temperature increases by 0.05K compared to DIR0 run. Inspection of the cloudiness change in Table 3.3 shows that the overall cloudiness increases by 0.15% in SON, while lower level clouds decreases. This implies that the high level clouds in SON increases, therefore trapping more outgoing long wave radiation, thus leading to the small temperature increase. The reason for the increase in high level clouds in SON is not clear; however, it could be due to the humidity penetrating the inversion at the boundary layer, producing an unstable layer, and creating larger deep convective clouds (Rudich et al., 2003; Andreae et al., 2004).

*3.3.2.3 Precipitation change due to aerosol radiative effect*

I now turn to a discussion of the model simulated precipitation impacts from aerosol-radiative effects (i.e., those effects that are strictly radiative: direct, semi-direct and 1$^{st}$ indirect effects). Table 3.2 shows that, on regional scales, the model simulations predict that the radiative effects of aerosols lead to a net decrease in rainfall. The largest relative decreases are seen in the fall (SON) and winter (DJF), which is consistent with the seasonal variation in aerosol loadings. By examining the three effects individually, it can be seen that: on average, 1) direct effect (DIR0) produces a precipitation reduction of -

4% and -7% in SON and DJF, with smaller changes in MAM and JJA; 2) the inclusion of semi-direct effect (DIRBC) enhances the precipitation reduction by another -1% in all four seasons; 3) the 1st indirect effect produces a relatively larger precipitation decrease in all seasons (-4% ~ -6%); 4) the total precipitation reduction reaches up to -10% and -13% in the fall and winter, and -5.5% and -6.4% in the spring and summer. As discussed in Giorgi et al. (2002), the precipitation reduction by these aerosol-radiative effects (i.e., direct, semi-direct and 1st indirect effects), is caused by the increase in thermal stability from the aerosol induced surface cooling and atmospheric heating in the case of DIRBC. This, in turn, tends to inhibit cloud formation (see Table 3.3) and thus precipitation.

In terms of the spatial distribution of the precipitation reduction, Figure 3.4 (DIR0 run) reveals significant portions of the eastern continental region with the precipitation changes of as much as 2cm $month^{-1}$ in SON and DJF. However, during the spring and summer (MAM and JJA), the precipitation change on average is generally small and negligible, with a noisy distribution of grids with increased and decreased precipitation of 0.5 ~ 2 cm $month^{-1}$ (MAM) and 1 ~ 5cm $month^{-1}$ (JJA). This reflects the inherent noise in the model-calculated precipitation difference due to more nonlinear and random nature of convective precipitation activities for these seasons (Giorgi et al., 2002). The 1st indirect effect (INDIR1) generates a pattern of precipitation reduction (Figure 3.5) that is quite similar to that of direct effect (DIR0), but with more pronounced reductions in DJF, SON and MAM.

As noted earlier, the CONT run of RegCM2 reproduces the basic features of the seasonal evolution of Eastern Asia climate, but overestimates the precipitation over the continental region, especially in spring and summer. Figure 3.5 presents the annual cycle

in the simulated monthly precipitation averaged over the model inner domain for INDIR1, TCALL and BHALL (see Table 3.1) experiments. It can be seen that, with the inclusion of aerosol direct and 1st indirect effects (INDIR1 run), the simulated precipitation bias becomes smaller, and thus better agree with the observations compared to the CONT run (see Figure 3.2b). In the fall and early winter, INDIR1 run reproduces the observed precipitation, and in the spring and summer, it reduces the model-observation difference by about 6%. It is also worth noting that in the summer (JJA), alternating east-west bands of precipitation increases and decreases are seen in both the DIRBC run (not shown) and INDIR1 run (Figure 3.4). These bands, may reflect the aerosol-radiative effects induced alterations in the vertical and latitudinal temperature gradient over China, that in turn affect the rate of appearance and retreat of the East Asian summer monsoonal rains over China (Boucher et al., 1998; Carrico et al., 2003; Menon et al., 2002b).

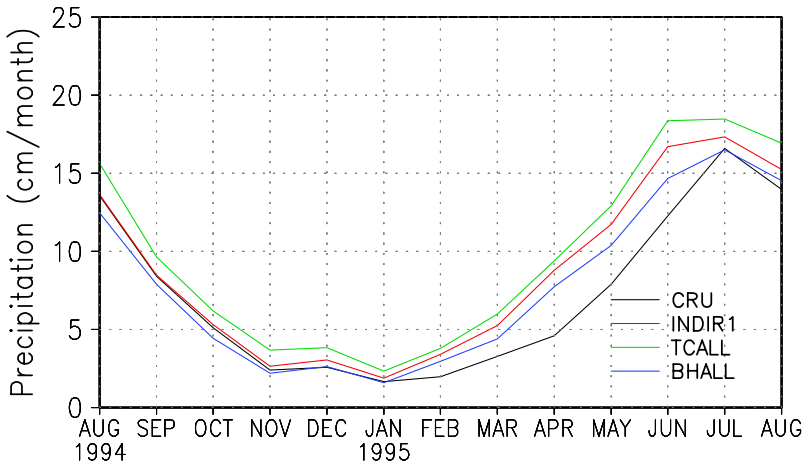


**Figure 3. 5** Seasonal variation of simulated monthly precipitation averaged over the model inner domain from three indirect experiments (INDIR1, TCALL and BHALL). Also listed is the observed CRU precipitation for comparison.

### 3.3.3 Aerosol 2nd Indirect Effect and Its Sensitivity to the Autoconversion Parameterizations

In this section, I discuss the aerosol 2nd indirect effect and its sensitivity to the two autoconversion parameterizations (discussed previously in Section 3.2.3) by comparing the experiments considering the 2nd indirect effect with their corresponding control runs. In the experiments TCIND2 and BHIND2, only 2nd indirect effect is considered, while TCALL and BHALL experiments included all four aerosol effects. Table 3.5 presents the changes in the annual mean cloud fractional cover and cloud liquid water path (weighted by cloud fraction), net cloud forcing, shortwave, long-wave and net radiative forcing at TOA averaged over the inner model domain (land grids only) for indirect experiments relative to the corresponding control experiments (INDIR1 vs CONT, TCIND2 vs TCCONT, TCALL vs TCCONT, and BHIND2 vs BHCONT, BHALL vs BHCONT). Also listed in Table 3.5 are the associated aerosol impact on surface air temperature and precipitation.

#### *3.3.3.1 The 2nd indirect effect on radiation and temperature*

As mentioned in Section 3.2.3, by acting as the cloud condensation nuclei, anthropogenic aerosols can increase the number concentration of cloud droplets, reduce the cloud effective radius, slow down the coalescence between the relative smaller cloud droplets, and thus lead to less efficient precipitation, more cloudiness and longer cloud lifetime. Table 3.5 shows that the 2nd indirect effect with BH94 scheme dramatically increases the cloud cover and cloud liquid water path by 6% and 31.5%, respectively. The TC80 scheme, on the other hand, has a much more modest impact, increasing the cloud cover and liquid water path by only 1.1% and 6%, respectively. The increase in the

cloud cover reflects more solar radiation back to the space (solar cooling), while the increase in the liquid water path tends to trap more outgoing long wave radiation (long-wave warming). The simulated net cloud forcing (SW cloud forcing plus LW cloud forcing) is negative at -0.6 W $m^{-2}$ and -3.6 W $m^{-2}$ with the 2$^{nd}$ indirect effect only for TC80 and BH94 scheme, respectively. In terms of solar and long-wave radiation forcing at the top of the atmosphere (TOA), the 2$^{nd}$ indirect effect produces a comparable magnitude in longwave heating as the solar cooling. Again the BH94 scheme generates a much larger impact than the TC80 scheme.

**Table 3. 5** Changes in annual mean cloud fractional cover (CLD) and cloud liquid water path (CLWP, weighted by cloud fraction), net cloud forcing (NCF), shortwave, long-wave and net radiative forcing at TOA (SWRF, LWRF and NRF), surface air temperature and precipitation averaged over the inner model domain (land grids only for the indirect experiments relative to the corresponding control experiments (i.e., INDIR1 vs CONT, TCIND2 vs TCCONT, TCALL vs TCCONT, and BHIND2 vs BHCONT, BHALL vs BHCONT). The relative change in cloud liquid water path is given in parenthesis.

| Experiments | INDIR1 | TCIND2 | TCALL | BHIND2 | BHALL |
|---|---|---|---|---|---|
| Δ CLD (%) | -0.8 | +1.1 | -0.5 | +6.1 | +5.7 |
| Δ CLWP (g $m^{-2}$) | -1.84 | +3.29 | +2.15 | +20.07 | +19.13 |
| | (-2.3) | (+6.0) | (+3.9) | (+31.5) | (+30.0) |
| Δ NCF (W $m^{-2}$) | -0.83 | -0.55 | -2.38 | -3.56 | -4.33 |
| SWRF (W $m^{-2}$) | -4.08 | -1.74 | -5.46 | -9.95 | -14.07 |
| LWRF (W $m^{-2}$) | -0.49 | +1.34 | +1.08 | +6.72 | +6.56 |
| NRF (W $m^{-2}$) | -4.57 | -0.40 | -4.38 | -3.23 | -7.49 |
| ΔT (K) | -0.35 | -0.03 | -0.31 | +0.08 | -0.25 |
| ΔP (%) | -9.3 | -2.7 | -10.0 | -20.4 | -27.7 |

Unlike the combined direct, semi-direct and 1st indirect effect (INDIR1), which generates a significant surface cooling (-0.35K), the temperature response to the 2nd indirect effect is smaller in magnitude and appears in both directions for TC80 and BH94 scheme. The temperature increase in BHIND2 mainly occurs in winter and early spring. By examining the changes in the vertical cloud liquid water path and the surface energy budget, it is found that with the 2nd indirect effect using the BH94 scheme, in the winter, the liquid water path from high level clouds increases by about 80-90%, while in the summer the increase is around 50%. Therefore, more long-wave radiation is trapped in the winter, and a temperature increase is produced. Additionally, the large reduction in precipitation (BHIND2, see next section), may lead to a decrease in surface evaporation, a decrease in evaporative cooling, and, in turn, an increase in surface temperature.

**Table 3. 6** Mean daily maximum and minimum surface air temperature difference in Kelvin, surface solar and longwave radiation forcings in W $m^{-2}$, overall cloud fraction in percent during the daytime and nighttime averaged over the model interior domain (see Figure 2.1, land grid only) in winter (BHIND2 vs BHCONT).

| | ΔT | SWRF | LWRF | ΔCLD |
|---|---|---|---|---|
| Daytime | +0.04[a] | -16.5 | +5.5 | +7.2 |
| Nighttime | +0.57[b] | n/a | +5.1 | +7.4 |
| Mean | +0.30 | -8.3 | +5.3 | +7.3 |

Note: [a] Daily maximum temperature ($T_{max}$ ), [b] Daily minimum temperature ($T_{min}$).

A further analysis regarding this temperature increase from the 2nd indirect effect using BH94 scheme is presented in the following. Table 3.6 lists mean daily maximum and minimum surface air temperature ( at 2 meters above surface) difference, surface solar and longwave radiation forcings, overall cloudiness change during the daytime and

nighttime averaged over the model interior domain (see Figure 2.1, land grid only) in winter, when the temperature increase appears to be largest. It can be seen that the mean temperature increases 0.3K, though the negative solar forcing is greater than the positive long wave heating. The temperature increases mainly occurs during the nighttime, with $T_{min}$ increases by 0.57K, while during the daytime, the temperature change is much smaller with slight increase in $T_{max}$ at 0.04K, and thus the diurnal temperature range (DTR) decreases at 0.53K. This simulated temperature change difference suggests that the nighttime temperature is more sensitive to the radiation changes, with a larger climate sensitivity ($\lambda$, a parameter to measure the global mean surface response $\Delta T$ to the radiative forcing $\Delta F$, see Ramaswamy, et al., (2001)) at 1.1K/(W $m^{-2}$) during the nighttime. Therefore, the 2nd indirect effect might be responsible for the observed nighttime warming as reported by Zhou et al. (2004) over the industrialized areas of China. On the other hand, the daytime surface temperature should decrease due to the larger reduction of solar radiation compared to the long wave heating. However, because of its counteracting greater boundary layer instability of the hotter and drier surface during the day, essentially no daytime cooling is computed. In addition, this temperature increase from 2nd indirect effect decreases the model cold bias in winter.

*3.3.3.2 The 2nd indirect effect on precipitation*

The 2nd indirect effect generally decreases the annual mean precipitation with the largest reduction at -20% with BH94 scheme, and -2.7% with TC80 scheme (Table 3.5). Figure 3.6 exhibits the seasonal variation of relative changes in monthly precipitation averaged over the inner domain (land grid only) from five pairs of experiments. The BH94 scheme reduces the precipitation by more than 30% in late fall and winter, and

around 10 ~ 20% in other seasons, while TC80 scheme only generates a small reduction in precipitation of -4% in the fall and winter and negligible changes in spring and summer. A possible reason for the seasonal variation in the magnitude of the 2nd indirect effects on precipitation might be related to the water vapor availability: in the wet/warm season, when there is generally a plentiful supply of water vapor, cloud droplets generally tend to be large enough to pass the autoconversion threshold and precipitate out even with the inclusion of the indirect effect. Moreover, in summer, convective precipitation processes dominate, and they are not directly affected by the 2nd indirect effect parameterized in this work.

The spatial distributions of the precipitation change in DJF and SON from the 2nd indirect effect are shown in Figure 3.7, when the simulated precipitation reductions are largest. The precipitation reduction is evident over a broad area from Sichuan Basin extending to the eastern coastal China. The maximum reduction in monthly precipitation

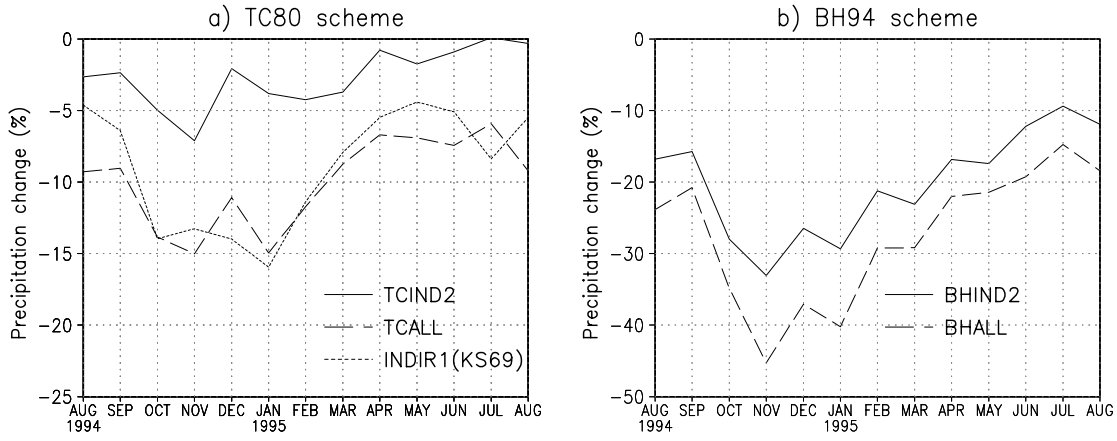


**Figure 3. 6** Seasonal variation of monthly precipitation changes averaged over the model inner domain, relative to their corresponding control runs (in percent) using a) TC80 scheme, b) BH94 scheme, also listed in a) is INDIR1 using KS69 scheme for comparison.

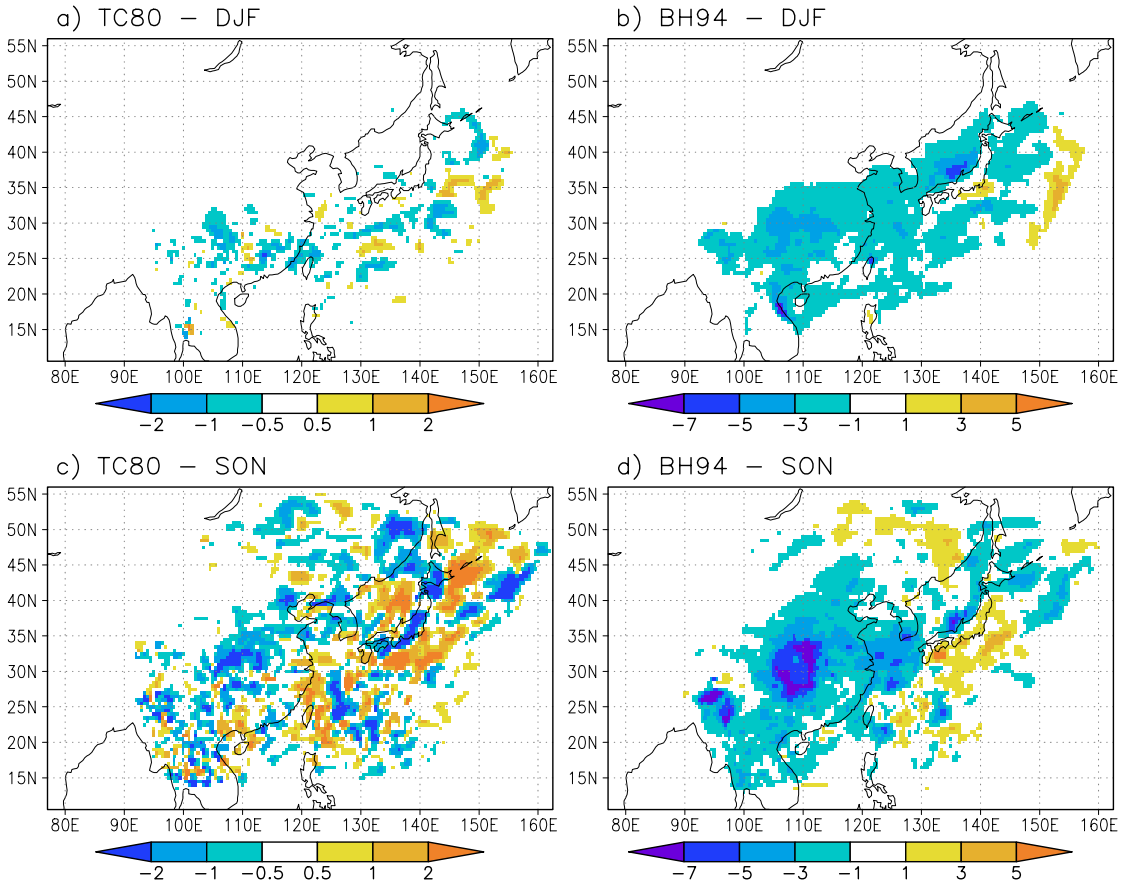


**Figure 3. 7** The spatial distribution of seasonal precipitation change in DJF and SON from 2nd indirect effect only experiments using TC80 and BH94 scheme. a) TC80 – DJF, b) BH94 – DJF, c) TC80 – SON, d) BH94 –SON, the unit is cm month$^{-1}$, note the different scale.

is generally found over the Sichuan Basin and reaches up to -3cm in DJF and -7cm in SON for the BH94 scheme, but only -1cm in DJF and -2 cm in SON for the TC80 scheme. The spatial distribution in the precipitation reduction distribution is generally well-correlated with the AOD spatial distribution in DJF and SON, but not in JJA and MAM (not shown for brevity).

The above discussion shows that the 2nd indirect effect using BH94 scheme dramatically alters the cloudiness and precipitation, while the changes are considerably smaller for the TC80 scheme. This is expected from Equations (3.6) and (3.7): the BH94 scheme is much more strongly dependent on the aerosol perturbation than the TC80 scheme. Thus the model estimation of 2nd indirect effect on precipitation is very sensitive to the autoconversion parameterization, and this in turn suggests that large uncertainty exists in this estimation. GCM studies found that the global annual mean liquid water path increases by about 20% (Jones et al., 2001), and 17% (Lohmann and Feichter, 1997) using BH94 scheme, while only around 5% increase with the TC80 scheme (Jones et al., 2001). These changes in cloud liquid water path are consistent with what are found in this work. Ackerman et al. (2004) recently assessed the cloud water change due to the 2nd indirect for the marine stratocumulus clouds. They argued that the change of cloud water by the 2nd indirect effect would depend on the competition between the moistening from the suppressed surface precipitation and the drying from the increased entrainment of overlying water, and concluded that the impact of 2nd indirect effect is likely to be small. This result is most consistent with my results using TC80 scheme. Takemura et al. (2005), on the other hand, found a strong signal from the 2nd indirect effect in regions where a

large amount of anthropogenic aerosols and cloud water co-exist. This result would seem to favor my results using BH80 scheme.

### 3.3.4 The Partitioning between the 2nd Indirect Effect and the Combined Direct, Semi-direct and 1st Indirect Effects

I now turn to a discussion of the relative contributions of the 2nd indirect and the combined direct/semi-direct/1st indirect effects by comparing the results from the experiments INDIR1 and TCALL, BHALL (the latter two runs include all the aforementioned aerosol effects, i.e., direct and semi-direct effect, and as well as the 1st, 2nd indirect effects using TC80 and BH94 scheme, respectively). From Table 3.5, it can be seen that the BHALL and TCALL experiments generally reinforce the aerosol impacts from the aerosol radiative effects (INDIR1) in all aspects, except for cloud cover, liquid water path and the corresponding long-wave radiative forcing at TOA. In the INDIR1 experiment, the negative solar forcing is dominant over the negative long-wave forcing; this negative long-wave forcing (-0.5 W $m^{-2}$) in INDIR1 run is caused by the overall decrease in cloud cover and liquid water path. On the other hand, with the 2nd indirect effect, the long-wave forcing becomes positive, because of the increased cloud liquid water, and approaches the magnitude of the negative solar forcing. Again the BH94 scheme generates relatively larger impacts than the TC80 scheme.

The net radiative forcing at TOA is always negative for all experiments in Table 3.5: -4.6 W $m^{-2}$ from the direct, semi-direct and 1st indirect effects; -3.2 W $m^{-2}$ with the 2nd indirect effect using BH94 scheme; and -0.4 W $m^{-2}$ with the 2nd indirect effect using TC80 scheme. With all effects included, the TOA negative forcing ranges from -4.4 W $m^{-2}$ using TC80 scheme to -7.5 W $m^{-2}$ using BH94 scheme. These results are broadly

consistent with the findings of Lohmann and Feichter (1997), Lohmann et al. (2000) and Jones et al. (2001).

Table 3.5 also shows that with the inclusion of all aerosol effects, the annual mean precipitation reduction reaches -28% using the BH94 scheme averaged over the inner domain (land grid only), and -10% using TC80 scheme. The aerosol radiative effects (INDIR1) generate a decrease in both surface temperature and precipitation, while the 2$^{nd}$ indirect effect mainly decreases the precipitation and likely increase the surface temperature.

Finally, I present the spatial distribution in the seasonal precipitation change from the BHALL run in Figure 3.8. (The precipitation change from TCALL run is similar to INDIR1 run, since the 2$^{nd}$ indirect effect using TC80 scheme only generates a small change in precipitation, and thus is not shown here.) It can be seen that the precipitation reduction appears in all seasons over continental China, with the largest reduction occurring over a broad region extending from the Sichuan Basin to the northeastern/eastern coast of China, a pattern reasonably consistent with the distribution of anthropogenic aerosol loading calculated by the model. In comparison to the precipitation change from INDIR1 run (Figure 3.4) and 2$^{nd}$ indirect effect by itself (Figure 3.7b and d), the 2$^{nd}$ indirect effect using the BH94 scheme produces a significant precipitation reduction in spring and summer, in addition to winter and fall. The local precipitation reduction reaches up to 4cm month$^{-1}$ in winter and 7 cm month$^{-1}$ in other seasons.

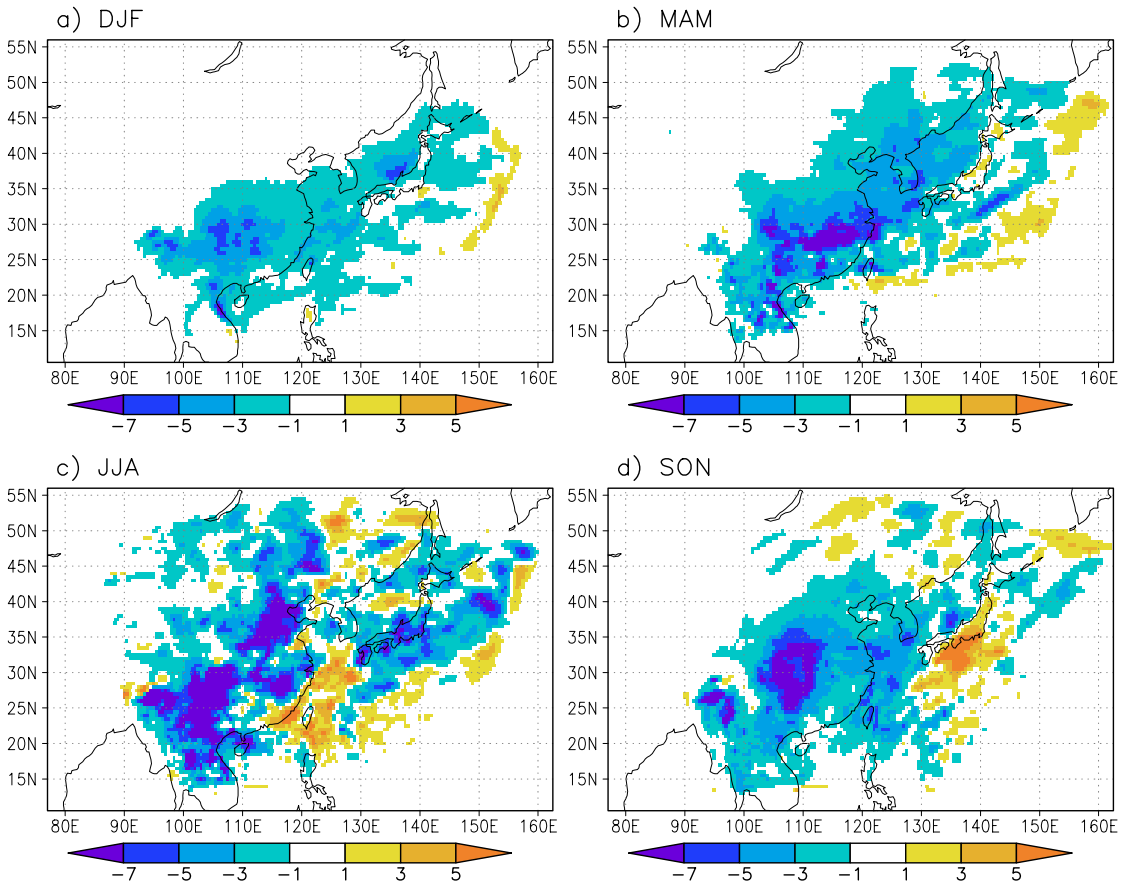


**Figure 3. 8** Similar to Figure 3.3, but for BHALL vs. BHCONT.

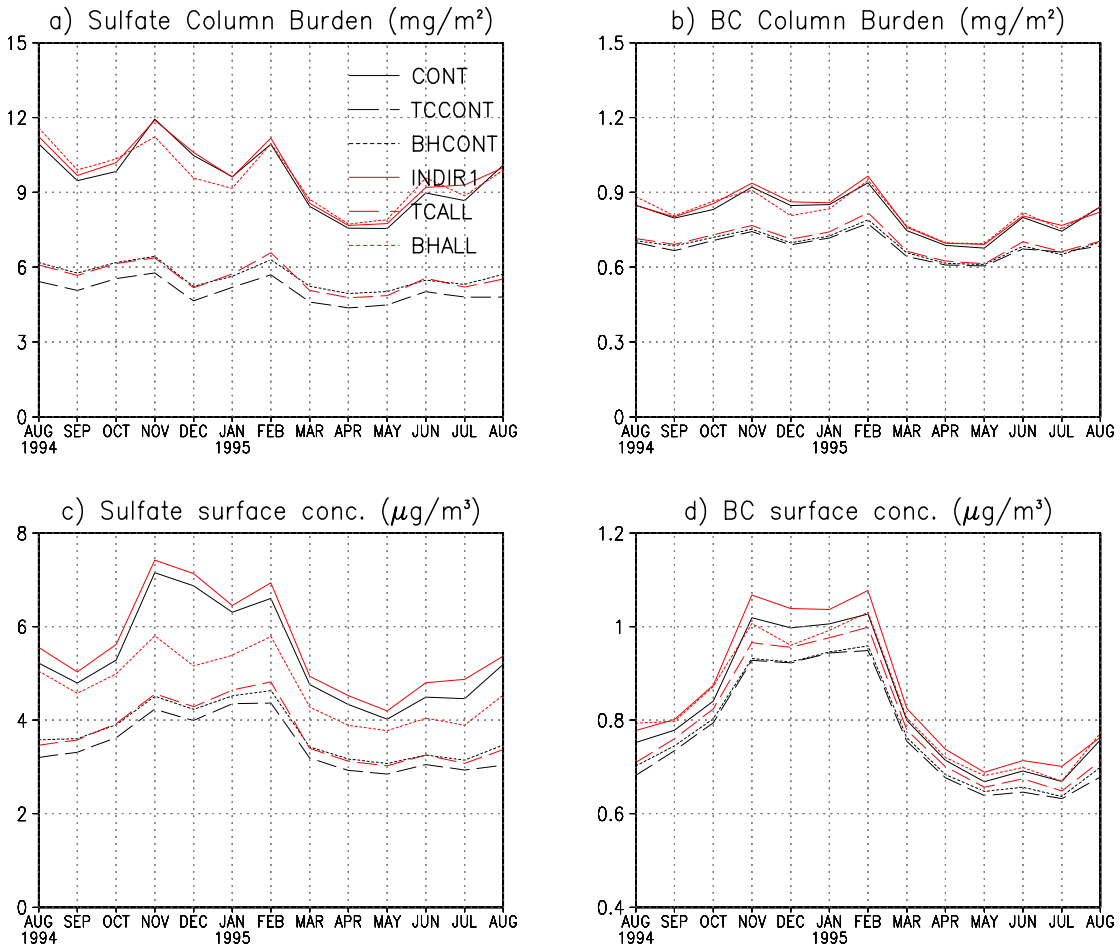


**Figure 3. 9** Seasonal variation of simulated sulfate and BC column burden and surface concentration from the control and indirect experiments (CONT, TCCONT, BHCONT, INDIR1, TCALL and BHALL). The unit for column burden is mg $m^{-2}$, and for surface concentration is μg $m^{-3}$.

### 3.3.5 Simulated Aerosol Distributions with Climatic Coupling

The spatial and temporal distribution of the model-simulated sulfate and carbonaceous aerosols from the CONT run were discussed and compared to the observations in Chapter 2. In brief, without interaction with climate using the KS69 scheme (CONT run), the model simulated aerosol were about 2/3 of the observed aerosol surface concentrations and aerosol optical depths (AOD) over East Asia. In this section, I present the results of simulations showing how the model-calculated aerosol distributions are affected by the inclusion of the climate-aerosol coupling parameterizations discussed above.

Before discussing the impact of including the climate-aerosol coupling, it is relevant to consider how the aerosol distributions are affected by the various auto-conversion parameterizations used here. This can be seen by comparing the sulfate and BC column burden and aerosol surface concentrations for CONT, TCCONT and BHCONT in Figure 3.9 (black lines). (The simulated OC variation is similar to BC, but approximately 10 times larger in magnitude, thus not shown.) Since the control runs using TC94 and BH80 schemes produce more precipitation (Figure 3.2b), and aerosols are removed by precipitation, the aerosol surface concentrations and column burdens are reduced in the TCCONT and BHCONT runs relative to those in the CONT run with KS69 scheme. The reductions of $SO_4^{2-}$ column burden (about 45% annually) are more pronounced than that of BC and OC (about 15%), because a significant fraction of the BC and OC is hydrophobic and unaffected by precipitation. The annual aerosol surface concentrations decrease by 35% and 6% for sulfate, and BC and OC, respectively. Thus, the simulated 'TOTAL' (see chapter 2 for the definition) surface aerosol concentration is reduced by ~

20%. The smaller reduction for aerosol surface concentration than the column burden is because wet removal occurs in clouds, which are generally above the boundary layer over the continental East Asia. Also notice that, among the three schemes, TC80 scheme produces the largest precipitation with the lowest aerosol loadings, while KS69 scheme generates the least precipitation with the highest aerosols loadings. Thus as in the case of the comparison between model simulated and observed precipitation, the use of the TC80 and BH94 parameterizations tends to worsen the agreement between model-simulated and observed aerosol concentrations. However, as will be discussed below, because the $2^{nd}$ indirect effect effectively reduces precipitation (especially for BH94 scheme), the inclusion of climate-aerosol coupling with the BH80 parameterization tends to bring the fully-coupled model-simulated aerosol concentrations closer to the observations when compared to their control runs.

As discussed earlier in Chapter 2, the aerosol concentration and column loading are determined by various processes, i.e. chemical conversion (both gas and aqueous phase), dry and wet removal processes, transport and emissions, etc. The climate change due to the aerosol effects could alter the production/removal/transport of aerosols, resulting in the increase (positive feedback) or decrease (negative feedback) of the initial aerosol perturbations. It can be seen from Table 3.7 that, with the $2^{nd}$ indirect effect only, the sulfate column burden increases by 68% and 9%, while the BC column burden increase by 15.5% and 2.5% for BH94 and TC80 schemes, respectively. On the other hand, the aerosol surface concentrations increase by about 20% and 3.5% for sulfate and carbonaceous aerosols, respectively, using BH94 scheme, and a nominal change is found using TC80 scheme. This is expected since the increase in cloud liquid water (Table 3.5)

favors the aqueous conversion from $SO_2$ to sulfate and the reduction in precipitation (see also Table 3.5) decreases the wet removal rate, especially for water soluble aerosols (i.e. sulfate). Thus a positive feedback between aerosols and climate is found here, with aerosols alternate climate in a manner that slows the removal of the aerosols and favors their further accumulation in the atmosphere. A similar positive feedback was also found by Qian and Giorgi (1999) who simulated the direct and 1$^{st}$ indirect effect of sulfate over the same region. In terms of the annual cycle of the aerosol loading and surface concentration with the aerosol-climate coupling, Figure 3.9 (red lines vs. black lines) reveals that the simulated aerosol loadings and concentrations from the INDIR1, TCALL and BHALL experiments all increase to some extent relative to their corresponding control runs, with the largest increase using BH94 scheme. Comparing to the aerosol observations, the simulated aerosols from the INDIR1 run using KS69 scheme are closest to the observed values among all coupling experiments.

**Table 3. 7** Relative changes in percent in annual mean sulfate and BC aerosol surface concentration and column burden for the indirect experiments to the corresponding control experiments (i.e., INDIR1 vs CONT, TCIND2 vs TCCONT, TCALL vs TCCONT, and BHIND2 vs BHCONT, BHALL vs BHCONT) .

| Experiments | INDIR1 | TCIND2 | TCALL | BHIND2 | BHALL |
|---|---|---|---|---|---|
| $\Delta SO_4^{2-}$-conc | +7.6 | +3.5 | +7.6 | +20.4 | +24.9 |
| ΔBC-conc | +3.6 | +0.9 | +3.7 | +2.8 | +6.4 |
| $\Delta SO_4^{2-}$-burden | +1.8 | +8.9 | +11.1 | +67.8 | +69.2 |
| ΔBC-burden | +1.5 | +2.5 | +3.2 | +15.5 | +17.5 |

### 3.3.6 Aerosol Induced Precipitation Signals in Climate Record

The results presented in Section 3.3.2 and 3.3.3 suggest that the anthropogenic aerosols cause a decrease in precipitation over East Asia. Depending upon the parameterization used for autoconversion, the model predicts that a precipitation reduction of as much as 28% may have occurred over the region as a result of the addition of anthropogenic aerosols to the atmosphere.

Over East Asia, anthropogenic emissions of aerosol precursors and primary aerosols has dramatically increased since the 1950s (Streets and Waldhoff, 2000; Tan et al., 2004). If the model results are correct, these emission increases should have had a significant impact on precipitation over the region. Now the question is: is there any aerosol-induced signal in the observed precipitation record of the past century to support these model results?

Figure 3.10 illustrates the spatial distribution of the observed linear trend for fall and winter precipitation (when the large scale precipitation generally dominates and the model predicts the largest aerosol impacts) over the last century based on the CRU 1901-2000 $0.5^{o}$ x $0.5^{o}$ monthly observed precipitation dataset over lands (developed by Mitchell et al. (2003)), interpolated onto the model grid used here. A decreasing trend (-1~ -2 mm per decade) is seen over the eastern coastal regions in both fall and winter seasons, and over the Sichuan Basin in the fall. This decreasing trend is consistent with the simulated maximum aerosol optical depth and precipitation reduction in the fall and winter, therefore, to some extent, it might be an indication of an aerosol induced signal.

However, since precipitation is affected by a combination of many different natural and anthropogenic influences (i.e. ENSO, increasing greenhouse gases concentrations,

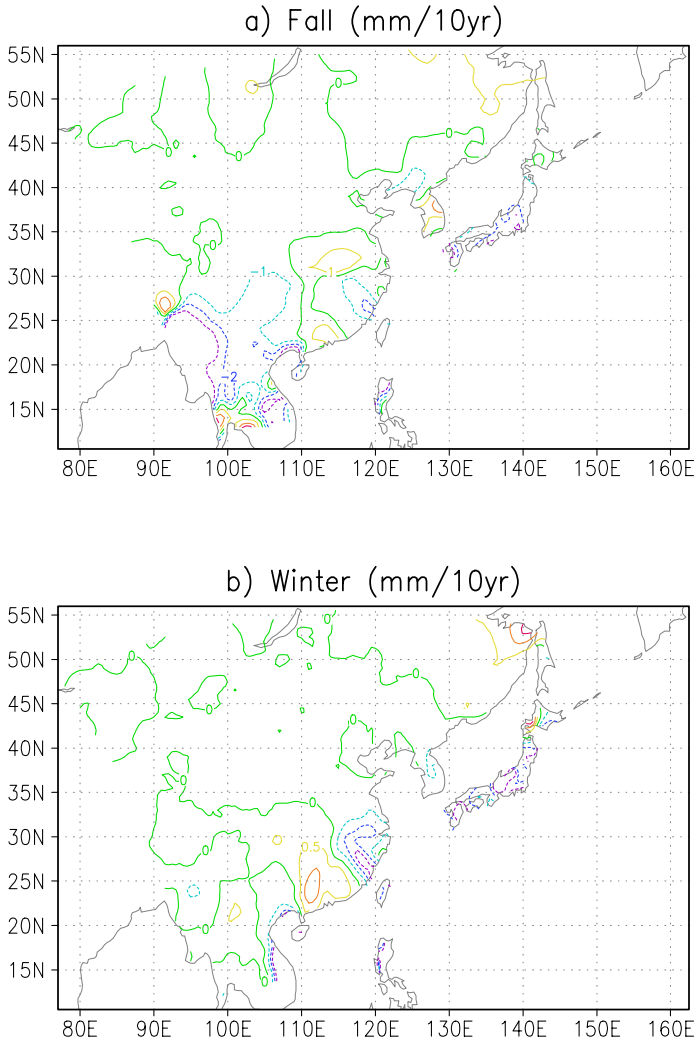


**Figure 3. 10** The spatial distribution of observed linear trends for the fall and winter precipitation using CRU monthly dataset. Unit is in mm/10yr, and the contour intervals are 1mm/10yr and 0.5mm/10yr for fall and winter, respectively.

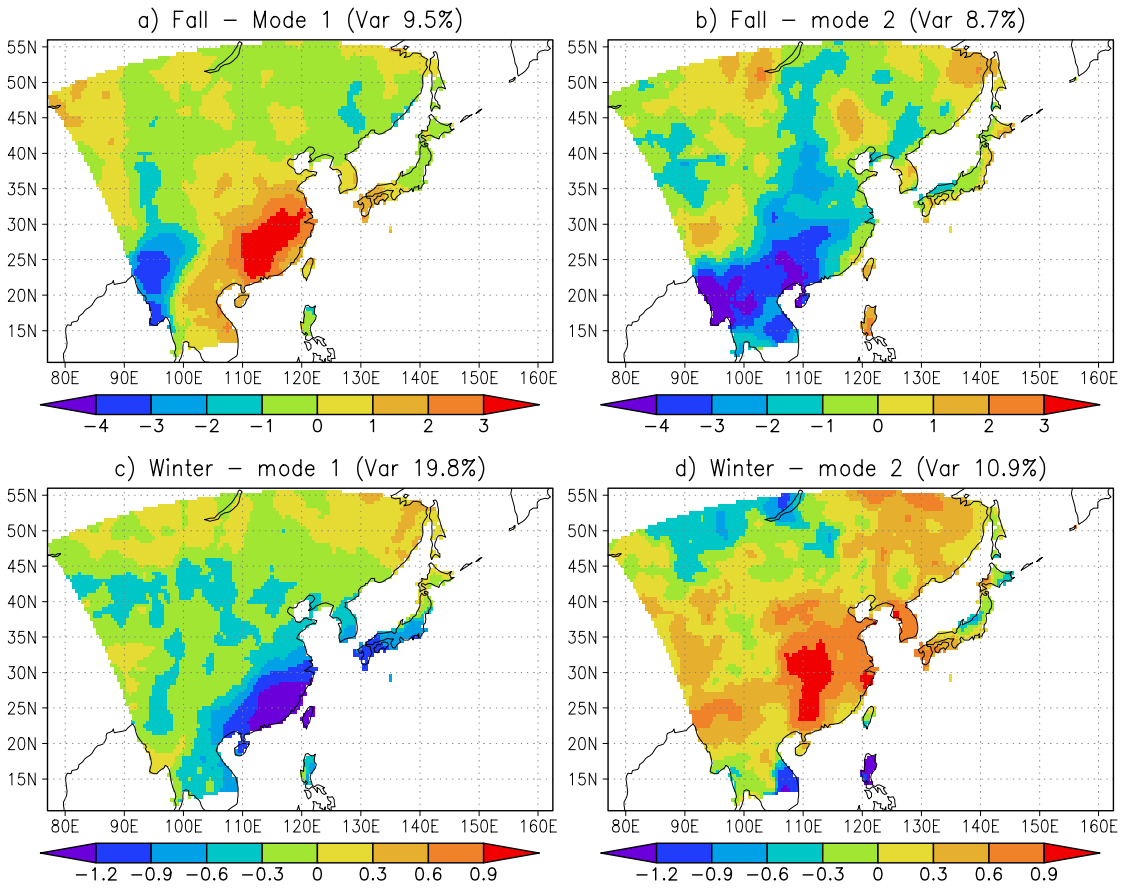


**Figure 3. 11** The spatial pattern of the 1st and 2nd EOF of fall and winter precipitation anomaly. Unit: mm/10yr. Note that the EOF loadings are converted into regionally aggregated precipitation anomalies associated with the principal component (PC).

and land use and land cover change, as well as aerosols), it is difficult to clearly identify the aerosol induced signal in the long term precipitation record by a simple linear least square regression method as used in Figure 3.10. Therefore, the 1901 ~ 2000 precipitation data was decomposed into different modes using Empirical Orthogonal Function (EOF) Analysis in an attempt to extract a potential aerosol-specific signal. Before the EOF analysis, the seasonal and annual precipitation anomalies were calculated, and normalized by their standard deviations. Figure 3.11 illustrates the spatial pattern of the 1st and 2nd leading EOF for the fall and winter precipitation anomalies, respectively, when the simulated precipitation reduction is largest. Table 3.8 gives the linear regression results (slopes and R-squares) for the time series of the associated 1st and 2nd principal coefficients (PC). It can be seen that the 2nd leading PC modes for the fall precipitation, and 1st leading PC mode for winter precipitation exhibit a decreasing trend of -1.27mm and -0.32mm per decade with an R-square of 0.17 and 0.05, respectively, and the trends are statistically significant using two-tailed t test given the number of samples of n=2472.

**Table 3. 8** Slopes and R-squares of linear regression equations for the 1st and 2nd principal components of the precipitation anomaly in the fall and winter.

| Principal Component (mm) | Slope (mm decade$^{-1}$) | R-square |
|---|---|---|
| Fall – PC1 | +0.90 | 0.07 |
| Fall –PC2 | -1.27 | 0.17 |
| Winter – PC1 | -0.32 | 0.05 |
| Winter – PC2 | +0.34 | 0.14 |

The 1st and 2nd leading modes explain 9.5% and 8.7% of the total variance for the fall precipitation, and larger variances (19.8% and 10.9%) for the winter precipitation. In terms of spatial distribution, in the fall, the 2nd leading EOF pattern (Figure 3.11b), exhibits a broad region of decreasing precipitation trend extending from Sichuan Basin to the east coastal area, while in the winter, the 1st leading EOF pattern (Figure 3.11c) shows a broad region of decreasing precipitation trend over the entire continental China. Thus the decreasing modes of the fall and winter observed precipitation appear to be qualitatively consistent with the model-predicted decrease in precipitation from aerosol impacts over the region. A more quantitatively comparison is presented below.

*3.3.6.1 Comparison between observed and model-predicted precipitation trends*

From Figure 3.7, it is seen that the decreasing modes for the fall and winter observed precipitation over the region yield downward trends of 2 ~ 3 mm/decade and 0.5 ~ 1.5 mm/decade, respectively. To estimate the trends predicted by the model calculations, first consider the spatial correlations between the simulated seasonally averaged aerosol optical depth and precipitation change between the INDIR1, TCALL and BHALL runs and their associated control runs over the inner domain land grids for the winter and fall season (Figure 3.12). In each case a negative slope is obtained. Give the number of samples (n=2472) and the $R^2$ values ranging from 0.16 to 0.60, the correlations are all statistically significant at the 95% confidence level. The magnitude of the slopes indicates the magnitude of the model-calculated precipitation reduction produced from one unit increase in AOD. For example, from the slopes illustrated in Figure 3.12a and b, one can infer that each unit increase of AOD results in a decrease in the monthly precipitation over the region of about 3.5 cm in SON, and 2.5 cm in DJF, respectively,

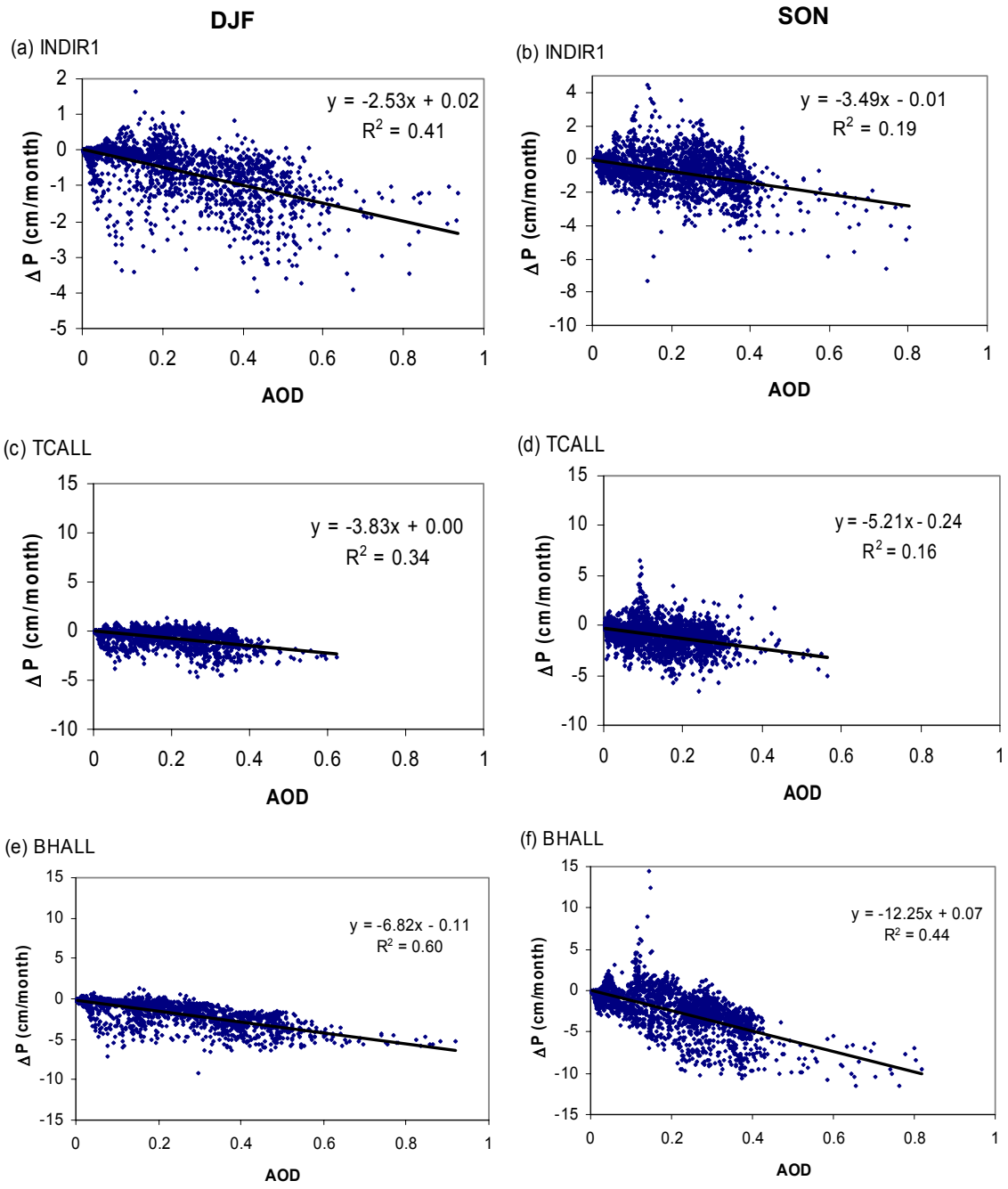


**Figure 3. 12** Scatterplots between seasonal precipitation change in cm/month and aerosol optical depth for INDIR1, TCALL and BHALL experiments in DJF (left column) and SON (right column) for land grids only over model inner domain, relative their corresponding control runs (CONT, TCCONT and BHCONT), respectively.

for INDIR1 run. The larger slopes from TCALL and BHALL experiments suggest that the inclusion of the second indirect effect enhances the simulated precipitation reduction for both winter and fall, and this enhancement is very large for BH94 scheme.

An estimate of the model-predicted precipitation trend can be obtained by multiplying the above slopes with the observed trend in AOD over the region. I adopt the AOD trend reported by Luo et al. (2001), where about +0.06 AOD increase per decade was obtained during 1961-1990 over the broad regions from Sichuan Basin extending eastward along the Yangtze River region. Given this AOD trend and the slopes of -3.5 and -2.5 from INDIR1 experiment, the simulated seasonal precipitation trend predicted by the INDIR1 run for the period of 1961-1990 can be estimated as the following

$$0.06\frac{AOD}{decade} * (-3.5\frac{cm}{month}\frac{1}{AOD}) = -0.2\frac{cm}{month}\frac{1}{decade} = -6\frac{mm}{decade}, \quad \text{in the fall}$$

$$0.06\frac{AOD}{decade} * (-2.5\frac{cm}{month}\frac{1}{AOD}) = -0.15\frac{cm}{month}\frac{1}{decade} = -4.5\frac{mm}{decade}, \quad \text{in the winter}$$

Given the larger negative slopes in Figure 3.12 for the TCALL and BHALL runs, the model predicted precipitation trends when the 2nd indirect effect is included are considerably larger than that indicated above. However, the decreasing trend in the 2nd leading EOF mode of the fall precipitation is only about 2 ~ 3 mm/decade and in the 1st leading EOF mode of the winter precipitation is only about 0.5 ~ 1.5mm/decade. Thus, while the model might be correctly predicting the direction of the precipitation change and the general geographic distribution from the anthropogenic aerosols, it is likely over-predicting the magnitude of the aerosol effect by a factor of 2 ~ 3. It is also possible that other processes not considered here (i.e. greenhouse gas effect, land cover change, etc) are damping the aerosol effects on precipitation in the observations.

From further inspection of Figure 3.12, it can be seen that, at larger AOD (i.e., > 0.4 in SON and > 0.6 in DJF), the slope tends to flatten. This implies that the effect of each unit increase of AOD would tend to produce a smaller precipitation reduction as the AOD gets larger. This suggests that the aerosol effect on precipitation is more pronounced and efficient at lower aerosol loadings over relative clean regions, and becomes saturated over highly polluted regions with large aerosol loadings. While not shown here, this also tends to be the case of radiative forcing and surface temperature changes.

## 3.4 Conclusions and Discussion

In this chapter, a fully coupled climate-chemistry-aerosol model is used to assess the anthropogenic sulfate and carbonaceous aerosol effects on regional climate over East Asia, with a focus on precipitation, and the long term seasonal precipitation data was analyzed in an attempt to extract the aerosol induced signal in the climate record. The primary conclusions can be summarized as follows:

1) The direct and 1$^{st}$ indirect aerosol effects generate a negative solar forcing at the surface while the semi-direct effect by BC absorption produces a positive atmospheric forcing and enhances the negative forcing at surface. The surface cooling (~ -0.35K) caused by the reduction of surface solar radiation, along with the atmospheric heating by the absorbing aerosol (BC), increases the atmospheric thermal stability, and thus tends to inhibit precipitation. In fall and winter, the direct effect decreases the precipitation by -4 ~ -7%, and the inclusion of 1$^{st}$ indirect effect further decrease the precipitation up to -10% ~ -13%. The precipitation reduction is largest in the fall and winter. The semi-direct effect slightly reduces the precipitation on average (~ -1%). In spring and summer, the precipitation reduction is relatively small.

2) The 2nd indirect effect is strongly dependent on the autoconversion scheme. The BH94 scheme produces a comparable long-wave heating as the solar cooling due to the increased cloud liquid water, and thus increase the surface air temperature, in particular the nighttime warming of 0.5K in winter. It also results a very large precipitation reduction (around -30%) for SON and DJF, and less reduction (about -15%) for JJA and MAM averaged over the model inner domain. The TC80 scheme only generates -3% reduction in precipitation for SON and DJF and a negligible effect in JJA and MAM.

3) The precipitation reduction by the aerosol effects simulated in the fully-coupled model, generally leads to a better agreement with observations. By allowing for climate-aerosol feedbacks, the discrepancies between the model-simulated and observed precipitation and aerosol loadings over East Asia generally decrease.

4) The EOF analysis on precipitation over last century confirms a decreasing trend in 2nd leading EOF mode of the fall precipitation and 1st mode of the winter precipitation over most of the continental China. The associated EOF spatial pattern is generally consistent with the distribution of the model simulated precipitation reduction from aerosols. However, the model simulates a larger reduction in precipitation from the aerosols than that seen in the observations, even without the inclusion of the 2nd indirect effect.

The large precipitation reductions from aerosols obtained here are consistent with the studies of Giorgi et al (2002 and 2003), who included the direct and 1st indirect effects. However, Menon et al. (2002b) found, using a global model with a prescribed aerosol distribution, that aerosols (primarily as a result of absorbing black carbon) cause an increase in precipitation over south China, and a decrease in north China in summer. In

this work, while the overall change in precipitation in the summer was small, the model-simulated summer precipitation change from DIRBC run tended to show alternating bands of increasing and decreasing precipitation from south to north china, possibly due to the BC induced vertical temperature profile changes. Thus while not totally consisted, the results reported here and in Menon et al. (2002b) show some similarities.

Several uncertainties and limitations are present here. First, the organic carbon emission was tripled to account for the underestimation of OC inventory and to better agree the observed aerosol optical depth. Second, the various mixing states between BC and other aerosols (external, core-coated and internal) lead to a large range of observed mass absorption coefficient, and the consequent radiative effect and the climate effect. The assumption of the core-coated BC mixing state in this work produces larger radiative forcing compared to the external mixing in the previous work of Giorgi et al. (2002). It can be expected that the effect from the internal mixing would be even larger. Third, the $1^{st}$ and $2^{nd}$ indirect effect was implemented by using the empirical relation between the cloud droplet number concentration and aerosol mass concentration and then diagnosing the cloud effective radius. As mentioned in Section 3.2.2, a number of the empirical relations and prognostic methods are available in the literature, which yields a considerable range of radiative forcing, hence the large uncertainty in the simulated precipitation reduction. Furthermore, model simulated precipitation reduction via $2^{nd}$ indirect effect is strongly dependent on the autoconversion schemes (TC80 and BH94, both are used in the literature to investigate the $2^{nd}$ indirect effect). More sensitivity tests and investigation on black carbon aerosol and $1^{st}$ and $2^{nd}$ indirect need to be performed in

the future in order to better understand the various aerosol effects, in particular, the interactions among the aerosols, clouds and precipitation.

# CHAPTER 4

# CONCLUSIONS

In this thesis, an aerosol module was developed and coupled with a regional climate model to assess the various aerosol effects on climate with a focus on precipitation over East Asia. Significant advances in this study include:

- The inclusion of all three major anthropogenic aerosols (i.e., sulfate, black carbon and organic carbon).
- The use of a fully coupled climate-chemistry-aerosol model allowing for the feedbacks between aerosol and climate.
- The implementation of various aerosol effects (i.e., direct, semi-direct, 1$^{st}$ and 2$^{nd}$ indirect effect), enabling the assessment of the relative impacts of these effects on precipitation, in addition to the radiative forcing and temperature, individually and in concert.
- Analysis of the long term precipitation record in an attempt to find an aerosol fingerprint that is consistent with the simulated precipitation change by aerosol effects over the region.

The major results and implications of this thesis are summarized in Section 4.1 and future research plans are given in Section 4.2.

## 4.1 Major Results and Implications

Six prognostic equations for $SO_2$, $SO_4^{2-}$, hydrophobic and hydrophilic BC and hydrophobic and hydrophilic OC are considered in the aerosol module, which include the various processes, i.e. emission, advection, dry and wet deposition, chemical production

and conversion. The simulated spatial and seasonal distributions of sulfate and carbonaceous aerosol are generally consistent with the observations, showing a maximum over Sichuan Basin and a broad region of high concentration extending to the eastern/northeastern coast of China. The aerosol concentrations are higher in winter and lower in summer. Comparing with the limited available observations, the model simulated 'TOTAL' aerosol concentration and optical depth are about 2/3 of the observed value. These results suggest that the model is capable of representing the anthropogenic sulfate and carbonaceous aerosol cycle over East Asia reasonably but conservatively.

Upon the implementation of various aerosol climatic effects, the fully coupled regional climate-chemistry-aerosol model is used to assess the aerosols' impacts on climate over East Asia. The direct, semi-direct and 1$^{st}$ indirect aerosol effects produce a surface cooling via a reduction of surface solar radiation. The semi-direct effect also heats the atmosphere by BC absorption. Together, these effects increase the atmospheric stability and tend to inhibit precipitation, generating a precipitation reduction of up to -10% in the fall and winter. The 2$^{nd}$ indirect aerosol effect is strongly dependent on the autoconversion precipitation schemes. It produces a large precipitation reduction of about -30% in the fall and winter, and about -15% in the spring and summer using BH94 scheme, while less than -5% using TC80 scheme.

The fully coupled model allows feedbacks to operate between the aerosol perturbation and climate change. These feedbacks act to decreases the precipitation and increase aerosol loadings, and, as a result, decrease the discrepancies between the model-simulated and observed precipitation and aerosols concentrations over East Asia.

The EOF analysis of the climatological precipitation from last century over East Asia reveals a decreasing trend in one of two EOF leading modes in the fall and winter. The associated EOF spatial pattern is generally consistent with the distribution of the model-simulated precipitation reduction from aerosols. However, the inferred model-simulated precipitation reduction is larger than that in the observations by a factor of 2 ~ 3, even without considering the 2nd indirect effect.

In conclusion, the preliminary finding of this study is that the anthropogenic aerosols decrease the precipitation over East Asia. This is supported by two aspects: 1) by allowing the interaction between aerosols and precipitation, the model-simulated precipitation decreases, and in turn better agrees with the observation; 2) a decreasing mode is seen in the EOF leading modes in the fall and winter precipitation when the model-simulated aerosol induced precipitation reduction is largest. This finding has several implications as following:

- The over-predicting precipitation reduction from the model suggests that the model might be sensitive in simulating the aerosol induced precipitation. A recent study by Ackermann et al (2004) assessed the cloud water change from the 2nd indirect effect, and argued that the 2nd indirect effect is likely to be small due to the competition between the moistening from the suppressed precipitation and entrainment of overlying dry air. This is most consistent with the simulation using TC80 scheme in this thesis, and thus, suggesting a weaker 2nd indirect effect.
- The precipitation reduction from the aerosols over East Asia, tends to slow down the hydrological cycle (Ramanathan et al., 2001b; Liepert et al., 2004), and this impact is in opposite direction as the effect of the greenhouse gases, which generally increase the

precipitation and exaggerates the water cycle. This implies that the anthropogenic aerosols play a crucial role in counteracting the greenhouse effect in precipitation, in addition to temperature, which has been neglected but may be important. Therefore, the emission control for sulfur species and carbonaceous aerosols in developed and some developing countries might be accelerating the greenhouse gas effect.

- The above offset also implies that the over-prediction in aerosol induced precipitation reduction is possibly caused by the other processes not considered in this model (i.e. greenhouse gas effect, land cover change, etc), which are damping the aerosol effect signal in the observed precipitation trend.
- Moreover, the reduction of precipitation at one place must be balanced by enhanced precipitation elsewhere, and as a result, the redistribution of precipitation from the most polluted areas to the cleaner areas, and in turn, the drought in polluted areas and flooding in other areas. Because the large amount of latent heat energy released from precipitation, these precipitation shifts are likely to cause shifts in the global circulation of atmosphere, including storm tracks.
- On the other hand, with the environmental regulation of pollution control to reduce the sulfur and carbonaceous aerosol emission in China (China SEPA, 2003), due to their short lifetime (~ 1 week or less), the atmospheric aerosol loadings will be decreasing provided the regulations take effect. Based on the positive feedbacks between the aerosol and precipitation found in this thesis, this reduction in aerosol loadings could results in precipitation increase, which can improve the water shortage problem, i.e. agriculture irrigation, desertification, and consequently lead to increase in crop yields and less frequency in dust events in China.

## 4.2 Future Research Plans

As discussed in Chapter 2 and 3, several uncertainties and limitation are presented in this thesis work, which should be addressed in future research:

- Since the model seems sensitive in simulating the precipitation reduction due to the aerosol effects comparing to the observed trend, and the aerosol indirect effect is the interactions between aerosols, clouds and hence precipitation, it might be useful to examine the model sensitivities of the parameterizations of indirect effects using the other aerosol-cloud relationships (i.e., prognostic methods, in which the number concentration of cloud droplet is explicitly represented by the aerosol concentration, cloud droplet nucleation, as well as the other relevant parameters). Considering the global and regional interactions might also improve the precipitation simulations since the precipitation change from aerosols are strongly affected by dynamical hydrological cycle (Takemura et al., 2004).

- On global annual mean basis, 60-70% of the absorbed solar radiation at the surface is balanced by the evaporation (Kiehl and Trenberth, 1997), thus, it is possible that a major fraction of the aerosol induced solar reduction is balanced by a reduction in rainfall and effectively spin down the hydrological cycle (Liepert et al, 2004). Therefore, further investigation regarding how aerosols affect the surface energy budget, and hence the precipitation will be necessary. In this regard, implementation of a more comprehensive land surface model using the satellite-derived simultaneous land cover data to better represent this land-atmosphere interaction would be a good step.

- Absorption by BC aerosols (mainly biomass burning) has received increasing attention in the aerosol-climate research area. Due to the complication in the mixing

states, and the relative location to the clouds, the estimation of its radiative and climatic effects varies at a large range. Observations in Amazonia show that, smoke suppresses the clouds, and on the other land, heats the clouds to make the updraft stronger. It would be interesting to apply this fully coupled model in the region to investigate the precipitation change from smoke aerosols there.

# REFERENCES


Ackerman, A. S., M. P. Kirkpatrick, D. E. Stevens and O. B. Toon (2004). The impact of humidity above stratiform clouds on indirect aerosol climate forcing, *Nature*, **432**, 1014 – 1017.

Ackerman, A.S., O.B. Toon, D.E. Stevens and J.A. Coakley Jr. (2003). Enhancement of cloud cover and suppression of nocturnal drizzle in stratocumulus polluted by haze, *Geophysical Research Letters*, **30**, 1381, doi: 10.1029/2002GL016634.

Ackerman, A.S., O.B. Toon, D.E. Stevens, A.J. Heymsfield, V. Ramanathan and E.J. Welton (2000). Reduction of tropical cloudiness by soot, *Science*, **288**, 1042-1047.

Ackerman, T.P. and O.B. Toon (1981). Absorption of visible radiation in atmosphere containing mixtures of absorbing and non-absorbing particles, *Applied Optics*, **20**, 3661-3668.

Albrecht, B.A. (1989). Aerosols, cloud microphysics, and fractional cloudiness, *Science*, **245**, 1227-1230.

Anderson, T.L., R.J. Charlson, S.E. Schwartz, R. Knutti, O. Boucher, H. Rodhe and J. Heintzenberg (2003). Climate forcing by aerosols – a Hazy picture, *Science*, **300** (5622), 1103-1104.

Andreae, M.O. (1995). Climatic effects of changing atmospheric aerosol levels, in *World Survey of Climatology, Vol. 16: Future Climates of the World*, Edited by A. Henderson-Sellers, Elsevier, Amsterdam, pp. 341-392.

Andreae, M.O., D. Rosenfeld, P. Artaxo, A.A. Costa, G.P. Frank, K.M. Longo, and M.A.F. Silva-Dias (2004). Smoking rain clouds over the Amazon, *Science*, **303**, 1337-1341.

Angstrom, A. (1929). On the atmospheric transmission of sun radiation and on dust in the air, *Geograf. Ann. Deut.*, **11**, 156-166.

Angstrom, A. (1961). Techniques of determining the turbidity of the atmosphere, *Tellus*, **13**, 214-223.

Angstrom, A. (1964). The parameters of atmospheric turbidity, *Tellus*, **16**, 64-65.

Anthes, R.A. (1977). A cumulus parameterization scheme utilizing a one-dimensional cloud model, *Monthly Weather Review*, **105**, 270-286.

Anthes, R.A. E.Y. Hsie, and Y.H. Kuo (1987). Description of the Penn State/NCAR Mesoscale Model Version 4 (MM4), *NCAR Technical Note,* **NCAR/TN-282+STR**, National Center for Atmospheric Research, Boulder, Colorado.

Balkanski, Y., D. Jacob, G. Gardner, W. Graustein and K. Turekian (1993). Transport and residence time of tropospheric aerosol inferred from a global three-dimensional simulation of $^{210}$Pb, *Journal of Geophysical Research*, **98**, 20,573-20,586.

Ball, R.J. and G.P. Robinson (1982). The origin of haze in the central United States and its on solar radiation, *Journal of Applied Meteorology*, **21**, 171-188.

Barrie, L.A., Y. Yi, W.R. Leaitch, et al. (2001). A comparison of large-scale atmospheric sulfate aerosol models (COSAM): overview and highlights, *Tellus*, **53B**, 615-645.

Beheng, K.D. (1994). A parameterization of warm cloud microphysical conversion processes, *Atmospheric Research*, **33**, 193-206.

Benkovitz, C. M., S. E. Schwartz (1997). Evaluation of modeled sulfate and $SO_2$ over North America and Europe for four seasonal months in 1986 - 1987, *Journal of Geophysical Research*, **102**(D21), 25,305-25,338.

Benkovitz, C.M., M.T. Scholtz, J. Pacyna, et al. (1996) Global gridded inventories of anthropogenic emissions of sulfur and nitrogen, *Journal of Geophysical Research*, **101**(D22), 29,239-29,254.

Bergin, M. H, W. Greenwald, J. Xu, Y. Berta and W.L. Chameides (2001a). Influence of aerosol dry deposition on photosynthetically active radiation available to plants: a case study in the Yangtze delta region of China, *Geophysical Research Letters*, **28**, 3605-3608.

Bergin, M. H., et al. (2004). Hong Kong and the Pearl River Delta Pilot Air Monitoring Project: Pilot study on the use of atmospheric measurements to manage air quality in Hong Kong and the Pearl River Delta, Project 2: Fine particulate matter ($PM_{2.5}$) in the Pearl River Delta (Final Report).

Bergin, M.H., G. R. Cass, J. Xu, C. Fang, L. M. Zeng, T. Yu, L.G. Salmon, C. S. Kiang, X. Y. Tang, Y. H. Zhang and W. L. Chameides (2001b). Aerosol radiative, physical, and chemical properties in Beijing during June 1999, *Journal of Geophysical Research*, **106**, 17,969-17,980.

Bodhaine, B.A. (1995). Aerosol absorption measurements at Barrow, Mauna Loa and the South Pole, *Journal of Geophysical Research*, **100**, 8967-8975.

Boucher, O. and U. Lohmann (1995). The sulfate-CCN-cloud albedo effect - A sensitivity study with two general circulation models, *Tellus*, **47B**, 281-300.

Boucher, O., Pham, M. and Sadourny, R. (1998). General circulation model simulations of the Indian summer monsoon with increasing levels of sulfate aerosols, *Annals of Geophysicae*, **16**, 346-352.

Brenguier, J.-L., H. Pawlowska, L. Schuller, R. Preusker, J. Fischer and Y. Fouquart (2000). Radiative properties of boundary layer clouds: Droplet effective radius versus number concentration, *Journal of the Atmospheric Sciences*, **57**(6), 803-821.

Briegleb, B.P. (1992). Delta-Eddington approximation for solar radiation in the NCAR Community Climate Model, *Journal of Geophysical Research*, **97**, 7603-7612.

Carrico, C. M., M. H. Bergin, J. Xu, K. Baumann, and H. Maring (2003). Urban aerosol radiative properties: Measurements during the 1999 Atlanta Super-site Experiment, *Journal of Geophysical Research*, **108**(D7), 8422, doi: 10.1029/2001JD001222.

Chameides, W.L. (1984). Photochemistry of a remote marine stratiform cloud, *Journal of Geophysical Research,* **89**, 4739-4755.

Chameides, W.L. (1995). The Yantze Delta of China as an evolving metro-agro-plex, proposal to the National Aeronautics and Space Administration, 55pp, Georgia Institute of Technology, Atlanta, GA.

Chameides, W.L., C. Luo, R. Saylor, D. Streets, Y. Huang, M. Bergin and F. Giorgi (2002). Correlation between model-calculated anthropogenic aerosols and satellite-derived cloud optical depths: Indication of indirect effect? *Journal of Geophysical Research,* **107**(D10), doi: 10.1029/2000JD000208.

Chameides, W.L., H. Yu, S.C. Liu, M. Bergin, X. Zhou, L. Mearns, G. Wang, C.S. Kiang, R.D. Saylor, C. Luo, Y. Huang, A. Steiner and F. Giorgi (1999a). Case study of the effects of atmospheric aerosols and regional haze on agriculture: An opportunity to enhance crop yields in China through emission controls? *Proceedings of National Academy of Sciences*, **96**, 13,626-13,633.

Chameides, W.L., P.S. Kasibhatla, H. Levy and W.J. Moxim (1994). Growth of continental scale metro-agro-plexes, regional ozone pollution and world food production, *Science*, **264**, 74-77.

Chameides, W.L., X. Li, X. Tang, X. Zhou, C. Luo, C.S. Kiang, J. St John, R.D. Saylor, S.C. Liu, K.S. Lam, T. Wang, F. Giorgi (1999b). Is ozone pollution affecting crop yields in china? *Geophysical Research Letters*, **26**, 867-870.

Charlson, R.J., J. Langner and H. Rodhe (1990). Sulfate aerosol and climate, *Nature*, **348**, 22.

Charlson, R.J., J. Langner and H. Rodhe, et al. (1991). Perturbation of the Northern Hemispheric radiative balance by backscattering form anthropogenic sulfate aerosols, *Tellus*, **43A**, 152-163.

Charlson, R.J., S.E. Schwartz, J. M. Hales, R.D. Cess, J. A. Coakley, Jr., J. E. Hansen and D. J. Hofmann (1992). Climate forcing by anthropogenic aerosols, *Science*, **255**, 423-430.

Chin, M., D.J. Jacob (1996). Anthropogenic and natural contributions to tropospheric sulfate: A global model analysis, *Journal of Geophysical Research*, **101**(D13), 18,691-18,700.

Chin, M., D.J. Jacob, G.M. Gardner, et al. (1996). A global three-dimensional model of tropospheric sulfate, *Journal of Geophysical Research*, **101**(D13), 18,667-18,690.

Chin, M., D.L. Savoie, B. J. Huebert, et al. (2000a). Atmospheric sulfur cycle simulated in the global model GOCART: Comparison with field observations and regional budgets, *Journal of Geophysical Research*, **105**(D20), 24,689-24,712.

Chin, M., R.B. Rood, S.-J. Lin, J.-F. Müller, A.M. Thompson (2000b). Atmospheric sulfur cycle simulated in the global model GOCART: Model description and global properties, *Journal of Geophysical Research*, **105**(D20), 24,671-24,688.

China, State Environmental Protection Administration (2003). Report on the state of the environment in China 2002, Beijing, China.

Chuang, C.C. and J.E. Penner (1995). Effects of anthropogenic sulfate on cloud drop nucleation and optical properties, *Tellus*, **47B**, 566-577.

Chuang, C.C. J.E. Penner, J.M. Prospero, et al. (2002). Cloud susceptibility and the first aerosol indirect forcing: Sensitivity to black carbon and aerosol concentration, *Journal of Geophysical Research*, **107**(D21), 4654, doi: 10.1029/2000JD000215.

Chuang, C.C., J.E. Penner, K.E. Taylor, A.S. Grossmann and J.J. Walton (1997). An assessment of the radiative effects of anthropogenic sulfate, *Journal of Geophysical Research,* **102**, 3761-3778.

Coakley, J.A. Jr., R.D. Cess and F.B. Yurevich (1983). The effect of tropospheric aerosols on the Earth's radiation budget: A parameterization for climate models, *Journal of the Atmospheric Sciences*, **40**, 116-138.

Coakley, J.A. Jr., R.L. Bernstein and P.A. Durkee (1987). Effect of ship-track effluents on cloud reflectivity, *Science*, **273**, 1020-1022.

Cooke, W.F. and Wilson J.J.N. (1996). A global black carbon aerosol model, *Journal of Geophysical Research,* **101**, 19,395-19,409.

Cooke, W.F., C. Liousse, Cachier, H. and Feichter J. (1999). Construction of a 1x1 fossil fuel emission data set for carbonaceous aerosol and implementation and radiative impact in the ECHAM4 model, *Journal of Geophysical Research,* **104**, 22,137-22,162.

Cotton, W.R. (1985). Atmospheric convection and nuclear winter, *American Scientist*, **73**(3), 275-280.

Crutzen, P.J., I.E. Galbally, C. Bruhl (1984). Atmospheric effects from post-nuclear fires, *Climatic Change*, **6**, 323-364.

DeMore, W.B., S. P. Sander, D. M. Golden, R.F. Hampson, M. J. Kurylo, C. J. Howard, A.R. Ravishankara, C. E. Kolb and M.J. Monila (1994). Chemical kinetics and photochemical data for use in stratospheric modeling, *Jet Propulsion Laboratory Pub*., **11**, 94-26.

Dennis, A.S. (1980). Weather modification by cloud seeding, *International Geophysics Series*, **24**, Academic Press, New York, 267pp.

Dickinson, R.E., A. Henderson-Selers and P.J. Kennedy (1993). Biosphere-atmosphere transfer scheme (BATS) version 1e as coupled to the NCAR Community Climate Mode, 72pp, *NCAR Technical Note*, **NCAR/TN-387+STR**, National Center for Atmospheric Research, Boulder, Colorado.

Ding, G., et al (1995). About acid deposition in china (in Chinese), China National Key Project about Acid Rain, China National Council of Sciences, Beijing, P.R. China.

Durkee, P.A., F. Pfeil, E. Frost and R. Shema (1991). Global Analysis of aerosol particle characteristics, *Atmospheric Environment*, **25A**, 2457-2471.

Eck, T. F., B. N. Holben, D.E. Ward, O. Dubovik, J.S. Reid, A. Smirnov, M. M. Mukelabai, N. C. Hsu, N.T. O'Neill and I. Slutsker (2001). Characterization of the optical properties of biomass burning aerosols in Zambia during the 1997 ZIBBEE field campaign, *Journal of Geophysical Research*, **106**, 3425-3448.

Feingold, G., W. L. Eberhard, D. E. Veron and M. Previdi (2003). First measurements of the Twomey indirect effect using ground-based remote sensors, *Geophysical Research Letters*, **30**, 1287, doi: 10.1029/2002GL016633.

Frisbie, P.R. and J.G. Hudson (1993). Urban cloud condensation nuclei spectral flux, *Journal of Applied Meteorology*, **32**, 666-676.

Fuller, K.A., W.C. Malm and S.M. Kreidenweis (1999). Effects of mixing on extinction by carbonaceous particles, *Journal of Geophysical Research*, **104**, 15,941-15,954.

Ganzeveld, L., J. Lelieveld, and G. J. Roelofs (1998). A dry deposition parameterization for sulfur oxides in a chemistry and general circulation model, *Journal of Geophysical Research*, **103**, 5679-5694.

Ghan, S.J., N. Laulainen, R. Easter, R. Wagener, S. Nemesure, E. Chapman, Y. Zhang and R. Leung (2001a). Evaluation of aerosol direct radiative forcing in MIRAGE, *Journal of Geophysical Research*, **106**, 5295-5316.

Ghan, S.J., R.C. Easter, E.G. Chapman, H. Abdul-Razzak, Y. Zhang, L.R. Leung, N.S. Laulainen, R. D. Saylor and R. Z. Zaveri (2001b). A physically based estimate of radiative forcing by anthropogenic sulfate aerosol, *Journal of Geophysical Research*, **106**, 5279-5293.

Ghan, S.J., R.C. Easter, J. Hudson and F,-M. Breon (2001c). Evaluation of aerosol indirect radiative forcing in MIRAGE, *Journal of Geophysical Research*, **106**, 5317-5334.

Giorgi, F. and G. Visconti (1989). Two-dimensional simulations of a possible mesoscale effects of nuclear war fires. 2. Model results, *Journal of Geophysical Research*, **94**, 1145-1163.

Giorgi, F. and L. O. Mearns (1991). Approaches to the simulation of regional climate change: A review, *Reviews of Geophysics*, **29**, 191-216.

Giorgi, F. and M.R. Marinucci (1996). An investigation of the sensitivity of simulated precipitation to model resolution and its implications for climate studies, *Monthly Weather Review*, **124**, 148-166.

Giorgi, F. and W. L. Chameides (1986). Rainout lifetimes of highly soluble aerosols and gases as inferred from simulations with a general circulation model, *Journal of Geophysical Research*, **91**, 14,367-14,376.

Giorgi, F., M.R. Marinucci, and G.T. Bates (1993a). Development of a second-generation regional climate model (RegCM2). Part I: Boundary-layer and radiative transfer processes. *Monthly Weather Review*, **121**, 2794-2813.

Giorgi, F., M.R. Marinucci, G.T. Bates, and G. De Canio (1993b). Development of a second-generation regional climate model (RegCM2). Part II: Convective processes and assimilation of lateral boundary conditions. *Monthly Weather Review*, **121**, 2814-2832.

Giorgi, F., Y. Huang, K. Nishizawa and C. Fu (1999). A seasonal cycle simulation over eastern Asia and its sensitivity to radiative transfer and surface processes. *Journal of Geophysical Research*, **104**, 6403-6423.

Giorgi, G. and C. Shields (1999). Tests of precipitation parameterizations available in the latest version of the NCAR regional climate model (RegCM) over continental U.S., *Journal of Geophysical Research*, **104**, 6353-6375.

Giorgi, G., X. Q. Bi and Y. Qian (2002). Direct radiative forcing and regional climatic effects of anthropogenic aerosols over East Asia: a regional coupled climate-chemistry/aerosol model study, *Journal of Geophysical Research*, **107**, 4439, doi: 10.1029/2001JD001066.

Giorgi, G., X. Q. Bi and Y. Qian (2003). Indirect vs. direct effects of anthropogenic sulfate on the climate of East Asia as simulated with a regional coupled climate-chemistry/aerosol model, *Climatic Change*, **58**, 345-376.

Golding, B.W., P. Goldsmith, N.A. Machin, A. Slingo (1986). Importance of local mesoscale factors in any assessment of nuclear winter, *Nature*, **319**, 301-303.

Graf, Hans-F. (2004). The complex interaction of aerosols and clouds, *Sciences*, **303**, 1309-1311.

Grell, G.A., J. Dudhia and D.R. Stauffer (1994). A description of the fifth-generation Penn State/NCAR mesoscale model (MM5). *NCAR Technical Note*, **NCAR/TN-398+STR**, 117 pp.

Gunn, R. and B.B. Phillips (1957). An experimental investiagation of the effect of air pollution on the initiation of rain, *Journal of the Atmospheric Sciences*, **14**, 272-280.

Han, Q. W.B. Rossow, J. Chou and R.M. Welch (1998a). Global variation of column droplet concentration in low-level clouds, *Geophysical Research Letters*, **25**, 1419-1422.

Han, Q. W.B. Rossow, J. Chou and R.M. Welch (1998b). Global survey of the relationships of cloud albedo and liquid water path with droplet size using ISCCP, *Journal of Climate*, **11**, 1516-1528.

Han, Q., W.B. Rossow and A.A. Lacis (1994). Near-global survey of effective droplet radii in liquid water clouds using ISCCP data, *Journal of Climate*, **7**, 465-497.

Hansen, J., M. Sato, A. Lacis, R. Ruedy, I. Tegen and E. Matthews (1998). Climate forcings in the Industrial Era, *Proceedings of National Academy of Sciences* **95**, 12,753-12,758.

Hansen, J.E, M. Sato and R. Ruedy (1995). Long-term changes of the diurnal temperature cycle: Implications about mechanisms of global climate change, *Atmospheric Research*, **37**, 175-209.

Hansen, J.E, M. Sato and R. Ruedy (1997). Radiative forcing and climate response, *Journal of Geophysical Research*, **102**, 6831-6864.

Hansen, J.E., A. Lacis, R. Ruedy, M. Sato and H. Wilson (1993). How sensitive is the world's climate? *National Geographic Research and Exploration*, **9**, 142-158.

Hansen, J.E., R. Ruedy, M. Sato, et al. (2001). A closer look at United States and global surface temperature change, *Journal of Geophysical Research*, **106**, 23,947-963.

Haywood, J.M. and K.P. Shine (1995). The effect of anthropogenic sulfate and soot on the clear sky planetary radiation budget, *Geophysical Research Letters*, **22**, 603-606.

Haywood, J.M. and O. Boucher (2000). Estimates of the direct and indirect radiative forcing due to the tropospheric aerosols: A review, *Reviews of Geophysics*, **38**, 513-543.

Haywood, J.M. and V. Ramaswamy (1998). Global sensitivity studies of the direct radiative forcing due to anthropogenic sulfate and black carbon aerosols, *Journal of Geophysical Research*, **103**, 6043-6058.

Haywood, J.M., D.L. Roberts, A. Slingo, J.M. Edwards and K.P. Shine (1997). General circulation model calculations of the direct radiative forcing by anthropogenic sulfate and fossil-fuel soot aerosol, *Journal of Climate,* **10**, 1562-1577.

Hegg, D. A. and P.V. Hobbs (1987). Comparisons of sulfate production due to ozone oxidation in cloud with a kinetic rate equation, *Geophysical Research Letters*, **14**, 719-721.

Hegg, D.A. (1994). Cloud condensation nucleus-sulfate mass relationship and cloud albedo, *Journal of Geophysical Research*, **99**, 25,903-25,907.

Hegg, D.A., R.J. Ferek and P.V. Hobbs (1993). Light scattering and cloud condensation nucleus activity of sulfate aerosols measured over the Northeast Atlantic Ocean, *Journal of Geophysical Research*, **98**, 14,887-14,894.

Heintzenberg, J., R. J. Charlson, A. D. Clarke, C. Liousse, V. Ramaswamy, K. P. Shine, M. Wendisch, and G. Helas (1997). Measurements and modeling of aerosol single-scattering albedo: Progress, problems and prospects. *Contributions to Atmospheric Physics,* **70**(4), 249-263.

Hobbs, P.V. and L.F. Radke (1969). Cloud condensation nuclei from a simulated forest fire, *Science*, **163**, 279-280.

Hobbs, P.V., H. Harrison and E. Robinson (1974). Atmospheric effects of pollutants, *Science*, **183**, 909-915.

Holtslag, A.A.M., E.I.F. de Bruijin, and H.L. Pan (1990). A high resolution air mass transformation model for short-range weather forecasting. *Monthly Weather Review*, **118**, 1561-1575.

Horvath, H. (1993). Atmospheric light absorption – a review, *Atmospheric Environment*, **27A**, 293-317.

Huang, Y. and H. Xu (1994). Seeding modeling on hail suppression with AgI particles, *Chinese Journal of Atmospheric Sciences*, **18**, 383-394.

Hudson, J.G. (1991). Observations of anthropogenic cloud condensation nuclei, *Atmospheric Environment*, **25A**, 2449-2455.

Hudson, J.G. and H. Li (1995). Microphysical contrasts in Atlantic stratus, *Journal of the Atmospheric Sciences*, **52**, 3031-3040.

Huebert, B.J., T. Bates, P. B. Russell, G. Shi, Y. J. Kim, K. Kawamura, G. Carmichael, T. Nakajima (2003). An overview of ACE-Asia: Strategies for quantifying the relationships between Asian aerosols and their climatic impacts, *Journal of Geophysical Research*, **108**(D23), 8633, doi:10.1029/2003JD003550.

Husar, R.B., J. M. Holloway and D.E. Patterson (1981). Spatial and temporal pattern of eastern U.S. haziness: A summary, *Atmospheric Environment*, **15**, 1919-1928.

Husar, R.B., J.D. Husar and L Martin (2000). Distribution of continental surface aerosol extinction based on visual range data, *Atmospheric Environment*, **34**, 5067-5078.

Husar, R.B., J.M. Prospero and L.L. Stowe (1997). Characterization of tropospheric aerosols over the oceans with the NOAA advanced very high resolution radiometer optical thickness operational product, *Journal of Geophysical Research*, **102**(D14), 16,889-16,909.

IPCC (1995). Climate change 1994: Radiative forcing of climate change and an evaluation of the IPCC IS92 emission scenarios, Edited by J.T. Houghton et al., 339p, Cambridge University Press, New York.

Jacobson, M.Z. (2000). A physically-based treatment of elemental carbon optics: Implications for global direct forcing of aerosols, *Geophysical Research Letters*, **27**, 217-220.

Jacobson, M.Z. (2001). Strong radiative heating due to the mixing state of black carbon in atmospheric aerosols, *Nature*, **409**, 695 - 697.

Jones, A. and Slingo A. (1996). Predicting cloud-droplet effective radius and indirect sulfate aerosol forcing using a general circulation model, *Quarterly Journal of the Royal Meteorological Society*, **122**, 1573-1595.

Jones, A., D.L. Roberts and A. Slingo (1994). A climate model study of indirect radiative forcing by anthropogenic aerosols, *Nature*, **370**, 450-453.

Jones, A., D.L. Roberts, M. J. Woodage and C. E. Johnson (2001). Indirect sulfate aerosol forcing in a climate model with an interactive sulfur cycle, *Journal of Geophysical Research*, **106**, 20,293-20,310.

Junge, C.E. (1975). The possible influence of aerosols on the general circulation and climate and possible approaches for modeling, Appendix 10 of *The physical Basic of climate and Climate Modeling*, GARP publications, **16**, WMO, Geneva.

Kaiser, D.P. and Y. Qian (2002). Decreasing trends in sunshine duration over China for 1954-1998: Indication of increased haze pollution? *Geophysical Research Letters*, **29**(21), 2042, doi: 10.1029/2002GL016057.

Karl, T.R., R.W. Knight, G. Kukla and G. Gavin (1995). Evidence for the radiative effects of anthropogenic sulfate aerosols in the observed climatic record, in Aerosol Forcing of Climate, edited by R. Charlson and J. Heintzenberg, p. 363-382, John Wiley, New York.

Kasibhatla, P., W.L. Chameides and J. St. John (1997). A three dimensional global model investigation of seasonal variation in the atmospheric burden of anthropogenic sulfate aerosols, *Journal of Geophysical Research*, **102**, 3737-3759.

Kaufman, Y. J., D. Tanré, L. A. Remer, E. F. Vermote, A. Chu, B. N. Holben (1997). Operational remote sensing of tropospheric aerosol over land from EOS moderate resolution imaging spectroradiometer, *Journal of Geophysical Research*, **102**(D14), 17,051-17,068, 10.1029/96JD03988.

Kaufman, Y.J. and R.S. Fraser (1997). The effect of smoke particles on clouds and climate forcing, *Science*, **277**, 1636-1639.

Kessler, E. (1969). On the distribution and continuity of water substance in atmospheric circulations, *Meteorological Monographs*, **32**, American Meteorological Society, Boston, MA, 84pp.

Kiehl, J. T., T. L. Schneider, P. J. Rasch, M. C. Barth and J .Wong (2000). Radiative forcing due to sulfate aerosols from simulations with the NCAR community Climate Model, *Journal of Geophysical Research*, **105**, 1441-2739.

Kiehl, J.T. and B.P. Briegleb (1993). The relative roles of sulfate aerosols and greenhouse gases in climate forcing, *Science*, **260**, 311-314.

Kiehl, J.T. and H. Rodhe (1995). Modeling geographical and seasonal forcing due to aerosols, in *Proceedings of the Dahlem Workshop on Aerosol Forcing of Climate*, Edited by R.J. Charlson and J. Heintzenberg, John Wiley & Sons, Chichester.

Kiehl, J.T. and K. E. Trenberth (1997). Earth's annual global mean energy budget, *Bulletin of the American Meteorological Society*, **78**, 197-208.

Kiehl, J.T., J.J. Hack, G.B. Bonan, B.A. Boville, B.P. Briegleb, D.L.Williamson, and P.J. Rasch (1996). Description of the NCAR Community Climate Model (CCM3), *NCAR Technical Note*, **NCAR/TN-420+STR**, 152pp.

King, M.D., L.F. Radke and P.V. Hobbs (1993). Optical properties of marine stratocumulus clouds modified by ships, *Journal of Geophysical Research*, **98**, 2729-2739.

Koch D. (2001). Transport and direct radiative forcing of carbonaceous and sulfate aerosols in the GISS GCM, *Journal of Geophysical Research*, **106**, 20,311-20,332.

Koch, D., D. Jacob, I. Tegen, et al. (1999). Tropospheric sulfur simulation and sulfate direct radiative forcing in the Goddard Institute for Space Studies general circulation model, *Journal of Geophysical Research*, **104**, 23,799-23,822.

Koren, I., Y. J. Kaufman, L. A. Remer and J. V. Martins (2004). Measurement of the effect of Amazon smoke on inhibition of cloud formation, *Science*, **303**, 1342-1345.

Kuang, Z. and Y.L. Yung (2000). Reflectivity variations off the Peru coast: evidence for indirect effect of anthropogenic sulfate aerosols on clouds, *Geophysical Research Letters*, **27**, 2501-2504.

Langner, J. and H. Rodhe (1991). A global three-dimensional model of the tropospheric sulphur cycle, *Journal of Atmospheric Chemistry*, **13**, 225-263.

Langner, J., H. Rodhe, P.J. Crutzen and P. Zimmermann (1992). Anthropogenic influence on the distribution of tropospheric sulfate aerosol, *Nature*, **359**, 712-716.

Leaitch, W.R. and G.A. Isaac (1994). On the relationship between sulfate and cloud droplet number concentration, *Journal of Climate*, **7**, 206-212.

Leaitch, W.R., G.A. Isacc, J.W. Strapp, C.M. Banic and H.A. Wiebe (1992). The relationship between cloud droplet number concentrations and anthropogenic pollution: Observations and climatic implications, *Journal of Geophysical Research*, **97**, 2463-2474.

Levine, S.Z. and S.E. Schwartz (1982). In-cloud and below-cloud scavenging of nitric acid vapor, *Atmospheric Environment*, **16**, 1725-1734.

Li, X., X. Zhou, W. Li and L. Chen (1995). The cooling of Sichuan province in recent 40 years and its probably mechanisms, *Acta Meteorologica Sinica*, **9**, 57-68.

Liepert, G. G., J. Feichter, U. Lohmann and E. Roeckner (2004). Can aerosols spin down the water cycle in a warmer and moister world? *Geophysical Research Letters*, **31**, L06207, doi: 10.1029/2003GL019060.

Liousse, C., H. Cachier and S.G. Jennings (1993). Optical and thermal measurements of black carbon aerosol content in different environments: variation of the specific attenuation cross-section, sigma, *Atmospheric Environment*, **27A**, 1201-1211.

Liousse, C., J.E. Penner, C.C Chuang, J.J. Walton and H. Eddleman (1996). A global three dimensional model study of carbonaceous aerosols, *Journal of Geophysical Research*, **101**, 19,411-19,432.

Lohmann, U. and J. Feichter (1997). Impact of sulfate aerosols on albedo and lifetime of clouds: A sensitivity study with the ECHAM4 GCM, *Journal of Geophysical Research*, **102**, 13,685-13,700.

Lohmann, U. and J. Feichter (2001). Can the direct and semi-indirect aerosol effect compete with the indirect effect on a global scale? *Geophysical Research Letters*, **28**, 159-161.

Lohmann, U., J. Feichter, J. Penner and R. Leaitch (1999). Predicting the number of cloud droplets in ECHAM GCM, *Journal of Geophysical Research*, **104**, 9169-9198.

Lohmann, U., J. Feichter, J. Penner and R. Leaitch (2000). Indirect effect of sulfate and carbonaceous aerosols: A mechanistic treatment, *Journal of Geophysical Research*, **105**, 12,193-12,206.

Luo, C., J. St. John, X. Zhou, K.S. Lam, T. Wang and W.L. Chameides (2000). A nonurban ozone air pollution episode over eastern China: Observations and model simulations, *Journal of Geophysical Research*, **105**, 1889-1908.

Luo, Y. F., D. R. Lu, X. Zhou, W. Li and Q. He (2001). Characteristics of the spatial distribution and yearly variation of aerosol optical depth over China in last 30 years, *Journal of Geophysical Research,* **106**(D13), 14,501-14,513.

Malone, R.c., L.H. Auer, G.A. Glatmaier, M.C. Wood, O.B. Toon (1985). Influence of solar heating and precipitation scavenging on the simulated lifetime of post-nuclear war smoke, *Science*, **230**, 317-319.

Malone, R.C., L.H. Auer, G.A. Glatzmaier, M.C. Wood (1986). Nuclear winter: Three-dimensional simulations including interactive transport, scavenging, and solar heating of smoke, *Journal of Geophysical Research*, **91**, 1039-1053.

Martin, G.M., D.W. Johnson and A. Spice (1994). The measurements and parameterization of effective radius of droplets in warm stratocumulus clouds, *Journal of the Atmospheric Sciences*, **51**, 1823-1842.

Menon, S., A. D. Del Genio, D. Koch and G. Tselioudis (2002a). GCM simulations of the aerosol indirect effect: Sensitivity to cloud parameterization and aerosol burden, *Journal of the Atmospheric Sciences*, **59**, 692-713.

Menon, S., J. Hansen, L. Nazarenko and Y. Luo (2002b). Climate effects of black carbon aerosols in China and India, *Science*, **297**, 2250-2253.

Meszaros, E. (1992). Structure of continental clouds before the industrial era: A mystery to be solved, *Atmospheric Environment*, **26A**, 2469-2470.

Mitchell, T.D., T.R. Carter, P.D. Jones, M. Hulme and M. New (2003). A comprehensive set of high-resolution grids of monthly climate for Europe and the globe: the

observed record (1901-2000) and 16 scenarios (2001-2100). *Journal of Climate*, submitted.

Myhre. G., F. Stordal, K. Restad and I. S. A. Isaksen (1998). Estimation of the direct radiative forcing due to the sulfate and soot aerosols, *Tellus*, **50B**, 463-477.

NAPAP (1990). Acid Deposition: *State of science and technology, National Acid Precipitation Assessment Program, Summary Report*, Washington DC.

Nenes, A. and J. H. Seinfeld (2003). Parameterization of cloud droplet formation in global climate models, *Journal of Geophysical Research*, **108**(D14), 4415, doi: 10.1029/2002JD002911.

Novakov, T., C. Rivera-Carpio, J.E. Penner and C.F. Rogers (1994). The effect of anthropogenic sulfate aerosols on marine cloud droplet concentrations, *Tellus*, **46B**, 132-141.

Novakov, T., D.A. Hegg and P.V. Hobbs (1997). Airborne measurements of carbonaceous aerosols on the East Coast of the United States, *Journal of Geophysical Research*, **102**, 30,023-30,030.

NRC (National Research Council) (1996). *A plan for a research program on aerosol radiative forcing and climate change*, National Academic Press, Washington DC.

Penner, J.E., C.C. Chuang and K. Grant (1998). Climate forcing by carbonaceous and sulfate aerosols, *Climate Dynamics*, **14**, 839-851.

Penner, J.E., C.S. Atherton and T.A. Graedel (1994). Global emissions and models of photochemically active compounds, in *Global Atmospheric-Biospheric Chemistry*, Edited by R.G. Prinn, pp. 223-247, Plenum, New York.

Penner, J.E., H. Eddleman and T. Novakov (1993). Towards the development of a global inventory for black carbon emissions, *Atmospheric Environment*, **27A**, 1277-1295.

Penner, J.E., M. Andreae, H. Annegarn, L. Barrie, J. Feichter, D.A. Hegg, R. Leaitch, D. Murphy, J. Nganga, G. Pitari (2001). Aerosols, their direct and indirect effects, in *Climate Change 2001: The Scientific Basis, Contribution of Working group I to the Third Assessment Report of the Intergovernmental panel on climate Change (IPCC)*, Edited by J.T. Houghton et al., chapter 5, pp289-348, Cambridge University Press, New York.

Penner, J.E., R.E. Dickinson and C.A. O'Neill (1992). Effects of aerosol from biomass burning on the global radiation budget, *Science*, **256**, 1432-1434.

Penner, J.E., S.Y. Zhang, M. Chin, et al. (2002). A comparison of model- and satellite-derived aerosol optical depth and reflectivity, *Journal of the Atmospheric Sciences*, **59**(3), 441-460.

Pham, M., J.-F. Muller, G. Brasseur, C. Granier and G. Megie (1995). A three-dimensional study of the tropospheric sulfur cycle, *Journal of Geophysical Research*, **100**, 26,061-26,092.

Pincus, R. and M. Baker (1994). Precipitation, solar absorption and albedo susceptibility in marine boundary layer clouds, *Nature*, **372**, 250-252.

Pruppacher, H.R., and Klett J.D. (1997). Microphysics of clouds and precipitation, 2nd ed., Kluwer Acad., Dordrecht, The Netherlands.

Qian, Y. and F. Giorgi (1999). Interactive coupling of regional climate and sulfate aerosol models over eastern Asia, *Journal of Geophysical Research*, **104**, 6477-6499.

Qian, Y. and F. Giorgi (2000). Regional climatic effects of anthropogenic aerosols? The case of Southwestern China, *Geophysical Research Letters*, **27**, 3521-3524.

Qian, Y., F. Giorgi, Y. Huang, W. Chameides and C. Luo (2001). Regional simulation of anthropogenic sulfur over East Asia and its sensitivity to model parameters, *Tellus*, **53B**, 171-191.

Qian, Y., L. R. Leung, S. J. Ghan and F. Giorgi (2003). Regional climate effects of aerosols over China: modeling and observation, *Tellus*, **55B**, 914-934.

Radke, L.F. and P.V. Hobbs (1976). Cloud condensation nuclei on the Atlantic seaboard of the United States, *Science*, **193**, 999-1002.

Radke, L.F., C.A. Brock, J.H. Lyons, P.V. Hobbs and R.C. Schnell (1989a). Aerosol and lidar measurements of hazes in mid-latitude and polar air masses, Atmospheric Environment, **23**, 2417-2430.

Radke, L.F., J.A. Coakley, Jr. and M.D. King (1989b). Direct and remote sensing observations of the effects of ships on clouds, *Science*, 246, 1146-1149.

Raes, F., T. Bates, F. McGovern and M Van Liederkerke (2000). The 2nd Aerosol Chracterization Experiemnt (ACE-2), General overview and main results, *Tellus*, **52B**, 111-125.

Ramanathan, V., O. Boucher, J. Haigh, D. Hauglustaine, J. Haywood, G. Myhre, T. Nakajima, G. Y. Shi, S. Solomn (2001a). Radiative forcing of climate change, in *Climate Change 2001: The Scientific Basis, Contribution of Working group I to the Third Assessment Report of the Intergovernmental panel on climate Change (IPCC)*, Edited by J.T. Houghton et al., chapter 5, pp349-416, Cambridge University Press, New York.

Ramanathan, V., P. J. Crutzen, J. Kiehl and D. Rosenfeld (2001b). Aerosol, climate and the hydrological cycle, *Science*, **292**, 2119-2124.

Ramanathan, V., P. J. Crutzen, J. Lelieveld, et al. (2001c). Indian Ocean Experiments: An integrated analysis of the climate forcing and effects of the grate Indo-Asian haze, *Journal of Geophysical Research*, **106**, 28,371-398.

Rasch, P., M. Barth, J. Kiehl, S. Schwartz and C. Benkovitz (2000). A description of the global sulfur cyble and its controlling processes in the National Center for Atmospheric Research Community Climate Model, Version 3, *Journal of Geophysical Research*, **105**, 1367-1385.

Redemann, J., P.B. Russell, and P. Hamill (2001). Dependence of aerosol light absorption and single scattering albedo on ambient relative humidity for sulfate aerosols with black carbon cores, *Journal of Geophysical Research*, **106**, 27,485-495.

Roelofs, G.J., P. Kasibhatla; L.A. Barrie, et al. (2001). Analysis of regional budgets of sulfur species modeled for the COSAM exercise, *Tellus*, **53B**, 673-694.

Rogers, R. R. and Yau M. K. (1989). A short course in cloud physics, 3rd Ed., Pergamon, Oxford, UK.

Rosenfeld, D. (1999). TRMM observed first direct evidence of smoke from forest fires inhibiting rainfall, *Geophysical Research Letters*, **26**, 3105-3108.

Rosenfeld, D. (2000). Suppression of rain and snow by urban and industrial air pollution, *Science*, **287**, 1793-1796.

Rosenfeld, D. and G. Feingold (2003). Explanation of discrepancies among satellite observations of the aerosol indirect effects, *Geophysical Research Letters*, **30** (14), 1776, doi: 10.1029/2003GL017684.

Rosenfeld, D., Y. Rudich and R. Lahav (2001). Desert dust suppressing precipitation: A possible desertification feedback loop, *Proceedings of National Academy of Sciences*, **98**, 5975-5980.

Rotstayn, L.D. (1999). Indirect forcing by anthropogenic aerosols: A global climate model calculation of effective-radius and cloud-lifetime effects, *Journal of Geophysical Research*, **104**, 9369-9380.

Rudich Y., A. Sagi, D. Rosenfeld (2003). Influence of the Kuwait oil fires plume (1991) on the microphysical development of clouds, *Journal of Geophysical Research*, **108** (D15), 4478, doi: 10.1029/2003JD003472.

Santer, B.D., K.E. Taylor, T.M.L. Wigley, et al. (1995). Towards the detection and attribution of an anthropogenic effect on climate, *Climate Dynamics*, **12**, 77-100.

Santer, B.D., K.E. Taylor, T.M.L. Wigley, et al. (1996). A search for human influences on the thermal sturcutre of the atmosphere, *Nature*, **382**, 39-46.

Schimel, D., et al. (1996). Radiative forcing of climate change, in *Climate Change 1995: The Science of Climate Change, Contribution of Working Group I to the Second Assessment Report of the Intergovernmental Panel for Climate Change (IPCC)*, edited by J.T. Houghton et al., chapter 2, pp. 65-130, Cambridge University Press, New York.

Schwartz, S.E. (1996). The whitehouse effect – shortwave radiative forcing of climate by anthropogenic aerosols: An overview, *Journal of Aerosol Sciences*, **27**, 359-382.

Schwartz, S.E. and M.O. Andreae (1996). Uncertainty in climate change caused by aerosols, *Science*, **272**, 1121-1122.

Scorer, R.S. (1987). Ship trails, *Atmospheric Environment*, **21**, 1417-1425.

Seinfeld, J. H. and S. N. Pandis (1997). Atmospheric chemistry and physics: From air pollution to climate change, 1326pp, John Wiley, New York.

Steiner, A.L. (2004). The influence of atmospheric chemistry and climate on atmospheric-biosphere interactions, Ph.D thesis, school of Earth and Atmospheric Sciences, Georgia Institute of Technology, Atlanta, GA.

Streets, D. G., S. Gupta, S.T. Waldhoff, et al. (2001). Black carbon emissions in China, *Atmospheric Environment*, **35**, 4281-4296.

Streets, D.G. and S.T. Waldhoff (2000). Present and future emissions of air pollutants in China: $SO_2$, $NO_x$, and CO, *Atmospheric Environment*, **34**, 363-374.

Streets, D.G., T.C. Bond, G.R. Carmichael, S.D. Fernandes, Q. Fu, D. He, Z. Klimont, S.M. Nelson, N.Y. Tsai, M.Q. Wang, J.-H. Woo, K.F. Yarber (2003). An inventory of gaseous and primary aerosol emissions in Asia in the year 2000, *Journal of Geophysical Research*, **108**, doi: 10.1029/2002JD003093.

Takemura, T., T. Nozawa, S. Emori, T. Y. Nakajima, and T. Nakajima (2005). Simulation of climate response to aerosol direct and indirect effects with aerosol transport-radiation model, *Journal of Geophysical Research,* **110**, D02202, doi: 10.1029/2004JD005029.

Tan, Q., W. L. Chameides, D. Streets, T. Wang, J. xu, M. Bergin and J. Woo (2004). An evaluation of TRACE-P emission inventories from China using a regional model and chemical measurements, *Journal of Geophysical Research,* **109***,* doi: 10.1029/2004JD005071.

Tan, Q., Y. Huang, W. L. Chameides (2002). Budget and export of anthropogenic $SO_x$ from East Asia during continental outflow conditions, *Journal of Geophysical Research,* **107***,* doi: 10.1029/2001JD000769.

Taylor, K.E and J.E. Penner (1994). Response of the climate system to atmospheric aerosols and greenhouse gases, *Nature*, **369**, 734-737.

Toon, O.B. (2000). How pollution suppresses rain, *Science*, **287**, 1763-1765.

Tripoli, G.J. and Cotton W.R. (1980). A numerical investigation of several factors contributing to the observed variable intensity of deep convection over South Florida, *Journal of Applied Meteorology*, **19**, 1037-1063.

Twomey, S. (1974). Pollution and the planetary albedo, *Atmospheric Environment*, **8**, 1251-1256.

Twomey, S., A.K. Davidson and K. J. Seton (1978). Results of five years' observations of cloud nucleus concentration at Roberton, New South Wales, *Journal of the Atmospheric Sciences*, **35**, 650-656.

U.S. Environmental Protection Agency (1996). *Review of National Ambient Air Quality Standards for Ozone: Assessment of Scientific and Technical Information*, (Office of Air Quality Planning and Standards, U.S. EPA, Research Triangle Park, NC), EPA/452/5-96-007, 152pp.

United Nations (1996). *United Nations Statistical Yearbook*, 41$^{th}$ Issue, United Nations Publication, 886pp, New York, NY.

Wang, T., T. F. Cheung, Y. S. Li, X. M. Yu and D.R. Blake (2002). Emission characteristics of CO, $NO_x$ and $SO_2$ and indications of biomass burning observed at a rural site in eastern China, *Journal of Geophysical Research*, **107**(D12), 4157, doi:10.1029/2001JD000724.

Wang, W. and T. Wang (1995). On the origin and the trend of acid deposition in China, *Water, Air and Soil Pollution*, **85**(4), 2295-2300.

Warner, J. (1968). A reduction in rainfall associated with smoke from sugar-cane fires: An inadvertent weather modification? *Journal of Applied Meteorology*, **7**, 247-251.

Warner, J. and S. Twomey (1967). The production of cloud nuclei by cane fires and the effect on cloud droplet concentration, *Journal of the atmospheric Sciences*, **24**, 704-706.

World Climate Program, WCP-112 (1986). A preliminary cloudless standard atmosphere for radiation computations, WMO, WMO/TD-N24, Geneva, 53pp.

World Climate Program, WCP-55 (1983). Report of the expert meeting on aerosols and their climatic effects (Eds. A. Deepak, and H. E. Gerber), WMO, Geneva, 83pp.

Xu, J., M.H. Bergin and R. Greenwald (2003). Direct aerosol radiative forcing in the Yangtze delta region of China: Observation and model estimation, *Journal of Geophysical Research*, **108**(D2) 4060, doi:10.1029/2002JD002550.

Xu, J., M.H. Bergin, X. Yu, G. Liu, J. Zhao, C.M. Carrico and K. Baumann (2002). Measurement of aerosol chemical, physical and radiative properties in the Yangtze Delta region of China, *Atmospheric Environment*, **36**, 161-173.

Xu, Q. (2001). Abrupt change of the mid-summer climate in central east China by the influence of atmospheric pollution, *Atmospheric Environment*, **35**, 5029-5040.

Yan, P., C. Luo, X. Xu, R. Xiang, G. Ding, J. Tang, M. Wang, and X. Yu (1997). The study of distribution character of $O_3$, $NO_x$ and $SO_2$ at rural areas in China, *Quarterly Journal of Applied Meteorology*, **8**, 53-60.

Yu, H., R.E. Dickinson, M. Chin, Y.J. Kaufman, B.N. Holben, I.V. Geogdzhayev, and M.I. Mishchenko (2003). Annual cycle of global distributions of aerosol optical depth from integration of MODIS retrievals and GOCART model simulations, *Journal of Geophysical Research*, **108**(D3), 4128, doi:10.1029/2002JD002717.

Yu, H., R.E. Dickinson, M. Chin, Y.J. Kaufman, M. Zhou, L. Zhou, Y. Tian, O. Dubovik, and B.N. Holben (2004). The direct radiative effect of aerosols as determined from a combination of MODIS retrievals and GOCART simulations, *Journal of Geophysical Research*, **109,** D03206, doi: 10.1029/2003JD003914.

Yu, H., S.C. Liu, and R.E. Dickinson (2002). Radiative effects of aerosols on the evolution of the atmospheric boundary layer, *Journal of Geophysical Research*, **107**(D12), 4142, doi: 10.1029/2001JD000754.

Zhai, P.-M. and X.-H. Pan (2003). Trends in temperature extremes during 1951-1999 in China, *Geophysical Research Letters*, **30**(17), 1913, doi: 10.1029/2003GL018004.

Zhou, L., R. E. Dickinson, Y. Tian, et al. (2004). Evidence for a significant urbanization effect on climate in China, *Proceedings of National Academy of Sciences*, **101**, 9540-9544.

# VITA

Yan Huang was born in Qidong, Jiangsu Province, P. R. China. In 1985, she entered Nanjing Institute of Meteorology, Nanjing, China, where she received her B. S. in Atmospheric Physics in 1989. Then she studied towards to a M.S. majored in Atmospheric Physics during 1989 to 1992 at the Institute of Atmospheric Physics, Chinese Academy of Sciences, Beijing. After graduation, she worked there as a research scientist for five years. In 1997, she moved to the National Center for Atmospheric Research, Boulder, CO, and worked there for one and half years as a visiting scholar. She began her Ph.D. in Atmospheric Chemistry at Georgia Institute of Technology in the fall of 1999. After six years as a research and teaching assistant, she received her Ph.D. from the School of Earth and Atmospheric Sciences in February 2005.